NCAR/TN-417+STR
NCAR TECHNICAL NOTE

January 1996

A Land Surface Model (LSM version 1.0) for Ecological, Hydrological, and Atmospheric Studies: Technical Description and User's Guide

Gordon B. Bonan

CLIMATE AND GLOBAL DYNAMICS DIVISION

NATIONAL CENTER FOR ATMOSPHERIC RESEARCH
BOULDER, COLORADO

NCAR TECHNICAL NOTES

The Technical Note series provides an outlet for a variety of NCAR manuscripts that contribute in specialized ways to the body of scientific knowledge but which are not suitable for journal, monograph, or book publication. Reports in this series are issued by the NCAR Scientific Divisions; copies may be obtained on request from the Publications Office of NCAR. Designation symbols for the series include:

EDD – *Engineering, Design, or Development Reports*

Equipment descriptions, test results, instrumentation, and operating and maintenance manuals.

IA – *Instructional Aids*

Instruction manuals, bibliographies, film supplements, and other research or instructional aids.

PPR – *Program Progress Reports*

Field program reports, interim and working reports, survey reports, and plans for experiments.

PROC – *Proceedings*

Documentation of symposia, colloquia, conferences, workshops, and lectures. (Distribution may be limited to attendees.)

STR – *Scientific and Technical Reports*

Data compilations, theoretical and numerical investigations, and experimental results

The National Center for Atmospheric Research is operated by the University Corporation for Atmospheric Research and is sponsored by the National Science Foundation. Any opinions, findings, conclusions, or recommendations expressed in this publication are those of the author(s) and do not necessarily reflect the views of the National Science Foundation.

TABLE OF CONTENTS

LIST OF FIGURES

LIST OF TABLES

INTRODUCTION

Ecological, hydrological, and atmospheric models often parameterize the same processes, though with vastly different complexity. For example, soil water is an important determinant of net primary production and biogeographical vegetation patterns. Soil water, through its effects on the partitioning of net radiation into latent and sensible heat, is also an important determinant of climate. Ecological models often use a simple bucket model, updated monthly, to model soil water. In contrast, hydrologists might use the Richards equation for vertical water flow to model soil water. The non-linearity of this equation requires short time steps (seconds to minutes) and high spatial resolution of the soil column (millimeters to centimeters). Some of the land surface parameterizations for atmospheric models use the Richards equation, though with much fewer soil layers (e.g., three layers corresponding to diurnal, seasonal, and annual time scales).

Stomatal physiology is important for many ecological studies because it determines the rate of CO_2 uptake during photosynthesis and is important for many hydrologic and atmospheric studies because of its effect on the latent heat flux. Ironically, the most detailed parameterizations of stomatal physiology, including the response of stomata to environmental factors such as light, temperature, soil water, etc., are often found in the land surface models used with atmospheric models. The long (monthly) time step of many ecological models prevents them from explicitly modeling photosynthesis as a diffusion process that varies with stomatal resistance. Instead, optimal rates of carbon uptake are decremented for sub-optimal environmental conditions using relative growth factors ranging from zero to one.

Other common processes include: phenology, which is important due to the effects of leaf area on the absorption of solar radiation at the surface, sensible heat flux, and latent heat flux; the absorption, reflection, and transmittance of solar radiation, which is important energetically as part of the net radiation at the surface

and ecologically due to the effects of the vertical light profile on vegetation structure, composition, and biogeochemical fluxes; and soil heat fluxes, which are important due to the effects of soil temperatures on biogeochemical fluxes, the surface energy budget, and soil hydrology.

It is clear that many ecological, hydrological, and atmospheric processes are so intertwined that these cannot be considered separate disciplines. Successful modeling of net primary production, carbon storage, and trace gas emissions (e.g., methane, non-methane hydrocarbons, nitrous oxide) requires an accurate model of the micrometeorological and hydrological environments in addition to the traditional ecological emphasis on vegetation and biogeochemical controls. Successful modeling of latent and sensible heat fluxes requires an accurate description of the ecological state and biogeochemical controls in addition to the traditional emphasis on the physical environment.

Several years ago, I became interested in combining the relevant biophysical, biogeochemical, hydrologic, and ecosystem processes into a comprehensive model of land-atmosphere interactions that was physically and biologically realistic (see Bonan 1993c and 1995c for a discussion of some of the important issues). The first such model (Bonan 1991a, 1991b, 1993a) did so, but at a daily time step, and was very similar in nature to the FOREST-BGC and BIOME-BGC ecosystem models developed by Steve Running and colleagues at the University of Montana (Running et al. 1989), though with more biophysical and hydrologic detail. Like FOREST-BGC, this model proved to be very successful at simulating annual net primary production along large climatic gradients (Bonan 1993b).

The land surface model described in this document is an extension of this earlier model development, but now applied at sub-hourly time scales (e.g., 30 minutes) to resolve the diurnal cycle. The model is a blend of the ecological processes found in many ecosystem models, the hydrologic processes found in many hydrologic models,

and the surface fluxes common to the land surface models used with atmospheric models. With the requirement that the model be implemented globally, many other surface types (e.g., glaciers, lakes, savanna, etc.) needed to be included in addition to the initial needleleaf evergreen and broadleaf deciduous forests.

This technical note describes version 1 of this LSM land surface model. In this model, land surface processes are described in terms of biophysical fluxes (latent heat, sensible heat, momentum, reflected solar radiation, emitted longwave radiation) and biogeochemical fluxes (CO_2) that depend on the ecological and hydrologic state of the land. Consequently, ecological and hydrologic sub-models are needed to simulate temporal changes in terrestrial biomass and water. Component processes and their interactions are illustrated in Figure 1. Scientific justification for many of the parameterizations used in this model can be found in Bonan (1994), Bonan (1995a) [CO_2 fluxes], Bonan (1995b) [lakes], and Bonan (1996) [infiltration].

Figure 1. Schematic diagram of the biophysical, biogeochemical, hydrologic, and ecosystem processes simulated by the model, interactions among these component processes, and the interaction between the land and atmosphere. The biophysical and biogeochemical fluxes depend on the ecological and hydrologic state of the land, which are updated by ecological and hydrologic sub-models. Text within boxes indicates specific processes. Italics text indicates processes not currently considered. The biomass and water boxes indicate terrestrial state variables that affect and are affected by the component processes.

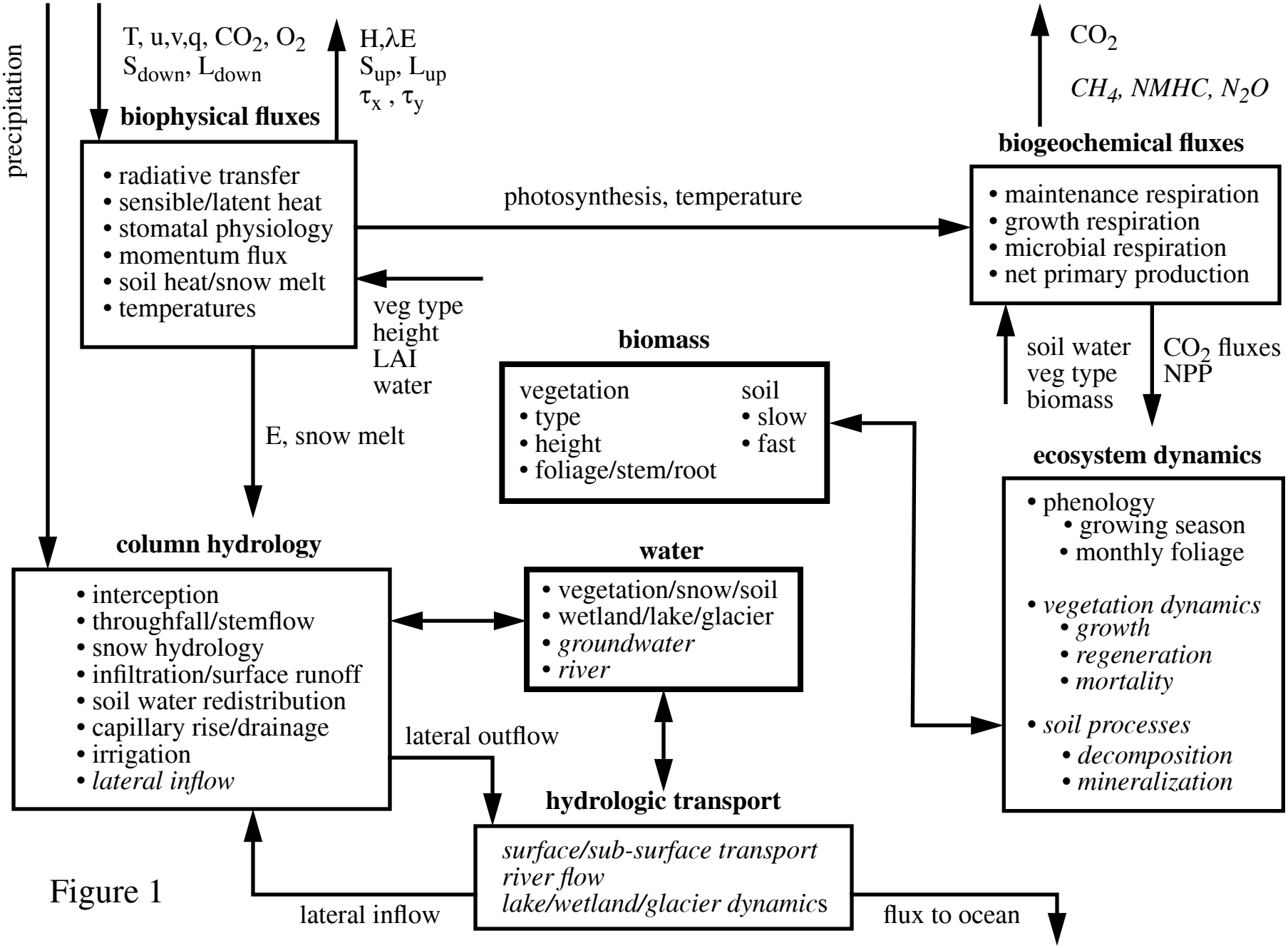
precipitation
T, u,v,q, CO_2, O_2
S_{down}, L_{down}
biophysical fluxes
H,λE
S_{up}, L_{up}
τ_x , τ_y
• radiative transfer
• sensible/latent heat
• stomatal physiology
• momentum flux
• soil heat/snow melt
• temperatures
photosynthesis, temperature
CO_2
CH_4, NMHC, N_2O
biogeochemical fluxes
• maintenance respiration
• growth respiration
• microbial respiration
• net primary production
veg type
height
LAI
water
E, snow melt
biomass
vegetation
• type
• height
• foliage/stem/root
soil
• slow
• fast
soil water
veg type
biomass
CO_2 fluxes
NPP
ecosystem dynamics
• phenology
• growing season
• monthly foliage
• *vegetation dynamics*
• *growth*
• *regeneration*
• *mortality*
• *soil processes*
• *decomposition*
• *mineralization*
column hydrology
• interception
• throughfall/stemflow
• snow hydrology
• infiltration/surface runoff
• soil water redistribution
• capillary rise/drainage
• irrigation
• *lateral inflow*
water
• vegetation/snow/soil
• wetland/lake/glacier
• *groundwater*
• *river*
lateral outflow
hydrologic transport
surface/sub-surface transport
river flow
lake/wetland/glacier dynamics
lateral inflow
flux to ocean

Figure 1

PART I: TECHNICAL DESCRIPTION

The land surface model is a one-dimensional model of energy, momentum, water, and CO_2 exchanges between the atmosphere and land accounting for

- ecological differences among vegetation types;
- thermal and hydrological differences among soil types; and
- multiple surface types, including lakes and wetlands, within a grid cell.

Vegetated surfaces are comprised of multiple plant types so that, for example, a mixed broadleaf deciduous-needleleaf evergreen forest consists of patches of needleleaf evergreen trees, broadleaf deciduous trees, and bare ground. Lakes and wetlands, if present, form additional patches for a total of up to five subgrid points. The model is run for each subgrid point independently, with the same grid-averaged atmospheric forcing. Grid-averaged surface variables are obtained using the subgrid fractional areas. Processes simulated for each subgrid point are:

ecosystem dynamics

- vegetation phenology (section 1.3);

biophysical processes

- absorption, reflection, and transmittance of solar radiation (sections 2, 3.1);
- absorption and emission of longwave radiation, allowing for emissivities less than one (sections 3.2);
- sensible and latent heat fluxes, partitioning latent heat into canopy evaporation, soil evaporation, and transpiration (section 4);
- momentum fluxes (section 4);
- heat transfer in a multi-layer soil or lake (sections 6, 7);
- stomatal physiology (section 9.1);

hydrologic processes

- interception, throughfall, and stemflow (section 8.1);
- snow accumulation and melt (section 8.2);
- infiltration and runoff (section 8.3);
- soil hydrology, including water transfer in a multi-layer soil (section 8.4);

biogeochemical processes

- photosynthesis, plant respiration, and microbial respiration (section 9); and
- net primary production (section 9).

Table 1. Atmospheric input to land model

reference height	z_{atm}	(m)
temperature at z_{atm}	T_{atm}	(K)
zonal wind at z_{atm}	u_{atm}	(m s^{-1})
meridional wind at z_{atm}	v_{atm}	(m s^{-1})
specific humidity at z_{atm}	q_{atm}	(kg kg^{-1})
pressure at z_{atm}	P_{atm}	(Pa)
partial pressure CO_2 at z_{atm}	355×10^{-6}	(mol mol^{-1})
partial pressure O_2 at z_{atm}	0.209	(mol mol^{-1})
surface pressure	P_{srf}	(Pa)
convective precipitation	q_{prcc}	(mm H_2O s^{-1})
large-scale precipitation	q_{prcl}	(mm H_2O s^{-1})
incident direct beam solar radiation $< 0.7\mu$m	$S_{\mathrm{atm}}\downarrow^{\mu}_{\mathrm{vis}}$	(W m^{-2})
incident direct beam solar radiation $\geq 0.7\mu$m	$S_{\mathrm{atm}}\downarrow^{\mu}_{\mathrm{nir}}$	(W m^{-2})
incident diffuse solar radiation $< 0.7\mu$m	$S_{\mathrm{atm}}\downarrow_{\mathrm{vis}}$	(W m^{-2})
incident diffuse solar radiation $\geq 0.7\mu$m	$S_{\mathrm{atm}}\downarrow_{\mathrm{nir}}$	(W m^{-2})
incident longwave radiation	$L_{\mathrm{atm}}\downarrow$	(W m^{-2})

Atmospheric potential temperature (θ_{atm}, K), vapor pressure (e_{atm}, Pa), and density (ρ_{atm}, kg m^{-3}) are also required, but are derived from T_{atm}, q_{atm}, P_{atm}, and P_{srf}

Table 2. Atmospheric output from land model

latent heat flux	λE	(W m^{-2})
sensible heat flux	H	(W m^{-2})
constituent flux	H_2O, CO_2	(kg m^{-2} s^{-1})
zonal momentum flux	τ_x	(kg m^{-1} s^{-2})
meridional momentum flux	τ_y	(kg m^{-1} s^{-2})
emitted longwave radiation	$L\uparrow$	(W m^{-2})
direct beam albedo $< 0.7\mu$m	$I\uparrow^{\mu}_{\rm vis}$	
direct beam albedo $\geq 0.7\mu$m	$I\uparrow^{\mu}_{\rm nir}$	
diffuse albedo $< 0.7\mu$m	$I\uparrow_{\rm vis}$	
diffuse albedo $\geq 0.7\mu$m	$I\uparrow_{\rm nir}$	

The model is developed with the assumption that the land and atmosphere are coupled with a fully-explicit time-stepping procedure. That is, the current state of the atmosphere (Table 1) is used to force the land model; surface energy, constituent, momentum, and radiative fluxes (Table 2) are then used to update the atmosphere.

Required surface data for each land grid cell are listed in Table 3. Latitude and longitude are used to calculate the solar zenith angle (section 2.3). The surface type defines the plant types, which differ in ecological characteristics, within the vegetated fraction of the grid cell (cf. Table 5). Soil color defines the saturated and dry soil albedos (Table 10). Percent sand, silt, and clay define soil thermal and hydrologic properties (sections 6.2, 8.4.1). The percent lake and wetland data define inland water subgrid points. Surface types were derived from Olson et al.'s (1983) 0.5^o by 0.5^o data, overlayed onto the NCAR Community Climate Model T42 (2.8^o by 2.8^o) grid. Soil colors were taken from the BATS T42 data set for use with the CCM (Dickinson et al. 1993). Sand, silt, and clay data were derived from Webb et

al.'s (1993) 1.0^o by 1.0^o data. Inland water data were derived from Cogley's (1991) 1.0^o by 1.0^o data for perennial freshwater lakes and swamps/marshes. Lakes can be either deep (50 m) or shallow (10 m) (section 7). Currently, all lakes are treated as deep lakes. Wetland "soils" are, when calculating temperatures, treated the same as soil except that the water content is kept at saturation.

Specific parameter values are introduced in the following sub-sections as appropriate. Physical constants are listed in Table 4.

Table 3. Required surface data

latitude and longitude at center of grid cell
surface type
soil color type
percent sand, percent silt, percent clay
percent of grid cell covered with lakes
percent of grid cell covered with wetlands

Table 4. Physical constants

gravitational acceleration	g	9.80616 m s^{-2}
von Karman constant	k	0.4
Stefan-Boltzmann constant	σ	5.67×10^{-8} W m^{-2} K^{-4}
latent heat of sublimation	λ	2.8440×10^{6} J kg^{-1}
latent heat of vaporization	λ	2.5104×10^{6} J kg^{-1}
heat capacity of dry air	C_p	1004.64 J kg^{-1} K^{-1}
at constant pressure		
gas constant dry air	R	287.04 J kg^{-1} K^{-1}
heat capacity of water	c_w	4.188×10^{6} J m^{-3} K^{-1}
heat capacity of ice	c_i	2.094×10^{6} J m^{-3} K^{-1}
thermal conductivity of water	k_w	0.6 W m^{-1} K^{-1}
thermal conductivity of ice	k_i	2.2 W m^{-1} K^{-1}
bulk density of water	ρ_w	1000 kg m^{-3}
freezing point	T_f	273.16 K
latent heat of fusion	h_{fus}	0.3336×10^{6} J kg^{-1}

1. Ecosystem Composition and Structure

1.1 Vegetation Composition

Vegetated surfaces are comprised of bare ground and several physiological plant types (Table 5). For example, mixed broadleaf deciduous and needleleaf evergreen forest is composed of broadleaf deciduous trees, needleleaf evergreen trees, and bare ground. Rather than using a blended mix (e.g., the average roughness length), the model performs separate flux calculations for each fractional area and then averages the fluxes. These plant types (Table 6) differ in important properties that influence surface fluxes: leaf and stem areas (Figures 2, 3); root profile, canopy height, leaf dimension, stem and root biomass, and soil carbon (Table 7); optical properties (Table 8); physiological properties that determine stomatal resistance and CO_2 fluxes (Tables 16, 17); and roughness length, displacement height, and other aerodynamic properties (Table 12). Currently, there are no physiological differences between cool and warm plant types, except cool C_3 and warm C_4 grasses, so that, for example, the cool broadleaf deciduous forest is equivalent to the warm broadleaf deciduous forest. Vegetation composition and fractional areas are currently time-invariant.

1.2 Vegetation Structure, Carbon, and Nitrogen

Vegetation structure is defined by time-varying leaf and stem areas (section 1.3) and time-invariant canopy height, root profile, leaf dimension, carbon, and nitrogen (Table 7). Canopy top z_{top} and bottom z_{bot} heights and leaf dimensions $\mathrm{d}_{\mathrm{leaf}}$ are from Bonan (1995a, 1995b). Relative root abundance in each soil layer r_i is calculated from Gale and Grigal's (1987) cumulative root profile $R_i = 1 - r_p^z$, where z is soil depth (cm). Vegetation common to dry regions (tropical seasonal tree, grass, evergreen shrub, deciduous shrub) have a larger portion of their roots in deep soil layers.

Stem and root biomass, soil carbon, and foliage nitrogen are needed for the biogeochemical fluxes. Vegetation stem biomass V_b^s, vegetation root biomass V_b^r, and soil carbon S_c are adapted from McGuire et al. (1992) to give reasonable values for each plant type. Foliage nitrogen N is used to adjust the rate of photosynthesis for nutrient limitations (section 9.1). Because the derivation of the photosynthetic parameters incorporates extant nitrogen limitations, foliage nitrogen is set to values that do not limit photosynthesis. These carbon and nitrogen pools are currently time-invariant.

1.3 Phenology

Leaf and stem area indices (Figure 2, 3) are updated daily using monthly values adapted from Dorman and Sellers (1989). In the Southern Hemisphere, these data are off-set by 6 months (Figure 4). These leaf and stem area indices are adjusted for burying by snow, $z_{\rm sno}$ m deep (section 8.2), using the fraction of the exposed canopy $0 \le 1 - \frac{z_{\rm sno} - z_{\rm bot}}{z_{\rm top} - z_{\rm bot}} \le 1$.

The photosynthetic growing season is defined as the period with vegetation temperature greater than some critical temperature $T_{\rm min}$ (section 9.1).

Figure 2. Daily leaf area index for the 12 plant types

Figure 3. Daily stem area index for the 12 plant types

Figure 4. Daily leaf area index for broadleaf deciduous trees and grass in the Northern Hemisphere (NH) and Southern Hemisphere (SH). Dashed lines indicated the monthly mean values.

Table 5. Plant types and fractional cover for each surface type

	surface type	plant	cover	plant	cover	plant	cover
	No Vegetation						
0	ocean	-	-	-	-	-	-
1	land ice	b	1.00	-	-	-	-
2	desert	b	1.00	-	-	-	-
	Forest						
3	cool needleleaf evergreen tree	net	0.75	b	0.25	-	-
4	cool needleleaf deciduous tree	ndt	0.50	b	0.50	-	-
5	cool broadleaf deciduous tree	bdt	0.75	b	0.25	-	-
6	cool mixed net and bdt	net	0.37	bdt	0.37	b	0.26
7	warm needleleaf evergreen tree	net	0.75	b	0.25	-	-
8	warm broadleaf deciduous tree	bdt	0.75	b	0.25	-	-
9	warm mixed net and bdt	net	0.37	bdt	0.37	b	0.26
10	tropical broadleaf evergreen tree	bet	0.95	b	0.05	-	-
11	tropical seasonal deciduous tree	tst	0.75	b	0.25	-	-
	Interrupted Woods						
12	savanna	wg	0.70	tst	0.30	-	-
13	evergreen forest tundra	net	0.25	ag	0.25	b	0.50
14	deciduous forest tundra	ndt	0.25	ag	0.25	b	0.50
15	cool forest crop	c	0.40	bdt	0.30	net	0.30
16	warm forest crop	c	0.40	bdt	0.30	net	0.30
	Non-Woods						
17	cool grassland	cg	0.60	wg	0.20	b	0.20
18	warm grassland	wg	0.60	cg	0.20	b	0.20
19	tundra	ads	0.30	ag	0.30	b	0.40
20	evergreen shrubland	es	0.80	b	0.20	-	-
21	deciduous shrubland	ds	0.80	b	0.20	-	-
22	semi-desert	ds	0.10	b	0.90	-	-
23	cool irrigated crop	c	0.85	b	0.15	-	-
24	cool crop	c	0.85	b	0.15	-	-
25	warm irrigated crop	c	0.85	b	0.15	-	-
26	warm crop	c	0.85	b	0.15	-	-
	Wetland						
27	forest wetland	bet	0.80	b	0.20	-	-
28	non-forest wetland	b	1.00	-	-	-	-

Table 6. Plant types

Plant Type	Acronym
needleleaf evergreen tree	net
needleleaf deciduous tree	ndt
broadleaf evergreen tree	bet
broadleaf deciduous tree	bdt
tropical seasonal tree	tst
cool C_3 grass	cg
evergreen shrub	es
deciduous shrub	ds
arctic deciduous shrub	ads
arctic grass	ag
crop	c
warm C_4 grass	wg
bare	b

Table 7. Vegetation structure, carbon, and nitrogen

Plant Type	r_p	z_{top} (m)	z_{bot} (m)	$\mathrm{d}_{\mathrm{leaf}}$ (m)	V_b^s (kg m^{-2})	V_b^r (kg m^{-2})	S_c (kg C m^{-2})	N %
needleleaf evergreen tree	0.94	17.0	8.50	0.04	3.6	7.2	11.0	-
needleleaf deciduous tree	0.94	14.0	7.00	0.04	3.6	7.2	11.0	-
broadleaf evergreen tree	0.94	35.0	1.00	0.04	9.0	18.0	15.0	-
broadleaf deciduous tree	0.94	20.0	11.50	0.04	6.2	12.4	11.0	-
tropical seasonal tree	0.97	18.0	10.00	0.04	4.5	9.0	8.0	-
C_3 grass	0.97	0.5	0.01	0.04	0.0	0.3	10.0	-
evergreen shrub	0.97	0.5	0.10	0.04	0.0	0.0	11.0	-
deciduous shrub	0.97	0.5	0.10	0.04	0.0	0.0	11.0	-
arctic deciduous shrub	0.94	0.5	0.10	0.04	0.1	0.4	18.0	-
arctic grass	0.94	0.5	0.01	0.04	0.1	0.4	18.0	-
crop	0.94	0.5	0.01	0.04	0.0	0.0	11.0	-
C_4 grass	0.97	0.5	0.01	0.04	0.0	0.3	10.0	-
bare	1.00	0.0	0.00	-	0.0	0.0	0.0	-

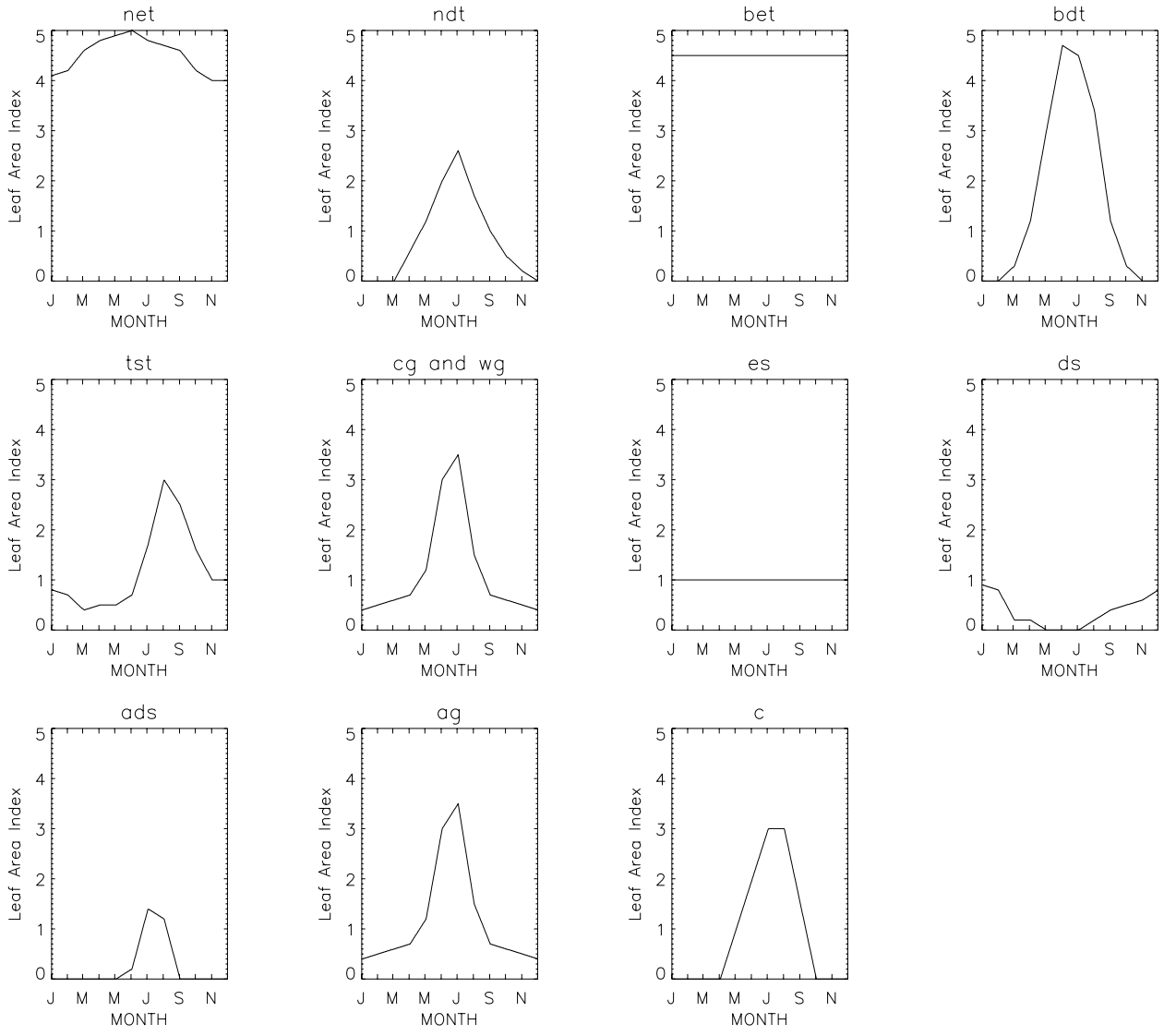
net
ndt
bet
bdt
tst
cg and wg
es
ds
ads
ag
c
Leaf Area Index
0
1
2
3
4
5
J M M J S N
MONTH

Figure 2

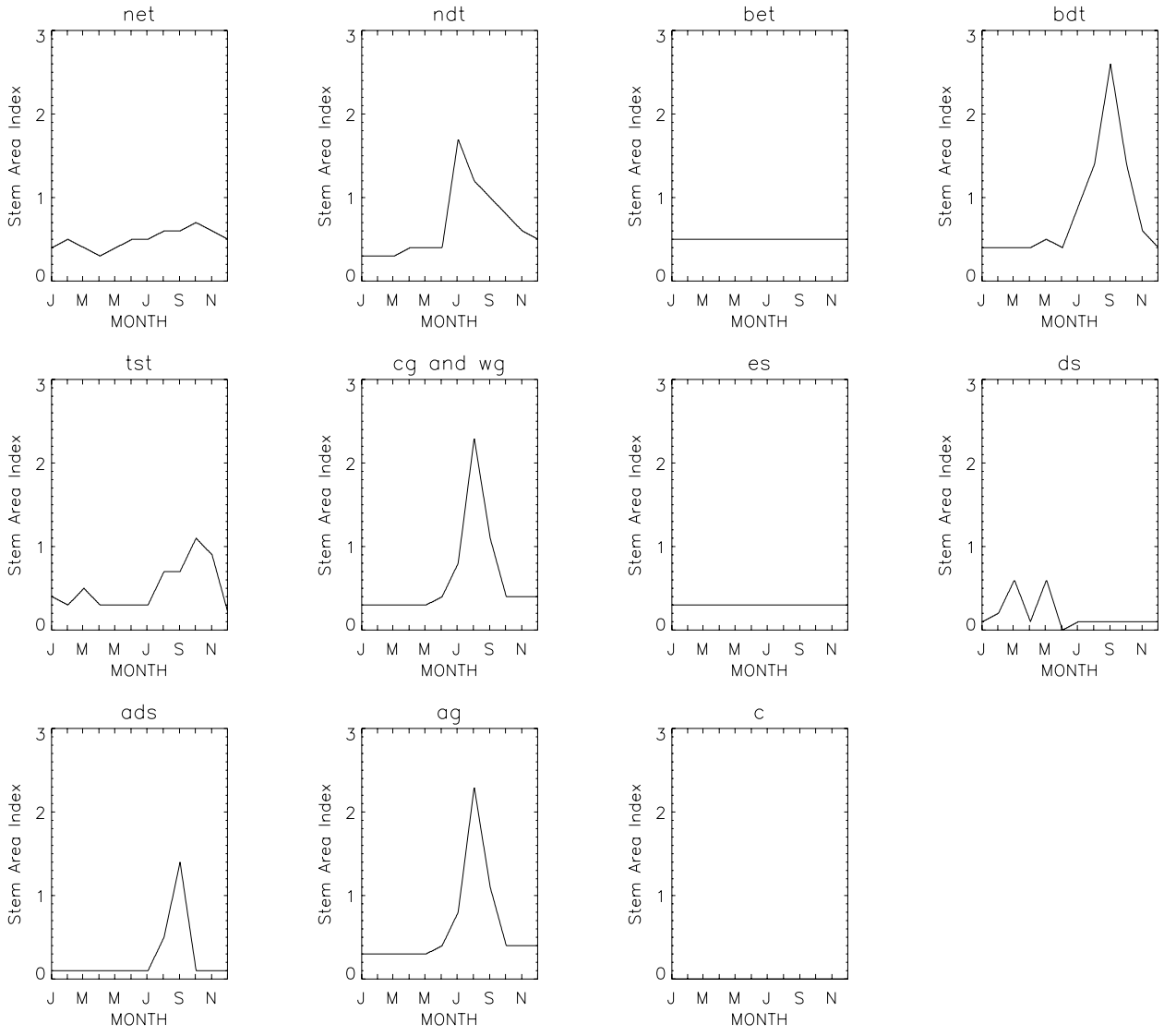
net
ndt
bet
bdt
tst
cg and wg
es
ds
ads
ag
c
Stem Area Index
0
1
2
3
J M M J S N
MONTH

Figure 3

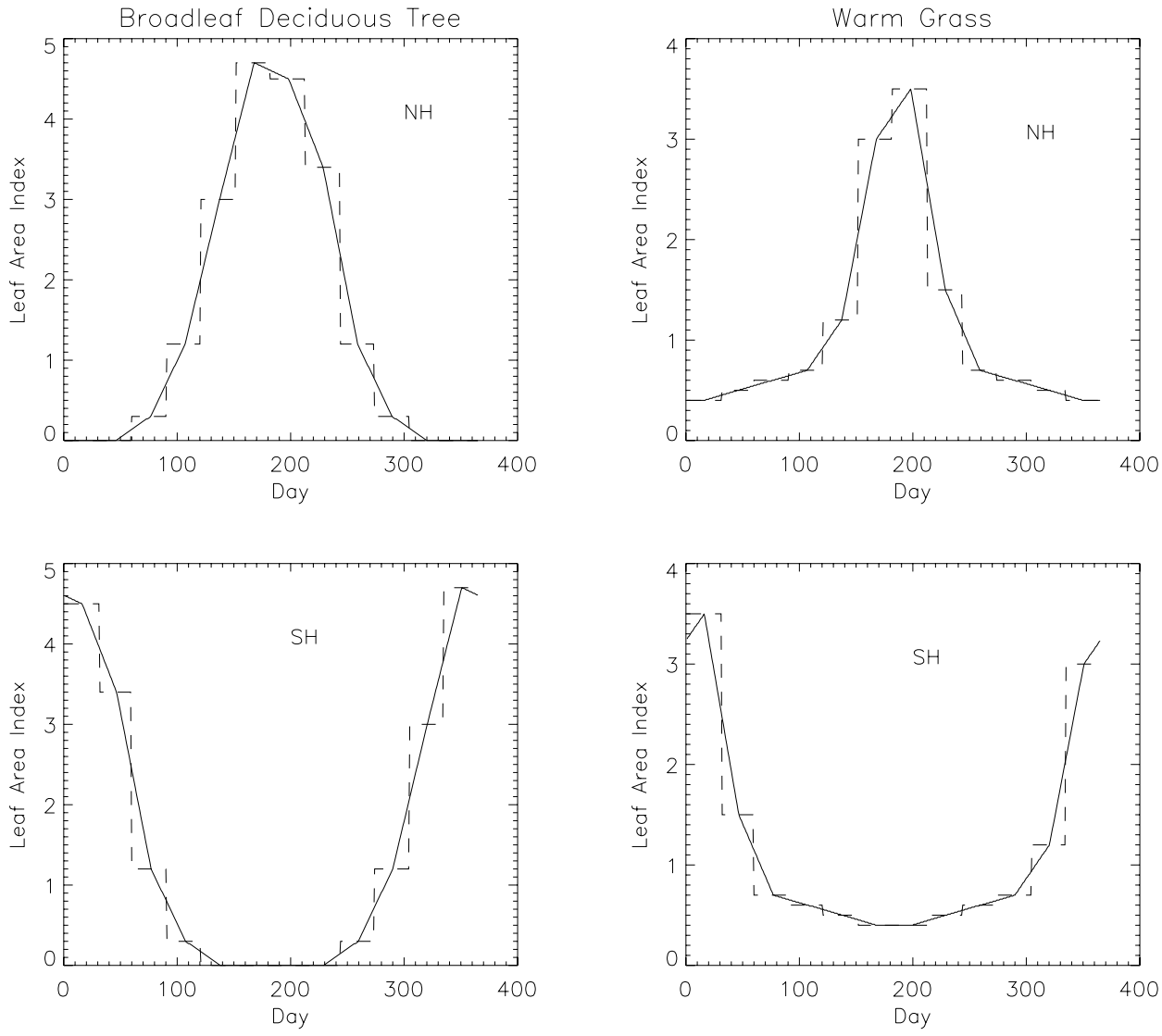
Broadleaf Deciduous Tree
Warm Grass
NH
NH
SH
SH
Leaf Area Index
Day
0
100
200
300
400
1
2
3
4
5

Figure 4

2. Surface Albedos

2.1 Canopy Radiative Transfer

Radiative transfer within vegetative canopies is calculated from the two-stream approximation of Dickinson (1983) and Sellers (1985)

$$-\bar{\mu}\frac{dI\uparrow}{d(L+S)} + [1-(1-\beta)\omega]I\uparrow - \omega\beta I\downarrow = \omega\bar{\mu}K\beta_0 e^{-K(L+S)}$$

$$\bar{\mu}\frac{dI\downarrow}{d(L+S)} + [1-(1-\beta)\omega]I\downarrow - \omega\beta I\uparrow = \omega\bar{\mu}K(1-\beta_0)e^{-K(L+S)}$$

where $I\uparrow$ and $I\downarrow$ are the upward and downward diffuse radiative fluxes per unit incident flux, $K = G(\mu)/\mu$ is the optical depth of direct beam per unit leaf and stem area, μ is the cosine of the zenith angle of the incident beam, $G(\mu)$ is the relative projected area of leaf and stem elements in the direction $\cos^{-1}\mu$, $\bar{\mu}$ is the average inverse diffuse optical depth per unit leaf and stem area, ω is a scattering coefficient, β and β_0 are upscatter parameters for diffuse and direct beam radiation, respectively, L is the leaf area index (section 1.3), and S is the stem area index (section 1.3). Given the direct beam albedo $\alpha^{\mu}_{g\Lambda}$ and diffuse albedo $\alpha_{g\Lambda}$ of the ground (section 2.2), these equations are solved to calculate the fluxes, per unit incident flux, absorbed by the vegetation, reflected by the vegetation, and transmitted through the vegetation for direct and diffuse radiation and for visible ($< 0.7\mu$m) and near-infrared ($\geq 0.7\mu$m) wavebands. The optical parameters $G(\mu)$, $\bar{\mu}$, ω, β, and β_0 are calculated based on work in Sellers (1985) as follows.

The relative projected area of leaves and stems in the direction $\cos^{-1}\mu$ is

$$G(\mu) = \phi_1 + \phi_2\mu$$

where $\phi_1 = 0.5 - 0.633\chi_L - 0.33\chi_L^2$ and $\phi_2 = 0.877(1-2\phi_1)$ for $-0.4 < \chi_L < 0.6$. χ_L is the departure of leaf angles from a random distribution and equals $+1$ for

horizontal leaves, 0 for random leaves, and -1 for vertical leaves.

The average inverse diffuse optical depth per unit leaf and stem area is

$$\bar{\mu} = \int_0^1 \frac{\mu'}{G(\mu')} d\mu' = \frac{1}{\phi_2}\left[1 - \frac{\phi_1}{\phi_2}\ln\left(\frac{\phi_1+\phi_2}{\phi_1}\right)\right]$$

where μ' is the direction of the scattered flux.

The optical parameters ω, β, and β_0, which vary with wavelength, are weighted combinations of values for vegetation and snow. If snow is intercepted by the canopy

$$\omega_\Lambda = \omega_\Lambda^{\rm veg}(1 - f_{\rm wet}) + \omega_\Lambda^{\rm sno} f_{\rm wet}$$

$$\omega_\Lambda \beta_\Lambda = \omega_\Lambda^{\rm veg}\beta_\Lambda^{\rm veg}(1 - f_{\rm wet}) + \omega_\Lambda^{\rm sno}\beta_\Lambda^{\rm sno} f_{\rm wet}$$

$$\omega_\Lambda \beta_{0,\Lambda} = \omega_\Lambda^{\rm veg}\beta_{0,\Lambda}^{\rm veg}(1 - f_{\rm wet}) + \omega_\Lambda^{\rm sno}\beta_{0,\Lambda}^{\rm sno} f_{\rm wet}$$

where $f_{\rm wet}$ is the wetted fraction of the canopy (section 8.1). The snow and vegetation weights are applied to the product $\omega_\Lambda\beta_\Lambda$ and $\omega_\Lambda\beta_{0,\Lambda}$ because these products are used in the two-stream equations. If there is no snow in the canopy,

$$\omega_\Lambda = \omega_\Lambda^{\rm veg}$$

$$\omega_\Lambda \beta_\Lambda = \omega_\Lambda^{\rm veg}\beta_\Lambda^{\rm veg}$$

$$\omega_\Lambda \beta_{0,\Lambda} = \omega_\Lambda^{\rm veg}\beta_{0,\Lambda}^{\rm veg} \; .$$

For vegetation, $\omega_\Lambda^{\rm veg} = \alpha_\Lambda + \tau_\Lambda$. α_Λ is a weighted combination of the leaf and stem reflectances ($\alpha_\Lambda^{\rm leaf}$, $\alpha_\Lambda^{\rm stem}$)

$$\alpha_\Lambda = \alpha_\Lambda^{\rm leaf} w_{\rm leaf} + \alpha_\Lambda^{\rm stem} w_{\rm stem}$$

where $w_{\rm leaf} = L/(L+S)$ and $w_{\rm stem} = S/(L+S)$. τ_Λ is a weighted combination of the leaf and stem transmittances ($\tau_\Lambda^{\rm leaf}$, $\tau_\Lambda^{\rm stem}$)

$$\tau_\Lambda = \tau_\Lambda^{\rm leaf} w_{\rm leaf} + \tau_\Lambda^{\rm stem} w_{\rm stem} \ .$$

The upscatter for diffuse radiation is

$$\omega_\Lambda^{\rm veg} \beta_\Lambda^{\rm veg} = \frac{1}{2}\left[\alpha_\Lambda + \tau_\Lambda + (\alpha_\Lambda - \tau_\Lambda)\left(\frac{1+\chi_L}{2}\right)^2\right]$$

and the upscatter for direct beam radiation is

$$\omega_\Lambda^{\rm veg} \beta_{0,\Lambda}^{\rm veg} = \frac{1+\bar{\mu}K}{\bar{\mu}K} a_s(\mu)_\Lambda$$

where the single scattering albedo is

$$\begin{aligned} a_s(\mu)_\Lambda =& \frac{\omega_\Lambda^{\rm veg}}{2}\int_0^1 \frac{\mu' G(\mu)}{\mu G(\mu') + \mu' G(\mu)} d\mu' \\ =& \frac{\omega_\Lambda^{\rm veg}}{2}\frac{G(\mu)}{\mu\phi_2 + G(\mu)}\left[1 - \frac{\mu\phi_1}{\mu\phi_2 + G(\mu)} \ln\left(\frac{\mu\phi_1 + \mu\phi_2 + G(\mu)}{\mu\phi_1}\right)\right] \ . \end{aligned}$$

The upward diffuse fluxes per unit incident direct beam and diffuse flux (i.e., the surface albedos) are

$$I\uparrow_\Lambda^\mu = \frac{h_1}{\sigma} + h_2 + h_3$$

$$I\uparrow_\Lambda = h_7 + h_8 \ .$$

The downward diffuse fluxes per unit incident direct beam and diffuse radiation, respectively, are

$$I\downarrow_\Lambda^\mu = \frac{h_4}{\sigma} e^{-K(L+S)} + h_5 s_1 + \frac{h_6}{s_1}$$

$$I\downarrow_\Lambda = h_9 s_1 + \frac{h_{10}}{s_1} \ .$$

The parameters h_1 to h_{10}, σ, and s_1 are from Sellers (1985) [note the error in h_4 in Sellers (1985)]:

$$b = 1 - \omega_\Lambda + \omega_\Lambda \beta_\Lambda$$

$$c = \omega_\Lambda \beta_\Lambda$$

$$d = \omega_\Lambda \bar{\mu} K \beta_{0,\Lambda}$$

$$f = \omega_\Lambda \bar{\mu} K (1 - \beta_{0,\Lambda})$$

$$h = \frac{\sqrt{b^2 - c^2}}{\bar{\mu}}$$

$$\sigma = (\bar{\mu} K)^2 + c^2 - b^2$$

$$u_1 = b - c/\alpha^{\mu}_{g\Lambda} \text{ or } u_1 = b - c/\alpha_{g\Lambda}$$

$$u_2 = b - c\alpha^{\mu}_{g\Lambda} \text{ or } u_2 = b - c\alpha_{g\Lambda}$$

$$u_3 = f + c\alpha^{\mu}_{g\Lambda} \text{ or } u_3 = f + c\alpha_{g\Lambda}$$

$$s_1 = \exp[-h(L+S)]$$

$$s_2 = \exp[-K(L+S)]$$

$$p_1 = b + \bar{\mu} h$$

$$p_2 = b - \bar{\mu} h$$

$$p_3 = b + \bar{\mu} K$$

$$p_4 = b - \bar{\mu} K$$

$$d_1 = \frac{p_1(u_1 - \bar{\mu}h)}{s_1} - p_2(u_1 + \bar{\mu}h)s_1$$

$$d_2 = \frac{u_2 + \bar{\mu}h}{s_1} - (u_2 - \bar{\mu}h)s_1$$

$$h_1 = -dp_4 - cf$$

$$h_2 = \frac{1}{d_1}\left[\left(d - \frac{h_1}{\sigma}p_3\right)\frac{(u_1 - \bar{\mu}h)}{s_1} - p_2\left(d - c - \frac{h_1}{\sigma}(u_1 + \bar{\mu}K)\right)s_2\right]$$

$$h_3 = \frac{-1}{d_1}\left[\left(d - \frac{h_1}{\sigma}p_3\right)(u_1 + \bar{\mu}h)s_1 - p_1\left(d - c - \frac{h_1}{\sigma}(u_1 + \bar{\mu}K)\right)s_2\right]$$

$$h_4 = -fp_3 - cd$$

$$h_5 = \frac{-1}{d_2}\left[\frac{h_4(u_2 + \bar{\mu}h)}{\sigma s_1} + \left(u_3 - \frac{h_4}{\sigma}(u_2 - \bar{\mu}K)\right)s_2\right]$$

$$h_6 = \frac{1}{d_2}\left[\frac{h_4}{\sigma}(u_2 - \bar{\mu}h)s_1 + \left(u_3 - \frac{h_4}{\sigma}(u_2 - \bar{\mu}K)\right)s_2\right]$$

$$h_7 = \frac{c(u_1 - \bar{\mu}h)}{d_1 s_1}$$

$$h_8 = \frac{-c(u_1 + \bar{\mu}h)s_1}{d_1}$$

$$h_9 = \frac{u_2 + \bar{\mu}h}{d_2 s_1}$$

$$h_{10} = \frac{-s_1(u_2 - \bar{\mu}h)}{d_2}$$

Vegetation optical parameters (Table 8) were taken from Dorman and Sellers (1989). Optical parameters for intercepted snow (Table 9) were taken from Sellers et al. (1986).

Figures 5, 6, and 7 show albedos as a function of zenith angle for semi-horizontal, random, and semi-vertical leaves. Albedos for all three leaf types are nearly constant for leaf area index > 2. Diffuse albedos have no zenith angle dependence and vary only slightly with leaf angle orientation. Direct beam albedos have negligible zenith angle dependence for semi-horizontal leaves (Figure 5), but strong dependence for random and semi-vertical leaves (Figures 6, 7). Direct beam albedos are very similar for the random and semi-vertical leaves.

Vegetation masking of snow albedos is illustrated in Figure 8. As leaf area index increases, the high underlying snow albedos are masked. In particular, albedos for leaf area index > 3 are comparable to the random leaves without snow (Figure 6). Visible albedos with intercepted snow ($f_{\rm wet} = 1$) are higher than without intercepted snow ($f_{\rm wet} = 0$), in part because of the higher values of ω (0.8 versus 0.15), but there are still much less than the snow albedos (leaf area index = 0). Albedos in the near-infrared waveband are less with intercepted snow than without due to the lower values of ω with snow (0.4) than without (0.7).

Table 8. Vegetation optical properties

Plant Type	χ_L	$\alpha_{\rm vis}^{\rm leaf}$	$\alpha_{\rm nir}^{\rm leaf}$	$\alpha_{\rm vis}^{\rm stem}$	$\alpha_{\rm nir}^{\rm stem}$	$\tau_{\rm vis}^{\rm leaf}$	$\tau_{\rm nir}^{\rm leaf}$	$\tau_{\rm vis}^{\rm stem}$	$\tau_{\rm nir}^{\rm stem}$
needleleaf evergreen tree	0.01	0.07	0.35	0.16	0.39	0.05	0.10	0.001	0.001
needleleaf deciduous tree	0.01	0.07	0.35	0.16	0.39	0.05	0.10	0.001	0.001
broadleaf evergreen tree	0.10	0.10	0.45	0.16	0.39	0.05	0.25	0.001	0.001
broadleaf deciduous tree	0.25	0.10	0.45	0.16	0.39	0.05	0.25	0.001	0.001
tropical seasonal tree	0.01	0.10	0.45	0.16	0.39	0.05	0.25	0.001	0.001
C_3 grass	-0.30	0.11	0.58	0.36	0.58	0.07	0.25	0.220	0.380
evergreen shrub	0.01	0.07	0.35	0.16	0.39	0.05	0.10	0.001	0.001
deciduous shrub	0.25	0.10	0.45	0.16	0.39	0.05	0.25	0.001	0.001
arctic deciduous shrub	0.25	0.10	0.45	0.16	0.39	0.05	0.25	0.001	0.001
arctic grass	-0.30	0.11	0.58	0.36	0.58	0.07	0.25	0.220	0.380
crop	-0.30	0.11	0.58	0.36	0.58	0.07	0.25	0.220	0.380
C_4 grass	-0.30	0.11	0.58	0.36	0.58	0.07	0.25	0.220	0.380

Table 9. Intercepted snow optical properties

	Waveband	
Parameter	vis	nir
$\omega^{\rm sno}$	0.8	0.4
$\beta^{\rm sno}$	0.5	0.5
$\beta_0^{\rm sno}$	0.5	0.5

Figure 5. Direct and diffuse albedos for visible and near-infrared wavebands as a function of cosine solar zenith angle and for leaf area indices of 0, 1, 2, 4, and 6. Data are for semi-horizontal broadleaf evergreen tree leaves ($\chi_L = 0.6$) with soil albedos $\alpha^{\mu}_{g\ \mathrm{vis}} = \alpha_{g\ \mathrm{vis}} = 0.10$ and $\alpha^{\mu}_{g\ \mathrm{nir}} = \alpha_{g\ \mathrm{nir}} = 0.20$.

Figure 6. As in Figure 5, but for random ($\chi_L = 0$) leaves.

Figure 7. As in Figure 5, but for semi-vertical ($\chi_L = -0.4$) leaves.

Figure 8. Direct and diffuse albedos for visible and near-infrared wavebands as a function of leaf area index. Data are for random leaves, with the same optical properties as in Figure 6, and $\mu = 0.71$. The ground albedos are typical of snow $\alpha^{\mu}_{g\ \mathrm{vis}} = \alpha_{g\ \mathrm{vis}} = 0.95$ and $\alpha^{\mu}_{g\ \mathrm{nir}} = \alpha_{g\ \mathrm{nir}} = 0.70$. Optical properties of snow (Table 9) are used when the canopy is wet ($f_{\mathrm{wet}} = 1$).

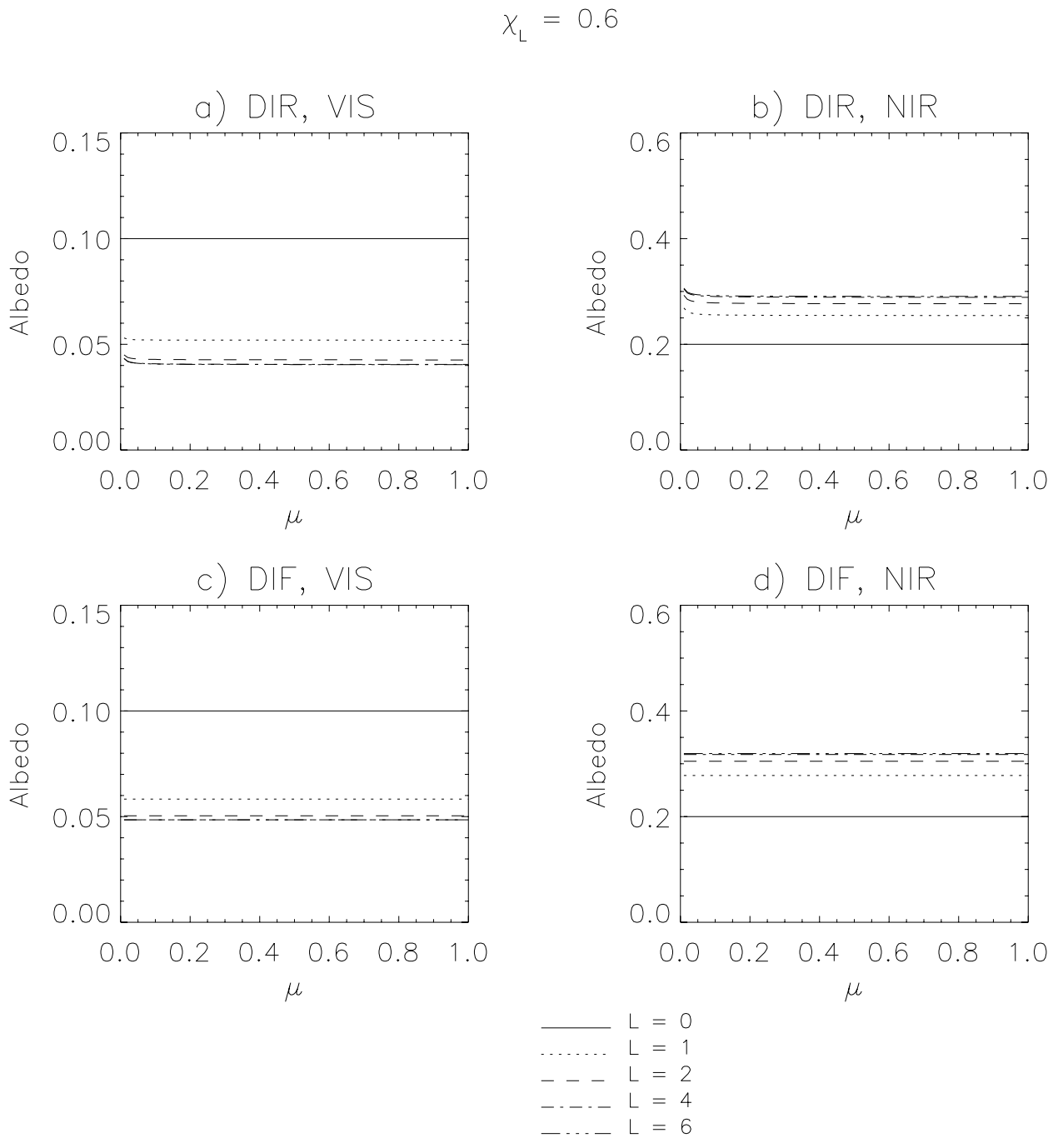
χ_L = 0.6
a) DIR, VIS
b) DIR, NIR
c) DIF, VIS
d) DIF, NIR
Albedo
μ
0.0
0.2
0.4
0.6
0.8
1.0
0.00
0.05
0.10
0.15
0.0
0.2
0.4
0.6
L = 0
L = 1
L = 2
L = 4
L = 6

Figure 5

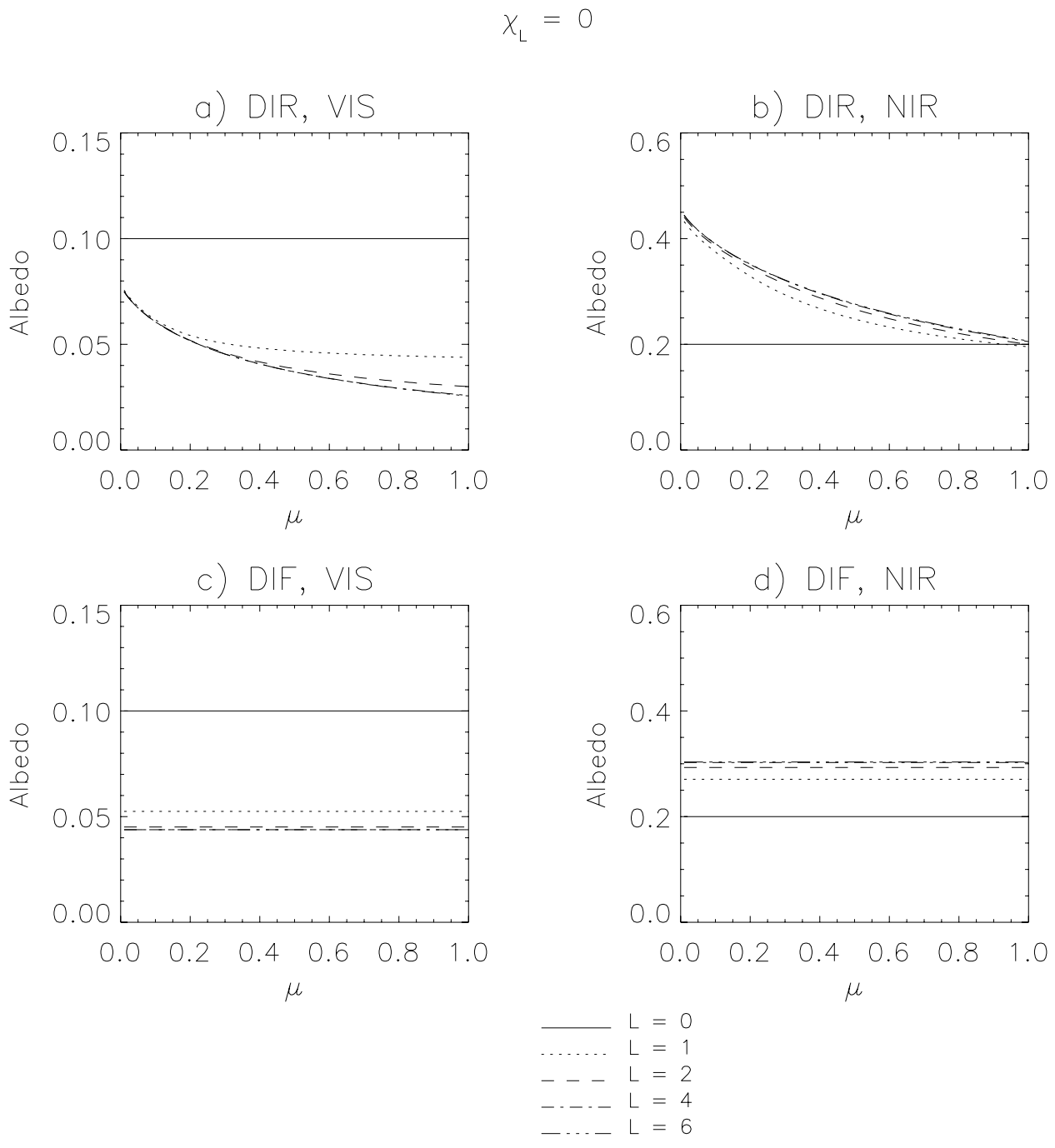
$\chi_L = 0$
a) DIR, VIS
b) DIR, NIR
c) DIF, VIS
d) DIF, NIR
Albedo
μ
0.00
0.05
0.10
0.15
0.0
0.2
0.4
0.6
0.8
1.0
L = 0
L = 1
L = 2
L = 4
L = 6

Figure 6

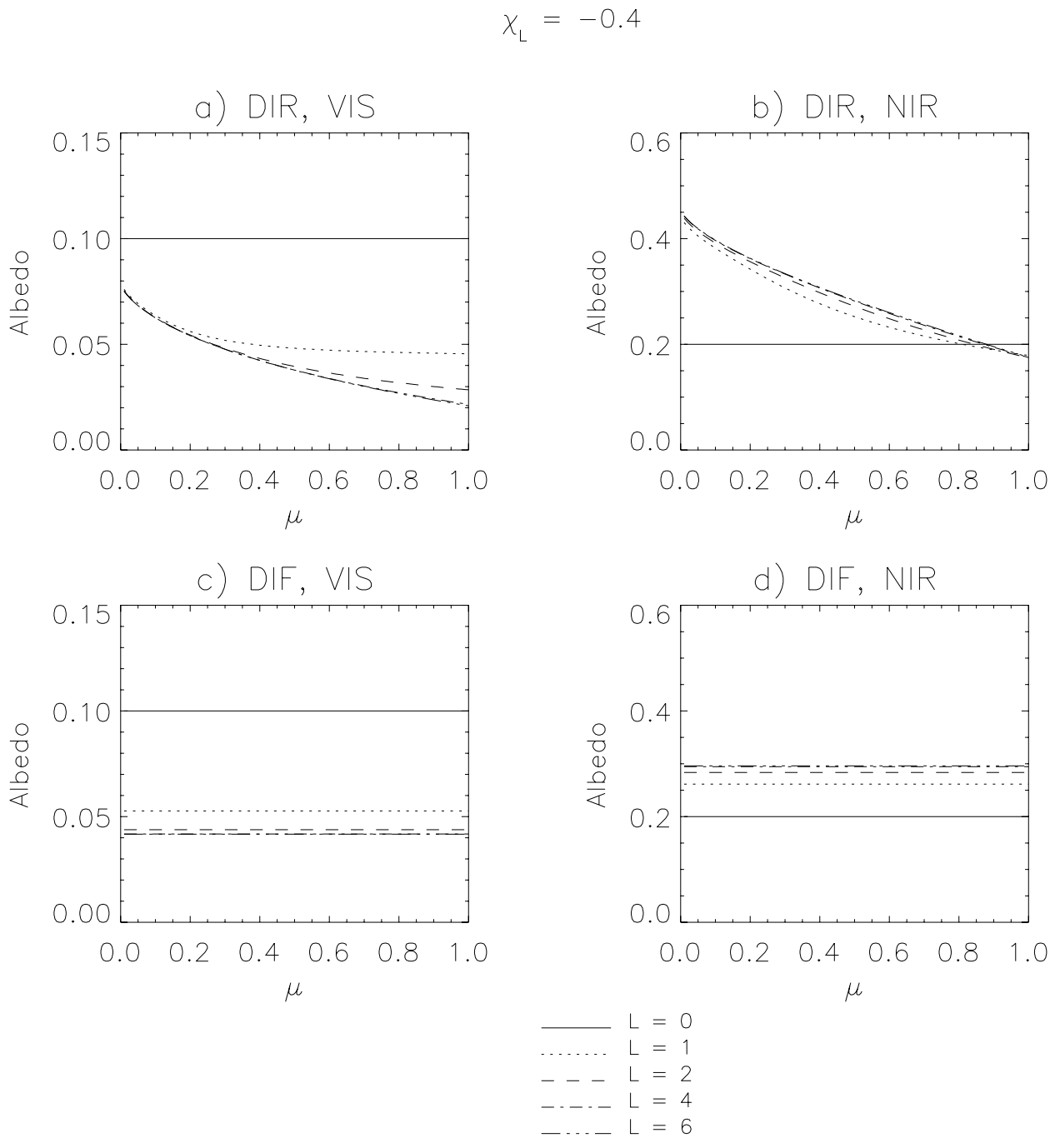
$\chi_L = -0.4$
a) DIR, VIS
b) DIR, NIR
c) DIF, VIS
d) DIF, NIR
Albedo
μ
0.00
0.05
0.10
0.15
0.0
0.2
0.4
0.6
0.8
1.0
L = 0
L = 1
L = 2
L = 4
L = 6

Figure 7

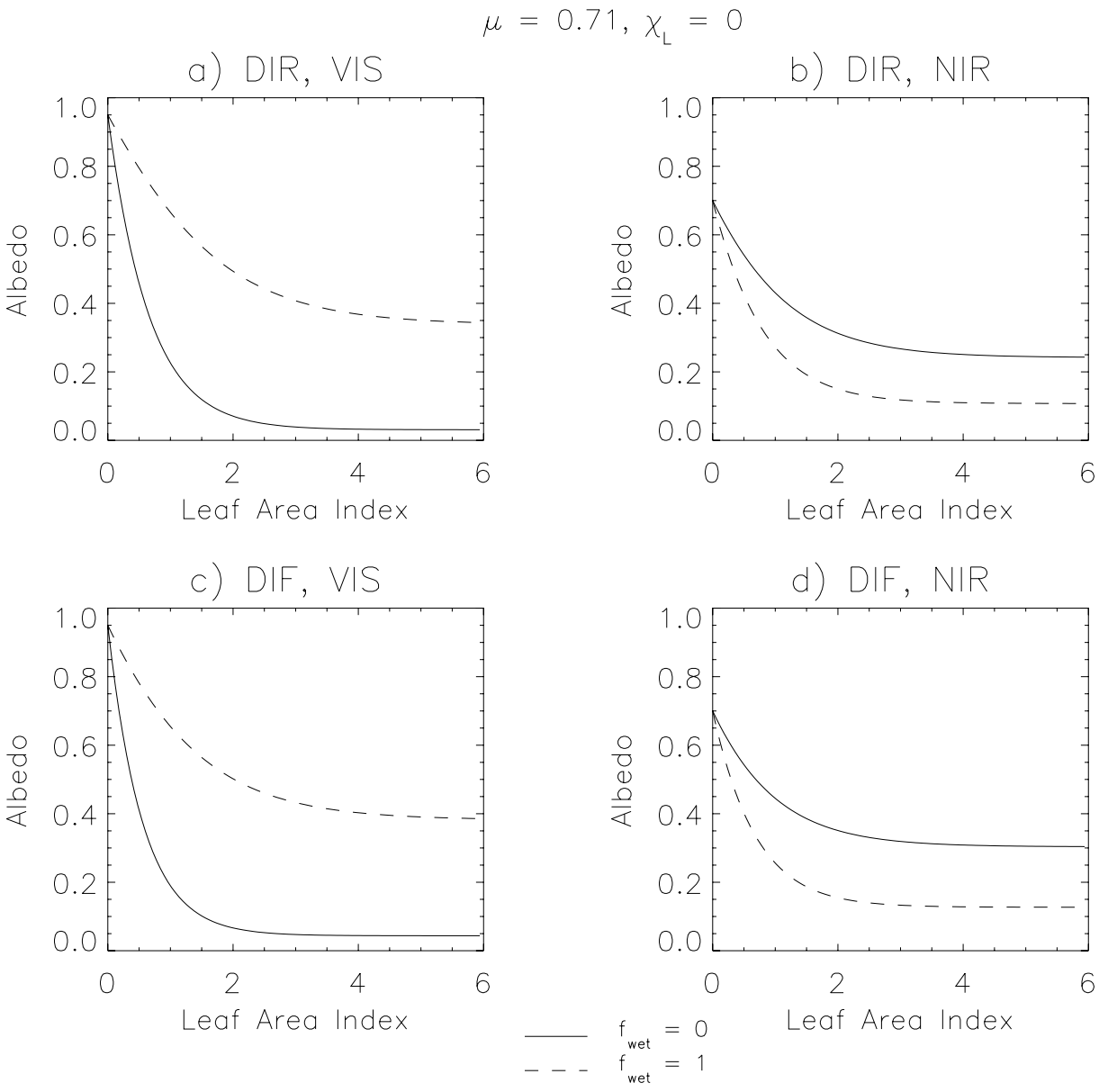
μ = 0.71, χL = 0
a) DIR, VIS
b) DIR, NIR
c) DIF, VIS
d) DIF, NIR
Albedo
Leaf Area Index
1.0
0.8
0.6
0.4
0.2
0.0
0
2
4
6
fwet = 0
fwet = 1

Figure 8

2.2 Ground Albedos

The overall direct beam $\alpha^{\mu}_{g\Lambda}$ and diffuse $\alpha_{g\Lambda}$ ground albedos are weighted combinations of "soil" and snow albedos

$$\alpha^{\mu}_{g\Lambda} = \alpha^{\mu}_{\mathrm{soi}\,\Lambda}(1 - f_{\mathrm{sno}}) + \alpha^{\mu}_{\mathrm{sno}\,\Lambda} f_{\mathrm{sno}}$$

$$\alpha_{g\Lambda} = \alpha_{\mathrm{soi}\,\Lambda}(1 - f_{\mathrm{sno}}) + \alpha_{\mathrm{sno}\,\Lambda} f_{\mathrm{sno}}$$

where f_{sno} is the fraction of the ground covered with snow (section 8.2).

$\alpha^{\mu}_{\mathrm{soi}\,\Lambda}$ and $\alpha_{\mathrm{soi}\,\Lambda}$ vary with glacier, lake, wetland, and soil surfaces. Glacier albedos are similar to BATS (Dickinson et al. 1993),

$$\alpha^{\mu}_{\mathrm{soi\ vis}} = \alpha_{\mathrm{soi\ vis}} = 0.80$$

$$\alpha^{\mu}_{\mathrm{soi\ nir}} = \alpha_{\mathrm{soi\ nir}} = 0.55\ .$$

Lake and wetland albedos depend on cosine solar zenith angle μ, based on data in Henderson-Sellers (1986) and Monteith and Unsworth (1990),

$$\alpha^{\mu}_{\mathrm{soi\ vis}} = \alpha^{\mu}_{\mathrm{soi\ nir}} = 0.06(\mu^{1.7} + 0.15)^{-1}$$

$$\alpha_{\mathrm{soi\ vis}} = \alpha_{\mathrm{soi\ nir}} = 0.06\ .$$

Frozen lake and wetland albedos are based on sea ice values used in BATS (Dickinson et al. 1993)

$$\alpha^{\mu}_{\mathrm{soi\ vis}} = \alpha_{\mathrm{soi\ vis}} = 0.60$$

$$\alpha^{\mu}_{\mathrm{soi\ nir}} = \alpha_{\mathrm{soi\ nir}} = 0.40\ .$$

As in BATS (Dickinson et al. 1993), soil albedos vary with color class

$$\alpha^{\mu}_{\mathrm{soi}\,\Lambda} = \alpha_{\mathrm{soi}\,\Lambda} = \alpha_{\mathrm{sat}\,\Lambda} + \Delta \leq \alpha_{\mathrm{dry}\,\Lambda}$$

where Δ depends on the volumetric water content of the first soil layer (section 8.4) as $\Delta = 0.11 - 0.40\theta_1 > 0$, and $\alpha_{\mathrm{sat}\,\Lambda}$ and $\alpha_{\mathrm{dry}\,\Lambda}$ are albedos for saturated and dry soil color classes (Table 10). The first eight color classes are as in BATS (Dickinson et al. 1993). The ninth class is a special class created to better match ERBE clear-sky albedos for desert and semi-desert surface types located in North Africa and the Arabian Peninsula. For this color class, albedos are also increased by 0.10.

Soil albedos as a function of soil water and lake albedos as a function of zenith angle are illustrated in Figure 9.

Table 10. Dry and saturated soil albedos

	Dry		Saturated	
Color Class	vis	nir	vis	nir
1 = light	0.24	0.48	0.12	0.24
2	0.22	0.44	0.11	0.22
3	0.20	0.40	0.10	0.20
4	0.18	0.36	0.09	0.18
5	0.16	0.32	0.08	0.16
6	0.14	0.28	0.07	0.14
7	0.12	0.24	0.06	0.12
8 = dark	0.10	0.20	0.05	0.10
9	0.27	0.55	0.15	0.31

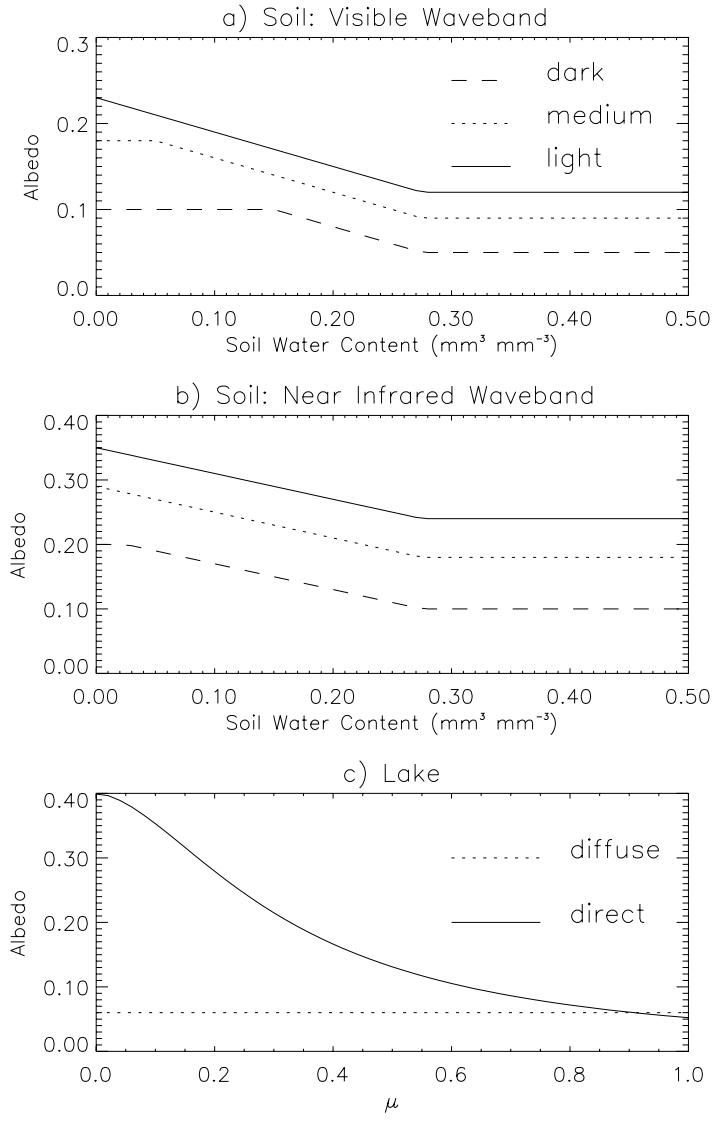
a) Soil: Visible Waveband
dark
medium
light
Albedo
0.0
0.1
0.2
0.3
0.00
0.10
0.20
0.30
0.40
0.50
Soil Water Content (mm³ mm⁻³)
b) Soil: Near Infrared Waveband
Albedo
0.00
0.10
0.20
0.30
0.40
0.00
0.10
0.20
0.30
0.40
0.50
Soil Water Content (mm³ mm⁻³)
c) Lake
diffuse
direct
Albedo
0.00
0.10
0.20
0.30
0.40
0.0
0.2
0.4
0.6
0.8
1.0
μ

Figure 9

Figure 9. a) Visible waveband soil albedos for light, medium, and dark soils as a function of soil water. b) Near-infrared waveband soil albedos for light, medium, and dark soils as a function of soil water. c) Unfrozen lake albedos as a function of zenith angle.

Snow albedos are based on the work of Marshall (1989). For soot content s (mass fraction) $< s_\Lambda^2$,

$$a_\Lambda(\mu) = a_\Lambda^h - (a_\Lambda^h - a_\Lambda^m)\exp\left[-k_\Lambda^{h1}\ln\left(\frac{s_\Lambda^2}{s}\right) + k_\Lambda^{h2}\left[\ln\left(\frac{s_\Lambda^2}{s}\right)\right]^2\right] \leq a_\Lambda^h$$

and for $s \geq s_\Lambda^2$,

$$a_\Lambda(\mu) = a_\Lambda^l + (a_\Lambda^m - a_\Lambda^l)\exp\left[-k_\Lambda^l\ln\left(\frac{s}{s_\Lambda^2}\right)\right] \geq a_\Lambda^l \ .$$

For direct beam radiation, $\alpha_{\mathrm{sno}\,\Lambda}^{\mu} = a_\Lambda(\mu)$ and for diffuse radiation $\alpha_{\mathrm{sno}\,\Lambda} = a_\Lambda(\mu = 0.65)$.

$a_\Lambda^m = 0.5(a_\Lambda^h + a_\Lambda^l)$ and a_Λ^l, k_Λ^l, k_Λ^{h1}, and k_Λ^{h2} are empirical parameters that vary with wavelength (Table 11).

$$s_\Lambda^2 = \exp\left(e_\Lambda + f_\Lambda\ln\sqrt{r_{e\,\Lambda}}\right)$$

where e_Λ and f_Λ are empirical constants (Table 11). $r_{e\,\Lambda}$ is an effective snow grain radius (μm), which adjusts snow albedos for zenith angle

$$r_{e\,\Lambda} = r\left(1 + \frac{\Delta\mu}{b_\Lambda}\right)^2$$

where b_Λ is an empirical constant (Table 11) and $\Delta\mu = \mu - 0.65$. Marshall (1989) lists typical values of snow grain radius r as: 50 μm for new snow, 100 μm for snow a few days old (or for Antarctica), 200 μm for cold snow, and 500 to 1000 μm for old

or melting snow. Rather than accounting for snow aging, she gives a simple snow grain radius parameterization that accounts for changes in albedo when melting

$$r = \left\{ \begin{array}{c} 80 \text{ for } T_a < 263.15 \\ e^{4.38+0.23(T_a-263.15)} \text{ for } 263.15 \leq T_a \leq 274.15 \\ 1000 \text{ for } T_a > 274.15 \end{array} \right\}$$

where T_a is the surface "aerodynamic" temperature (K) (section 4.1).

$$a^h_\Lambda = c^1_\Lambda + c^2_\Lambda \sqrt{r_{e\,\Lambda}} + c^3_\Lambda \ln(\sqrt{r_{e\,\Lambda}})$$

where c^1_Λ, c^2_Λ, and c^3_Λ are empirical constants (Table 11). Snow albedos in relation to grain radius, soot content, and zenith angle are illustrated in Figures 10 and 11. Snow albedos decrease as the the solar elevation angle (and μ) increases, the soot content increases, and the snow grain radius increases.

Figure 10. Snow albedos. a) As a function of zenith angle for snow grain radius of 80 and 1000 μm and with $s = 10^{-10}$. b) As in (a) but with $s = 10^{-6}$. c) As a function of soot for $\mu = 0.2$. d) As in (c) but for $\mu = 0.8$.

Figure 11. Snow albedos for snow grain radius of 80 and 1000 μm as a function of soot for $\mu = 0.65$.

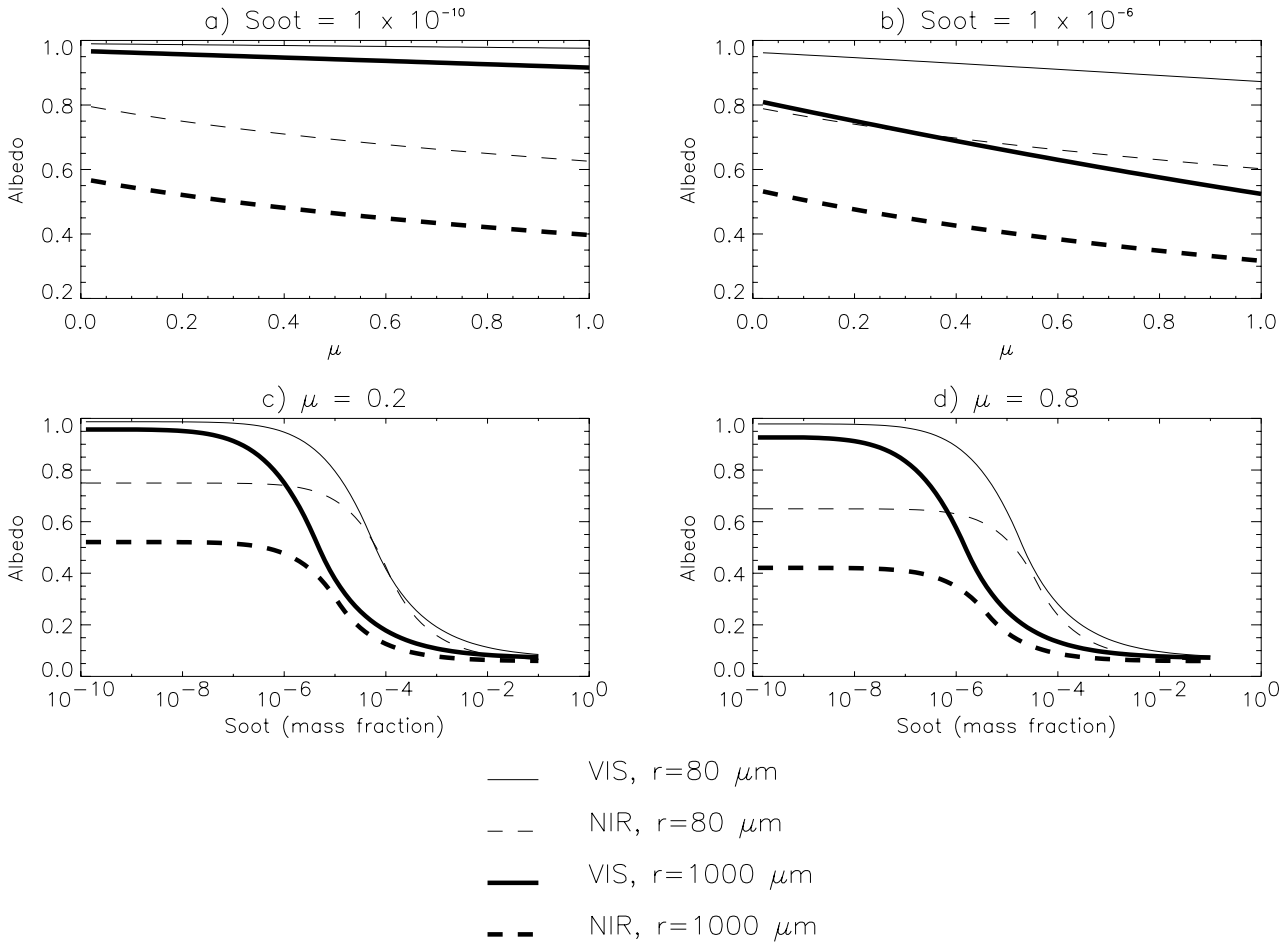
a) Soot = 1 x 10^-10
b) Soot = 1 x 10^-6
c) μ = 0.2
d) μ = 0.8
Albedo
μ
Soot (mass fraction)
VIS, r=80 μm
NIR, r=80 μm
VIS, r=1000 μm
NIR, r=1000 μm

Figure 10

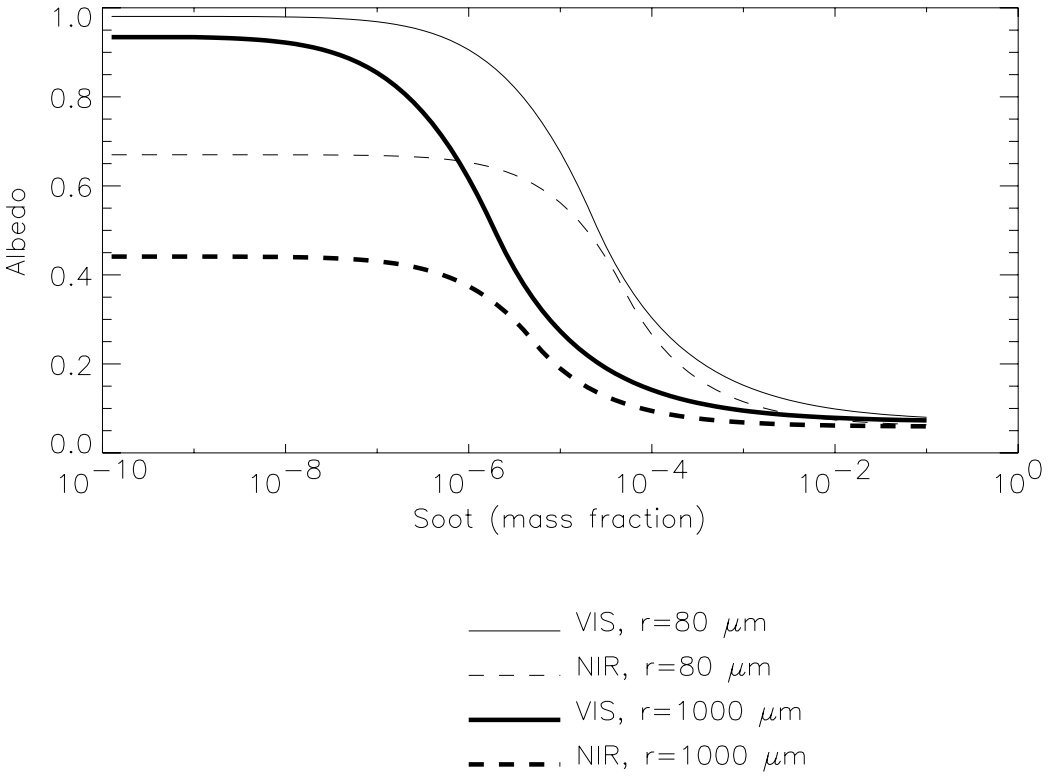
1.0
0.8
0.6
0.4
0.2
0.0
Albedo
10^{-10}
10^{-8}
10^{-6}
10^{-4}
10^{-2}
10^{0}
Soot (mass fraction)
VIS, r=80 μm
NIR, r=80 μm
VIS, r=1000 μm
NIR, r=1000 μm

Figure 11

Table 11. Snow albedo parameters

	Waveband	
Parameter	vis	nir
a^l	0.070	0.059
b	1.2812	1.2642
c^1	0.9988	1.0667
c^2	-0.0020	0
c^3	0	-0.1811
e	-6.3550	-5.9328
f	-1.9752	-1.8102
k^{h1}	0.450	0.580
k^{h2}	-0.040	-0.040
k^l	0.454	0.567

2.3 Solar Zenith Angle

The cosine of the solar zenith is

$$\mu = \sin\phi \sin\delta + \cos\phi \cos\delta \cos h$$

where ϕ is latitude (positive in the Northern Hemisphere), δ is the solar declination, and h is the solar hour angle (24 hour periodicity). The solar declination (radians) depends on the calendar day d

$$\begin{aligned}\delta = 0.006918 &- 0.399912\cos\Theta + 0.070257\sin\Theta \\ &- 0.006758\cos 2\Theta + 0.000907\sin 2\Theta \\ &- 0.002697\cos 3\Theta + 0.001480\sin 3\Theta\end{aligned}$$

where $\Theta = 2\pi\frac{d}{365}$. The solar hour angle (radians) is 15^o for every hour from local noon

$$h = \frac{360}{24}(t-12)\frac{\pi}{180} \ .$$

The local time t (hours) at longitude θ (radians, positive east of the Greenwich meridian) is obtained by adjusting m, the current seconds in the day at Greenwich, by 1 hour for every 15^o of longitude

$$t = \frac{m + \frac{\theta}{2\pi}86400}{3600} \ .$$

This calculation of μ, which depends on latitude, longitude, and Greenwich time, matches the algorithm used in the NCAR CCM2 to within ± 0.0001.

3. Radiative Fluxes

The net radiation at the surface is $(\overrightarrow{S}_v + \overrightarrow{S}_g) + (\overrightarrow{L}_v + \overrightarrow{L}_g)$ where $\overrightarrow{S}$ and $\overrightarrow{L}$ are the net solar and longwave fluxes absorbed by vegetation ("v") and the ground ("g"). The solar radiation absorbed by vegetation is partitioned into $\phi^{\rm sun}$ and $\phi^{\rm sha}$, the visible waveband solar radiation absorbed by sunlit and shaded leaves, for the stomatal resistance and photosynthesis calculations.

3.1 Solar Fluxes

With reference to Figure 12, the direct beam flux transmitted through the canopy, per unit incident flux, is $e^{-K(L+S)}$, and the direct beam and diffuse fluxes absorbed by the vegetation, per unit incident flux, are

$$\overrightarrow{I}^{\mu}_{\Lambda} = 1 - I\uparrow^{\mu}_{\Lambda} - (1-\alpha_{g\Lambda})I\downarrow^{\mu}_{\Lambda} - (1-\alpha^{\mu}_{g\Lambda})e^{-K(L+S)}$$

$$\overrightarrow{I}_{\Lambda} = 1 - I\uparrow_{\Lambda} - (1-\alpha_{g\Lambda})I\downarrow_{\Lambda} \quad .$$

$I\uparrow^{\mu}_{\Lambda}$ and $I\uparrow_{\Lambda}$ are the upward diffuse fluxes per unit incident direct beam and diffuse flux (section 2.1). $I\downarrow^{\mu}_{\Lambda}$ and $I\downarrow_{\Lambda}$ are the downward diffuse fluxes per unit incident direct beam and diffuse radiation (section 2.1). $\alpha^{\mu}_{g\Lambda}$ and $\alpha_{g\Lambda}$ are the direct beam and diffuse ground albedos (section 2.2).

The total solar radiation absorbed by the vegetation and ground are

$$\overrightarrow{S}_v = \sum_{\Lambda} S_{\rm atm}\downarrow^{\mu}_{\Lambda}\ \overrightarrow{I}^{\mu}_{\Lambda} + S_{\rm atm}\downarrow_{\Lambda}\ \overrightarrow{I}_{\Lambda}$$

$$\overrightarrow{S}_g = \sum_{\Lambda} S_{\rm atm}\downarrow^{\mu}_{\Lambda} e^{-K(L+S)}(1-\alpha^{\mu}_{g\Lambda}) +$$
$$(S_{\rm atm}\downarrow^{\mu}_{\Lambda} I\downarrow^{\mu}_{\Lambda} + S_{\rm atm}\downarrow_{\Lambda} I\downarrow_{\Lambda})(1-\alpha_{g\Lambda}) \ .$$

$S_{\rm atm}\downarrow^{\mu}_{\Lambda}$ and $S_{\rm atm}\downarrow_{\Lambda}$ are the incident direct beam and diffuse solar fluxes (W m^{-2}). The fraction of incident radiation absorbed by semi-horizontal, random, and semi-vertical leaves is shown in Figure 13. With a zenith angle of 45^o, 90% of the

Figure 12. Schematic diagram of direct beam solar radiation (top left), diffuse solar radiation (top right), and longwave radiation (bottom) absorbed, transmitted, and reflected by vegetation and the ground.

Figure 13. Fraction of incident direct and diffuse radiation absorbed by the canopy for visible and near-infrared wavebands as a function of leaf area index. Data are for semi-horizontal, random, and semi-vertical broadleaf evergreen tree leaves with $\mu = 0.71$ and soil albedos $\alpha^{\mu}_{g\,\mathrm{vis}} = \alpha_{g\,\mathrm{vis}} = 0.10$ and $\alpha^{\mu}_{g\,\mathrm{nir}} = \alpha_{g\,\mathrm{nir}} = 0.20$.

visible radiation is absorbed with leaf area index of 3 to 4. Absorption saturates at 95% with leaf area index equal to 6. In contrast, a maximum of only 60 to 70% of the near-infrared radiation is absorbed by the vegetation. Solar radiation is conserved as

$$\sum_{\Lambda} (S_{\mathrm{atm}} \downarrow^{\mu}_{\Lambda} + S_{\mathrm{atm}} \downarrow_{\Lambda}) = (\overrightarrow{S}_v + \overrightarrow{S}_g) + \sum_{\Lambda} (S_{\mathrm{atm}} \downarrow^{\mu}_{\Lambda} I \uparrow^{\mu}_{\Lambda} + S_{\mathrm{atm}} \downarrow_{\Lambda} I \uparrow_{\Lambda})$$

where the latter term is the reflected solar radiation. The visible and near-infrared reflectances are used to calculate the normalized difference vegetation index, at the surface, as $\frac{r_{\mathrm{nir}} - r_{\mathrm{vis}}}{r_{\mathrm{vis}} + r_{\mathrm{nir}}}$.

Photosynthesis and transpiration depend non-linearly on solar radiation, via the light response of stomata. A common way to integrate CO_2 and H_2O fluxes for the canopy is to divide the canopy into sunlit and shaded leaves (Campbell 1977, Landsberg 1986). The sunlit fraction of the canopy is

$$f_{\mathrm{sun}} = \frac{\int_0^{L+S} e^{-Kx} dx}{L+S} = \frac{1 - e^{-K(L+S)}}{K(L+S)}$$

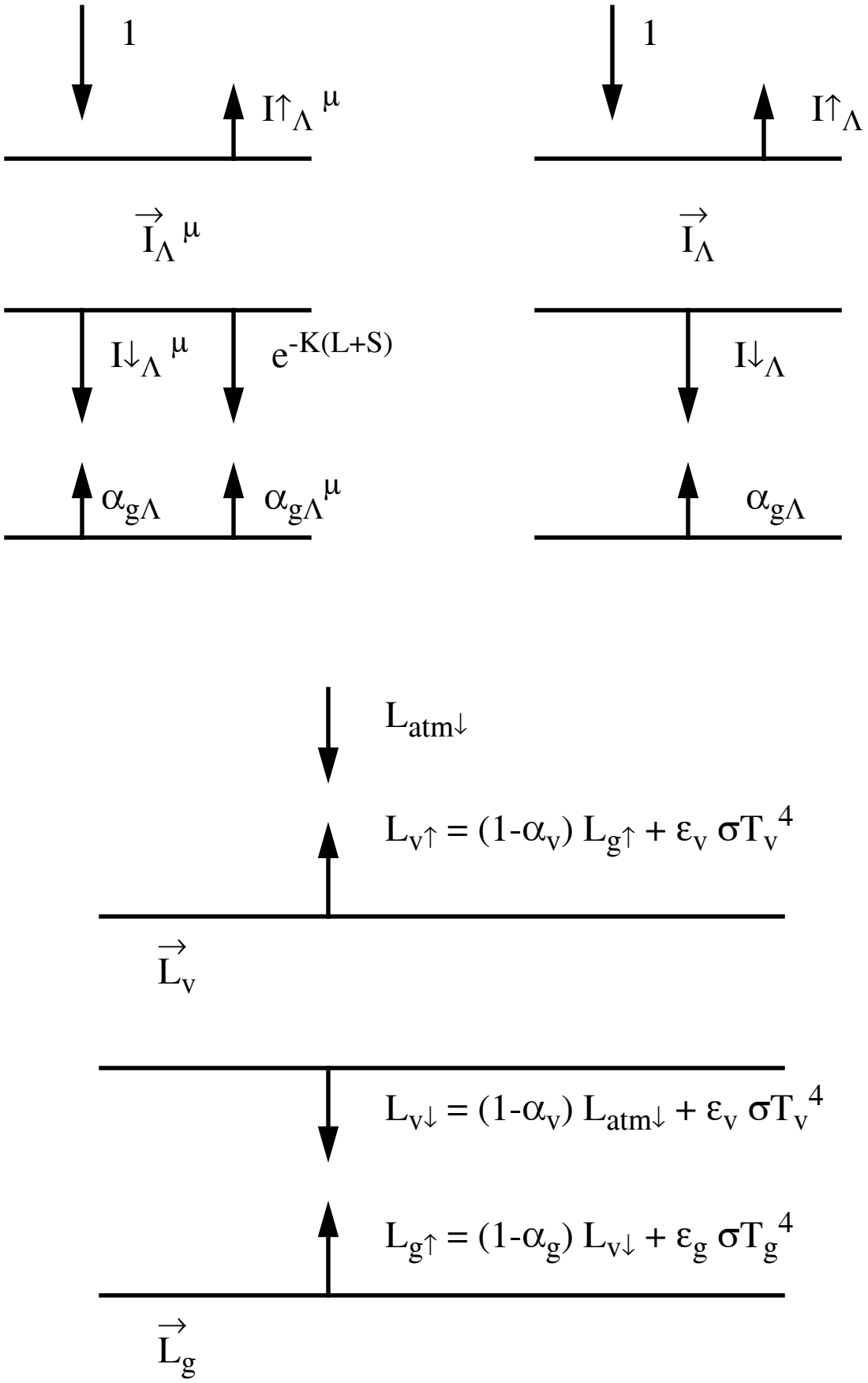
1
$I\uparrow_\Lambda{}^\mu$
$\vec{I}_\Lambda{}^\mu$
$I\downarrow_\Lambda{}^\mu$
$e^{-K(L+S)}$
$\alpha_{g\Lambda}$
$\alpha_{g\Lambda}{}^\mu$
1
$I\uparrow_\Lambda$
$\vec{I}_\Lambda$
$I\downarrow_\Lambda$
$\alpha_{g\Lambda}$
$L_{atm\downarrow}$
$L_{v\uparrow} = (1-\alpha_v)\, L_{g\uparrow} + \varepsilon_v\, \sigma T_v{}^4$
$\vec{L}_v$
$L_{v\downarrow} = (1-\alpha_v)\, L_{atm\downarrow} + \varepsilon_v\, \sigma T_v{}^4$
$L_{g\uparrow} = (1-\alpha_g)\, L_{v\downarrow} + \varepsilon_g\, \sigma T_g{}^4$
$\vec{L}_g$

Figure 12

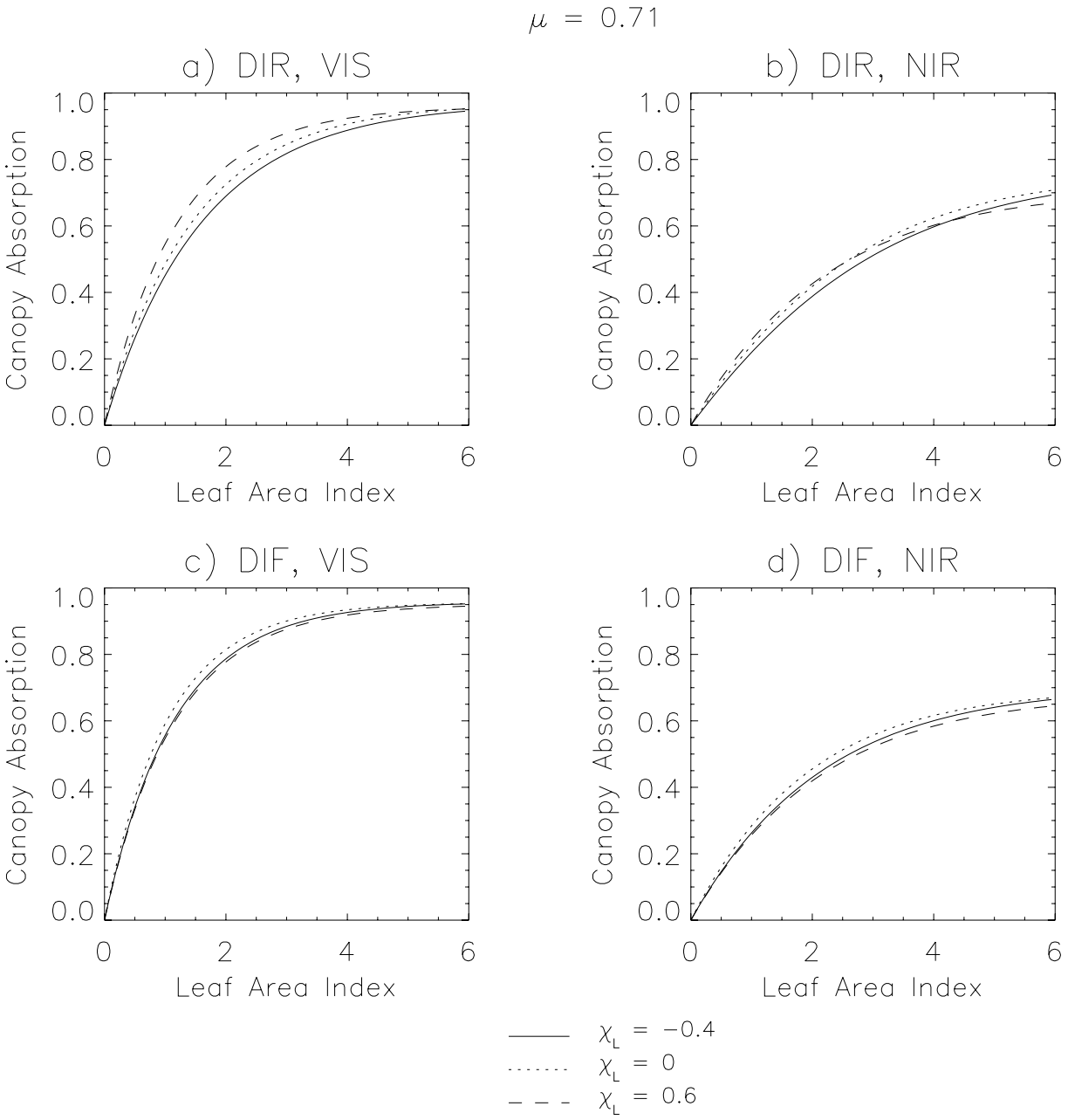
μ = 0.71
a) DIR, VIS
b) DIR, NIR
c) DIF, VIS
d) DIF, NIR
Canopy Absorption
Leaf Area Index
0.0
0.2
0.4
0.6
0.8
1.0
0
2
4
6
χ_L = −0.4
χ_L = 0
χ_L = 0.6

Figure 13

where $e^{-K(L+S)}$ is the fractional area of sunflecks on a horizontal plane below the leaf and stem area index $L+S$ (section 1.3). The shaded fraction is $f_{\rm sha} = 1 - f_{\rm sun}$, and the sunlit and shaded leaf areas indices are $L^{\rm sun} = f_{\rm sun} L$ and $L^{\rm sha} = f_{\rm sha} L$. In calculating $f_{\rm sun}$, $K = \frac{G(\mu)}{\mu}\sqrt{1-\omega_{\rm vis}^{\rm veg}}$, where $\sqrt{1-\omega_{\rm vis}^{\rm veg}}$ accounts for scattering within the canopy (Sellers 1985). To prevent numerical instabilities, $f_{\rm sun} = 0$ when the sunlit fraction is less than 1%.

The sunlit leaf area is illustrated in Figure 14 for horizontal $G(\mu) = \mu$, random $G(\mu) = 0.5$, and vertical $G(\mu) = \frac{2}{\pi}\sqrt{1-\mu^2}$ leaves. Horizontal leaves do not have a zenith angle dependence to sunlit leaf area; the sunlit fraction of random and vertical leaves increases as solar elevation angle (and μ) increase (Figure 14a, 14c). For low solar elevation angles ($\mu = 0.34$), sunlit leaf area saturates at low leaf area (Figure 14d). With higher sun angles ($\mu = 0.87$), more leaf area is illuminated in the vertical and random canopies (Figure 14b).

The solar radiation absorbed by the vegetation in the visible waveband ($< 0.7\mu$m) is partitioned to sunlit and shaded leaves to calculate the average absorbed photosynthetically active radiation for sunlit and shaded leaves. For $f_{\rm sun} > 0$

$$\phi^{\rm sun} = \frac{(S_{\rm atm}\downarrow_{\rm vis}^{\mu} \overrightarrow{I}_{\rm vis}^{\mu} + f_{\rm sun} S_{\rm atm}\downarrow_{\rm vis} \overrightarrow{I}_{\rm vis})\frac{L}{L+S}}{L^{\rm sun}}$$

$$\phi^{\rm sha} = \frac{(f_{\rm sha} S_{\rm atm}\downarrow_{\rm vis} \overrightarrow{I}_{\rm vis})\frac{L}{L+S}}{L^{\rm sha}} .$$

Figure 14. Sunlit leaf area of a broadleaf evergreen tree canopy with horizontal, random, and vertical leaves. a) Sunlit fraction as a function of cosine zenith angle for L=6. b) Sunlit leaf area as a function of leaf area index for $\mu = 0.87$. c) As in (a) but for L=2. d) As in (b) but for $\mu = 0.34$.

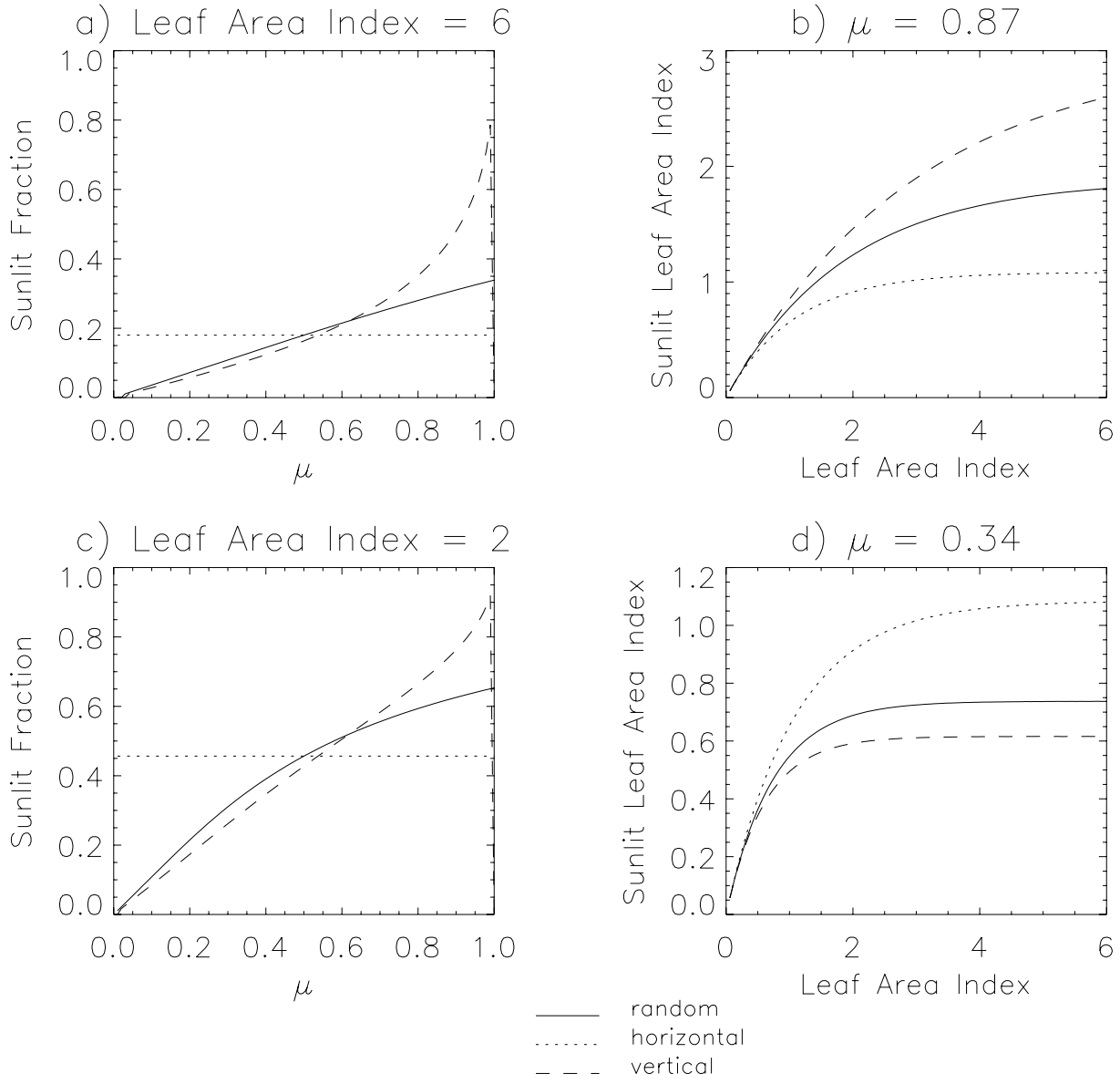
a) Leaf Area Index = 6
Sunlit Fraction
1.0
0.8
0.6
0.4
0.2
0.0
0.0 0.2 0.4 0.6 0.8 1.0
μ
b) μ = 0.87
Sunlit Leaf Area Index
3
2
1
0
0 2 4 6
Leaf Area Index
c) Leaf Area Index = 2
Sunlit Fraction
1.0
0.8
0.6
0.4
0.2
0.0
0.0 0.2 0.4 0.6 0.8 1.0
μ
d) μ = 0.34
Sunlit Leaf Area Index
1.2
1.0
0.8
0.6
0.4
0.2
0.0
0 2 4 6
Leaf Area Index
random
horizontal
vertical

Figure 14

These equations assume the sunlit leaves absorb the direct beam radiation, that all leaves absorb diffuse radiation, and that leaves absorb $\frac{L}{L+S}$ of the radiation absorbed by the vegetation. Although more complicated models of sunlit and shaded leaf radiation are available (Campbell 1977, Landsberg 1986), e.g., the leaf area illuminated by diffuse radiation could be found by integrating L^{sun} with respect to μ, the above equations are a reasonable approximation. If $f_{\text{sun}} = 0$, all the radiation is absorbed by the shaded leaves. This special condition is needed because $f_{\text{sun}} = 0$ if less than 1% of the canopy is sunlit, in which case direct beam radiation that would otherwise be absorbed by the sunlit canopy needs to be included in the shaded fraction.

3.2 Longwave Fluxes

The net longwave radiation (W m^{-2}) [positive towards the atmosphere] at the surface is

$$\overrightarrow{L} = -L_{\text{atm}} \downarrow + L \uparrow$$

where $L_{\text{atm}} \downarrow$ is the downward atmospheric longwave radiation and $L \uparrow$ is the upward longwave radiation (W m^{-2}). The radiative temperature is defined from the upward longwave flux as

$$T_{\text{rad}} = \left(\frac{L \uparrow}{\sigma} \right)^{1/4}$$

where σ is the Stefan-Boltzmann constant (W m^{-2} K^{-4}) (Table 4).

For non-vegetated surfaces,

$$\overrightarrow{L} = -\alpha_g L_{\text{atm}} \downarrow + \epsilon_g \sigma T_g^4$$

where α_g is the ground absorptivity, ϵ_g is the ground emissivity, and T_g is the ground temperature (K) (section 5). The upward longwave radiation is

$$L\uparrow = (1-\alpha_g)L_{\rm atm}\downarrow + \epsilon_g\sigma T_g^4 \ .$$

These equations allow for emissivity less than one, assuming absorptivity equals emissivity and $1-\alpha_g$ is reflected by the ground.

The net longwave radiation flux for vegetated surfaces is

$$\overrightarrow{L} = \overrightarrow{L}_v + \overrightarrow{L}_g$$

where, with reference to Figure 12, the net radiation fluxes for vegetation and ground (positive towards the atmosphere) are

$$\begin{aligned}
\overrightarrow{L}_v &= -\alpha_v(L_{\rm atm}\downarrow + L_g\uparrow) + 2\epsilon_v\sigma T_v^4 \\
&= -\alpha_v[1+(1-\alpha_v)(1-\alpha_g)]L_{\rm atm}\downarrow - \alpha_v\epsilon_g\sigma T_g^4 + \epsilon_v\sigma[2-\alpha_v(1-\alpha_g)]T_v^4 \\
\overrightarrow{L}_g &= -\alpha_g L_v\downarrow + \epsilon_g\sigma T_g^4 \\
&= -\alpha_g(1-\alpha_v)L_{\rm atm}\downarrow - \alpha_g\epsilon_v\sigma T_v^4 + \epsilon_g\sigma T_g^4 \ .
\end{aligned}$$

T_v and T_g are the vegetation and ground temperatures (K) (section 5), ϵ_v and ϵ_g are the vegetation and ground emissivities, and α_v and α_g are the vegetation and ground absorptivities. The downward longwave radiation below the vegetation canopy is

$$L_v\downarrow = (1-\alpha_v)L_{\rm atm}\downarrow + \epsilon_v\sigma T_v^4 \ .$$

The upward longwave radiation from the ground is

$$L_g\uparrow = (1-\alpha_g)L_v\downarrow + \epsilon_g\sigma T_g^4 \ .$$

The upward longwave radiation above the vegetation canopy is

$$L\uparrow = (1-\alpha_v)L_g\uparrow + \epsilon_v\sigma T_v^4 \ .$$

These equations allow for emissivities less than one, assuming absorptivity equals emissivity, $1-\alpha_v$ is transmitted through the canopy, and $1-\alpha_g$ is reflected by the ground.

The emissivity of the ground is $\epsilon_g = \epsilon_{\rm soi}(1-f_{\rm sno}) + \epsilon_{\rm sno} f_{\rm sno}$, where $f_{\rm sno}$ is the fraction of the ground covered by snow (section 8.2), $\epsilon_{\rm sno} = 0.97$ is the emissivity of snow, and $\epsilon_{\rm soi}$ equals 0.96 for soil, 0.97 for glaciers, 0.97 for lakes, and 0.96 for wetlands. The vegetation emissivity is $\epsilon_v = 1 - e^{-(L+S)/\bar{\mu}}$ where L and S are the one-sided leaf and stem area indices (section 1.3) and $\bar{\mu} = 1$ is the average inverse optical depth for longwave radiation.

4. Momentum, Sensible Heat, and Latent Heat Fluxes

The zonal τ_x and meridional τ_y momentum fluxes (kg m^{-1} s^{-2}), the sensible heat flux H (W m^{-2}), the water vapor flux E (kg m^{-2} s^{-1}), and the latent heat flux λE (W m^{-2}) between the atmosphere at reference height $z_{\rm atm}$ (m) [with zonal and meridional winds $u_{\rm atm}$ and $v_{\rm atm}$ (m s^{-1}), potential temperature $\theta_{\rm atm}$ (K), and specific humidity $q_{\rm atm}$ (kg kg^{-1})] and the surface [with u_s, v_s, θ_s, and q_s] are

$$\tau_x = -\rho_{\rm atm}\frac{(u_{\rm atm} - u_s)}{r_{am}}$$

$$\tau_y = -\rho_{\rm atm}\frac{(v_{\rm atm} - v_s)}{r_{am}}$$

$$H = -\rho_{\rm atm}C_p\frac{(\theta_{\rm atm} - \theta_s)}{r_{ah}}$$

$$E = -\rho_{\rm atm}\frac{(q_{\rm atm} - q_s)}{r_{aw}} \ .$$

These fluxes are derived in the next section from Monin-Obukhov similarity theory applied to the surface (i.e., constant flux) layer. In this derivation, u_s and v_s are defined to equal zero at height $z_{0m} + d$ (the apparent sink for momentum) so that r_{am} is the aerodynamic resistance (s m^{-1}) for momentum between the atmosphere at height $z_{\rm atm}$ and the surface at height $z_{0m} + d$. Likewise, θ_s and q_s are defined at heights $z_{0h} + d$ and $z_{0w} + d$ (the apparent sinks for heat and water vapor, respectively). Consequently, r_{ah} and r_{aw} are the aerodynamic resistance (s m^{-1}) to sensible heat and water vapor transfer between the atmosphere at height $z_{\rm atm}$ and the surface at heights $z_{0h} + d$ and $z_{0w} + d$, respectively. The heat capacity of air C_p (J kg^{-1} K^{-1}) is a constant (Table 4). Although λ, the latent heat of vaporization or sublimation (J kg^{-1}), depends on temperature, these values are taken as constants (Table 4). The atmospheric potential temperature is

$$\theta_{\rm atm} = T_{\rm atm} \left(\frac{P_{\rm srf}}{P_{\rm atm}} \right)^{\frac{R}{C_p}}$$

where $T_{\rm atm}$ is the air temperature (K) at height $z_{\rm atm}$, $P_{\rm srf}$ is the surface pressure (Pa), $P_{\rm atm}$ is the atmospheric pressure (Pa), and R is the gas constant (J kg^{-1} K^{-1}) (Table 4). By definition $\theta_s = T_s$. The density of moist air (kg m^{-3}) is

$$\rho_{\rm atm} = \frac{P_{\rm atm} - 0.378 e_{\rm atm}}{R T_{\rm atm}}$$

where the vapor pressure $e_{\rm atm}$ (Pa) at height $z_{\rm atm}$ is related to $q_{\rm atm}$ as

$$q_{\rm atm} = \frac{0.622 e_{\rm atm}}{P_{\rm atm} - 0.378 e_{\rm atm}} \, .$$

4.1 Monin-Obukhov Similarity Theory

Surface kinematic fluxes of momentum $\overline{u'w'}$ and $\overline{v'w'}$ (m^2 s^{-2}), sensible heat $\overline{\theta'w'}$ (K m s^{-1}), and latent heat $\overline{q'w'}$ (kg kg^{-1} m s^{-1}), where u', v', w', θ', and q' are zonal horizontal wind, meridional horizontal wind, vertical velocity, potential temperature, and specific humidity fluctuations about the mean, are defined from Monin-Obukhov similarity theory applied to the surface (i.e., constant flux) layer, as described by (Brutsaert 1982) and Arya (1988). This theory states that when scaled appropriately, the dimensionaless mean horizontal wind, mean potential temperature, and mean specific humidity profile gradients depend on unique functions of $\zeta = \dfrac{z-d}{L}$ as

$$\frac{k(z-d)}{u_*} \frac{\partial |\mathbf{u}|}{\partial z} = \phi_m(\zeta)$$

$$\frac{k(z-d)}{\theta_*} \frac{\partial \theta}{\partial z} = \phi_h(\zeta)$$

$$\frac{k(z-d)}{q_*} \frac{\partial q}{\partial z} = \phi_w(\zeta)$$

where $\mathbf{u} = \sqrt{u^2 + v^2}$, z is height in the surface layer (m), d is the displacement height (m), k is the von Karman constant (Table 4), and L is the Monin-Obukhov length scale (m). $\phi_m(\zeta)$, $\phi_h(\zeta)$, and $\phi_w(\zeta)$ are universal similarity functions that relate the constant fluxes of momentum, sensible heat, and latent heat to the mean profile gradients of $|\mathbf{u}|$, θ, and q in the surface layer. The velocity u_* (m s^{-1}), temperature θ_* (K), and moisture q_* (kg kg^{-1}) scales are

$$u_* u_* = \sqrt{(\overline{u'w'})^2 + (\overline{v'w'})^2} = \frac{|\boldsymbol{\tau}|}{\rho_{\mathrm{atm}}}$$

$$\theta_* u_* = -\overline{\theta' w'} = -\frac{H}{\rho_{\mathrm{atm}} C_p}$$

$$q_* u_* = -\overline{q' w'} = -\frac{E}{\rho_{\mathrm{atm}}}$$

where $|\boldsymbol{\tau}|$ is the shearing stress (kg m^{-1} s^{-2}), with zonal and meridional components $\overline{u'w'} = -\frac{\tau_x}{\rho_{\mathrm{atm}}}$ and $\overline{v'w'} = -\frac{\tau_y}{\rho_{\mathrm{atm}}}$, respectively, H is the sensible heat flux (W m^{-2}), E is the water vapor flux (kg m^{-2} s^{-1}), ρ_{atm} is the density of air (kg m^{-3}), and C_p is heat capacity of air (J kg^{-1} K^{-1}) (Table 4).

Accounting for the buoyancy effects of water vapor (p. 187 Arya 1988, p. 180 Stull 1988),

$$L = \frac{-u_*^3}{k \left(\frac{g}{T_{v\,\mathrm{atm}}}\right) \left(\frac{H_v}{\rho_{\mathrm{atm}} C_p}\right)}$$

where g is gravitational acceleration (m s^{-2}) (Table 4), H_v is the virtual sensible heat flux (W m^{-2}), and $T_{v\,\mathrm{atm}}$ is the virtual atmospheric temperature (K). $T_{v\,\mathrm{atm}}$ can be approximated from atmospheric temperature and specific humidity as $T_{v\,\mathrm{atm}} = T_{\mathrm{atm}}(1+0.61 q_{\mathrm{atm}})$ (p. 53, Arya 1988). The virtual sensible heat flux can be approximated as $H_v = H + 0.61 C_p\, T_{\mathrm{atm}}\, E$ (p. 187, Arya 1988). This definition of L is the same as that used by Beljaars and Viterbo (1994). $L > 0$ indicates stable

conditions. $L < 0$ indicates unstable conditions. $L = \infty$ for neutral conditions. A practical range is $1 \leq |L| \leq 1000$ (p. 158, Arya 1988).

Integrating $\frac{\partial |\mathbf{u}|}{\partial z}$, $\frac{\partial \theta}{\partial z}$, and $\frac{\partial q}{\partial z}$ between two arbitrary heights in the surface layer z_2 and z_1 ($z_2 > z_1$) with horizontal winds $|\mathbf{u}|_1$ and $|\mathbf{u}|_2$, potential temperatures θ_1 and θ_2, and specific humidities q_1 and q_2 results in

$$|\mathbf{u}|_2 - |\mathbf{u}|_1 = \frac{u_*}{k}\left[\ln\left(\frac{z_2 - d}{z_1 - d}\right) - \psi_m\left(\frac{z_2 - d}{L}\right) + \psi_m\left(\frac{z_1 - d}{L}\right)\right]$$

$$\theta_2 - \theta_1 = \frac{\theta_*}{k}\left[\ln\left(\frac{z_2 - d}{z_1 - d}\right) - \psi_h\left(\frac{z_2 - d}{L}\right) + \psi_h\left(\frac{z_1 - d}{L}\right)\right]$$

$$q_2 - q_1 = \frac{q_*}{k}\left[\ln\left(\frac{z_2 - d}{z_1 - d}\right) - \psi_w\left(\frac{z_2 - d}{L}\right) + \psi_w\left(\frac{z_1 - d}{L}\right)\right] .$$

The functions $\psi_m(\zeta)$, $\psi_h(\zeta)$, and $\psi_w(\zeta)$ are defined as

$$\psi_m(\zeta) = \int_{z_{0m}/L}^{\zeta} \frac{[1 - \phi_m(x)]}{x} dx$$

$$\psi_h(\zeta) = \int_{z_{0h}/L}^{\zeta} \frac{[1 - \phi_h(x)]}{x} dx$$

$$\psi_w(\zeta) = \int_{z_{0w}/L}^{\zeta} \frac{[1 - \phi_w(x)]}{x} dx$$

where z_{0m}, z_{0h}, and z_{0w} are the roughness lengths (m) for momentum, sensible heat, and water vapor, respectively.

Defining the surface values

$|\mathbf{u}|_1 = 0$ at $z_1 = z_{0m} + d$,

$\theta_1 = \theta_s$ at $z_1 = z_{0h} + d$, and

$q_1 = q_s$ at $z_1 = z_{0w} + d$,

and the atmospheric values at $z_2 = z_{\mathrm{atm}}$

$$|\mathbf{u}|_2 = |\mathbf{u}|_{\rm atm} = \sqrt{u_{\rm atm}^2 + v_{\rm atm}^2} \geq 1,$$

$$\theta_2 = \theta_{\rm atm}, \text{ and}$$

$$q_2 = q_{\rm atm},$$

the surface momentum, sensible heat, and latent heat fluxes are

$$|\mathbf{u}|_{\rm atm} = \frac{u_*}{k}\left[\ln\left(\frac{z_{\rm atm}-d}{z_{0m}}\right) - \psi_m\left(\frac{z_{\rm atm}-d}{L}\right)\right]$$

$$\theta_{\rm atm} - \theta_s = \frac{\theta_*}{k}\left[\ln\left(\frac{z_{\rm atm}-d}{z_{0h}}\right) - \psi_h\left(\frac{z_{\rm atm}-d}{L}\right)\right]$$

$$q_{\rm atm} - q_s = \frac{q_*}{k}\left[\ln\left(\frac{z_{\rm atm}-d}{z_{0w}}\right) - \psi_w\left(\frac{z_{\rm atm}-d}{L}\right)\right] .$$

The constraint $|\mathbf{u}|_{\rm atm} \geq 1$ is required simply for numerical reasons to prevent H and E from becoming small with small wind speeds.

Using the definitions of u_*, θ_*, and q_*, these equations can be used to calculate the surface momentum, sensible heat, and latent heat fluxes using atmospheric and surface values for $|\mathbf{u}|$, θ, and q except that L depends on u_*, θ_*, and q_*. However, the bulk Richardson number

$$R_{iB} = \left(\frac{\theta_{v\ {\rm atm}} - \theta_{v\ s}}{T_{v\ {\rm atm}}}\right)\frac{g(z-d)}{|\mathbf{u}|_{\rm atm}^2} ,$$

where the subscript "v" indicates virtual temperature, is related to $\zeta = \dfrac{z_{\rm atm}-d}{L}$ as

$$R_{iB} = \zeta\left[\ln\left(\frac{z_{\rm atm}-d}{z_{0h}}\right) - \psi_h(\zeta)\right]\left[\ln\left(\frac{z_{\rm atm}-d}{z_{0m}}\right) - \psi_m(\zeta)\right]^{-2}$$

and the inverse relationship $\zeta = f(R_{iB})$ can be used to calculate the surface fluxes from surface and atmospheric values of $|\mathbf{u}|$, θ, and q.

As discussed by Brutsaert (p.67, 1982)

$$\phi_m(\zeta)^2 = \phi_h(\zeta) = \phi_w(\zeta) = \frac{1}{\sqrt{1-16\zeta}} \quad \text{for } \zeta < 0 \quad \text{(unstable)}$$

$$\phi_m(\zeta) = \phi_h(\zeta) = \phi_w(\zeta) = 1 + 5\zeta \quad \text{for } 0 \leq \zeta \leq 1 \quad \text{(stable)} .$$

z_{0m}, z_{0h}, and z_{0w} are much smaller than L, and for practical purposes the lower limits in the ψ_m, ψ_h, and ψ_w integrations are replaced by zero (p. 70 Brutsaert 1982, p. 166 Arya 1988). Consequently, for unstable conditions ($\zeta < 0$),

$$\psi_h(\zeta) = \psi_w(\zeta) = 2\ln\left(\frac{1+x^2}{2}\right)$$

$$\psi_m(\zeta) = 2\ln\left(\frac{1+x}{2}\right) + \ln\left(\frac{1+x^2}{2}\right) - 2\tan^{-1}x + \frac{\pi}{2}$$

where $x = (1-16\zeta)^{1/4}$. For stable conditions ($0 \leq \zeta \leq 1$)

$$\psi_m(\zeta) = \psi_h(\zeta) = \psi_w(\zeta) = -5\zeta .$$

The limit $\zeta \leq 1$ is included because these equations are valid for only moderately stable conditions, as discussed by Brutsaert (1982). These stability functions are illustrated in Figure 15 for a range of ζ.

Figure 15. ψ_m and ψ_h as a function of ζ.

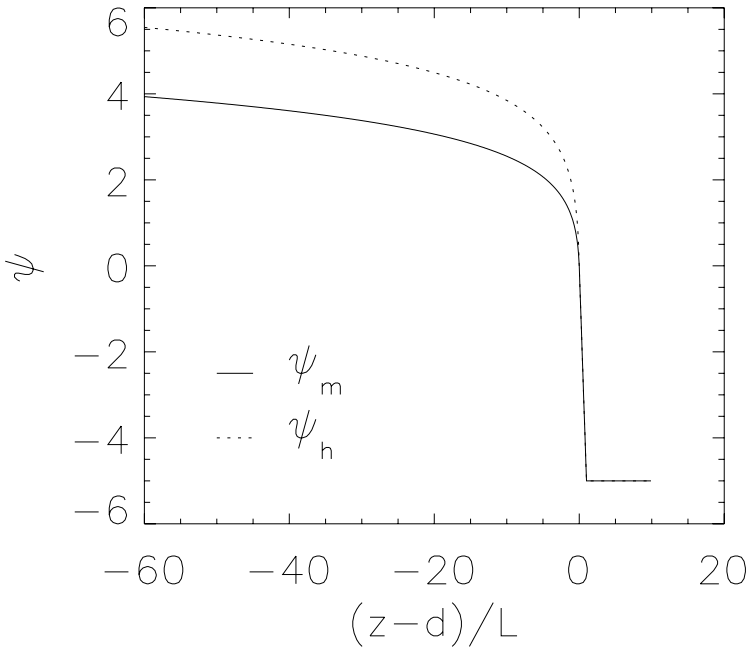

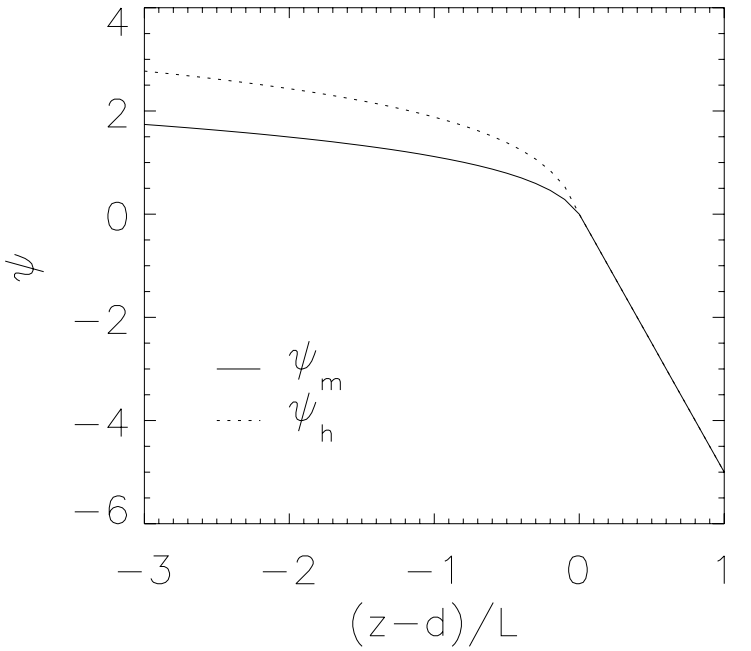

Figure 15

The momentum, sensible heat, and water vapor fluxes between the surface and the atmosphere can also be written in the form

$$\tau_x = -\rho_{\rm atm}\frac{u_{\rm atm}}{r_{am}}$$

$$\tau_y = -\rho_{\rm atm}\frac{v_{\rm atm}}{r_{am}}$$

$$H = -\rho_{\rm atm}C_p\frac{(\theta_{\rm atm}-\theta_s)}{r_{ah}}$$

$$E = -\rho_{\rm atm}\frac{(q_{\rm atm}-q_s)}{r_{aw}}$$

where with $\zeta = \dfrac{z_{\rm atm}-d}{L}$ the aerodynamic resistances (s m^{-1}) are

$$\begin{aligned} r_{am} =& \frac{1}{ku_*}\left[\ln\left(\frac{z_{\rm atm}-d}{z_{0m}}\right)-\psi_m(\zeta)\right] \\ =& \frac{1}{k^2|\mathbf{u}|_{\rm atm}}\left[\ln\left(\frac{z_{\rm atm}-d}{z_{0m}}\right)-\psi_m(\zeta)\right]\left[\ln\left(\frac{z_{\rm atm}-d}{z_{0m}}\right)-\psi_m(\zeta)\right] \end{aligned}$$

$$\begin{aligned} r_{ah} =& \frac{1}{ku_*}\left[\ln\left(\frac{z_{\rm atm}-d}{z_{0h}}\right)-\psi_h(\zeta)\right] \\ =& \frac{1}{k^2|\mathbf{u}|_{\rm atm}}\left[\ln\left(\frac{z_{\rm atm}-d}{z_{0m}}\right)-\psi_m(\zeta)\right]\left[\ln\left(\frac{z_{\rm atm}-d}{z_{0h}}\right)-\psi_h(\zeta)\right] \end{aligned}$$

$$\begin{aligned} r_{aw} =& \frac{1}{ku_*}\left[\ln\left(\frac{z_{\rm atm}-d}{z_{0w}}\right)-\psi_w(\zeta)\right] \\ =& \frac{1}{k^2|\mathbf{u}|_{\rm atm}}\left[\ln\left(\frac{z_{\rm atm}-d}{z_{0m}}\right)-\psi_m(\zeta)\right]\left[\ln\left(\frac{z_{\rm atm}-d}{z_{0w}}\right)-\psi_w(\zeta)\right] . \end{aligned}$$

For numerical reasons, these resistances are ≥ 1 s m^{-1}. The aerodynamic resistances are related to the dimensionaless exchange coefficients as $C_m = (r_{am}|\mathbf{u}|_{\rm atm})^{-1}$, $C_h = (r_{ah}|\mathbf{u}|_{\rm atm})^{-1}$, and $C_w = (r_{aw}|\mathbf{u}|_{\rm atm})^{-1}$. This definition of aerodynamic resistances and exchange coefficients is the same as that in Beljaars and Viterbo (1994), except that it excludes their free convection velocity scale ω_* in the calculation of $|\mathbf{u}|_{\rm atm}$.

It is useful to distinguish an "aerodynamic" temperature T_a at height $z_{0m} + d$ in addition to the "surface" temperature ($T_s = \theta_s$) at height $z_{0h} + d$

$$T_a - T_s = \frac{\theta_*}{k}\left[\ln\left(\frac{z_{0m}}{z_{0h}}\right) - \psi_h\left(\frac{z_{0m}}{L}\right)\right] .$$

The difference between z_{0m} and z_{0h}, compared to L, is small, and the term $\psi_h\left(\frac{z_{0m}}{L}\right) \approx 0$. The term $\frac{1}{k}\ln\left(\frac{z_{0m}}{z_{0h}}\right)$ is defined as B^{-1} and the excess resistance needed to account for differences in z_{0m} and z_{0h} is B^{-1}/u_* (p. 248, Monteith and Unsworth 1990). A typical value is $B^{-1} = 5.8$ so that $z_{0h} = 0.1\ z_{0m}$. However, B^{-1} may be > 20 (Beljaars and Holtslag 1991, Beljaars and Viterbo 1994).

A 2 m height "screen" temperature can be defined in a similar manner

$$T_{2m} - T_s = \frac{\theta_*}{k}\ln\left(\frac{2 + z_{0h}}{z_{0h}}\right)$$

where for convenience, "2 m" is defined as 2 m above the apparent sink for sensible heat.

4.2 Sensible and Latent Heat Fluxes for Non-Vegetated Surfaces

Surfaces are considered to be non-vegetated for the surface flux and temperature calculations if leaf plus stem area $L + S$ (section 1.3) equals zero. For these surfaces, the surface temperature T_s is also the ground temperature T_g so that the sensible heat flux (W m^{-2}) is, with reference to Figure 16,

$$H = -\rho_{\rm atm} C_p \frac{(\theta_{\rm atm} - T_g)}{r_{ah}}.$$

With specific humidity approximated from pressure P and vapor pressure e as $q \approx 0.622e/P$ and defining the psychrometric constant (Pa K^{-1}) as $\gamma = \frac{C_p P_{\rm atm}}{0.622\lambda}$, the latent heat flux is

$$\lambda E = -\frac{\rho_{\rm atm} C_p}{\gamma}\frac{[e_{\rm atm} - e_*(T_g)]}{r_{aw} + r_{\rm srf}}$$

Figure 16. Schematic diagram of sensible heat fluxes for non-vegetated surfaces (left) and vegetated surfaces (right).

Figure 17. Schematic diagram of latent heat fluxes for non-vegetated surfaces (top) and vegetated surfaces (bottom).

where $e_{\rm atm}$ is the vapor pressure (Pa) at height $z_{\rm atm}$ and $e_*(T_g)$ is the saturation vapor pressure (Pa) at the ground temperature. This equation is similar to that in previous section, but is derived, with reference to Figure 17, by assuming negligible capacity to store water vapor so that

$$-\frac{\rho_{\rm atm} C_p}{\gamma}\frac{[e_{\rm atm}-e_s]}{r_{aw}} = -\frac{\rho_{\rm atm} C_p}{\gamma}\frac{[e_s-e_*(T_g)]}{r_{\rm srf}}$$

and

$$e_s = \left[\frac{e_{\rm atm}}{r_{aw}} + \frac{e_*(T_g)}{r_{\rm srf}}\right] / \left[\frac{1}{r_{aw}} + \frac{1}{r_{\rm srf}}\right] .$$

$r_{\rm srf}$ is a surface resistance (s m^{-1}) that accounts for water vapor transfer between the soil with vapor pressure $e_*(T_g)$ and the apparent sink for water vapor with a vapor pressure e_s. This surface resistance, which increases as the soil becomes drier, is a linear combination of a resistance for the fraction of the ground covered by snow $f_{\rm sno}$ (section 8.2) and a soil resistance for $1-f_{\rm sno}$

$$r_{\rm srf} = 150 f_{\rm sno} + (1-f_{\rm sno})\frac{r_{aw}(1-\beta_e)}{\beta_e} .$$

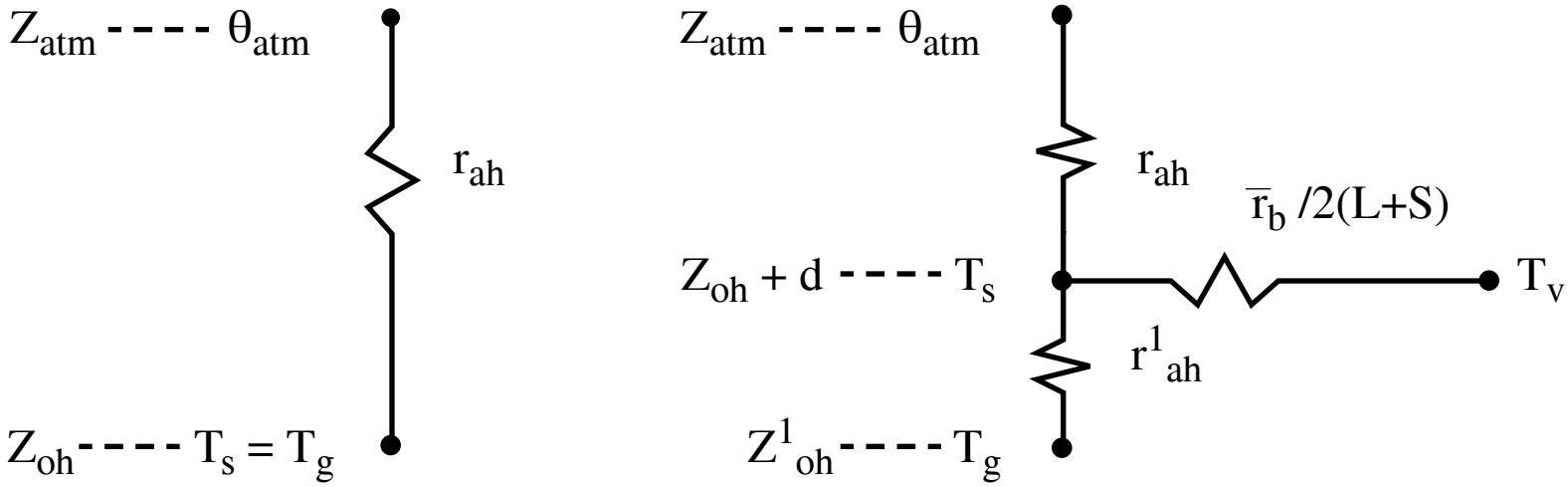
Z_{atm} ---- θ_{atm}
r_{ah}
Z_{oh} ---- $T_s = T_g$
Z_{atm} ---- θ_{atm}
r_{ah}
$\overline{r}_b$ /2(L+S)
Z_{oh} + d ---- T_s
T_v
r^1_{ah}
Z^1_{oh} ---- T_g

Figure 16

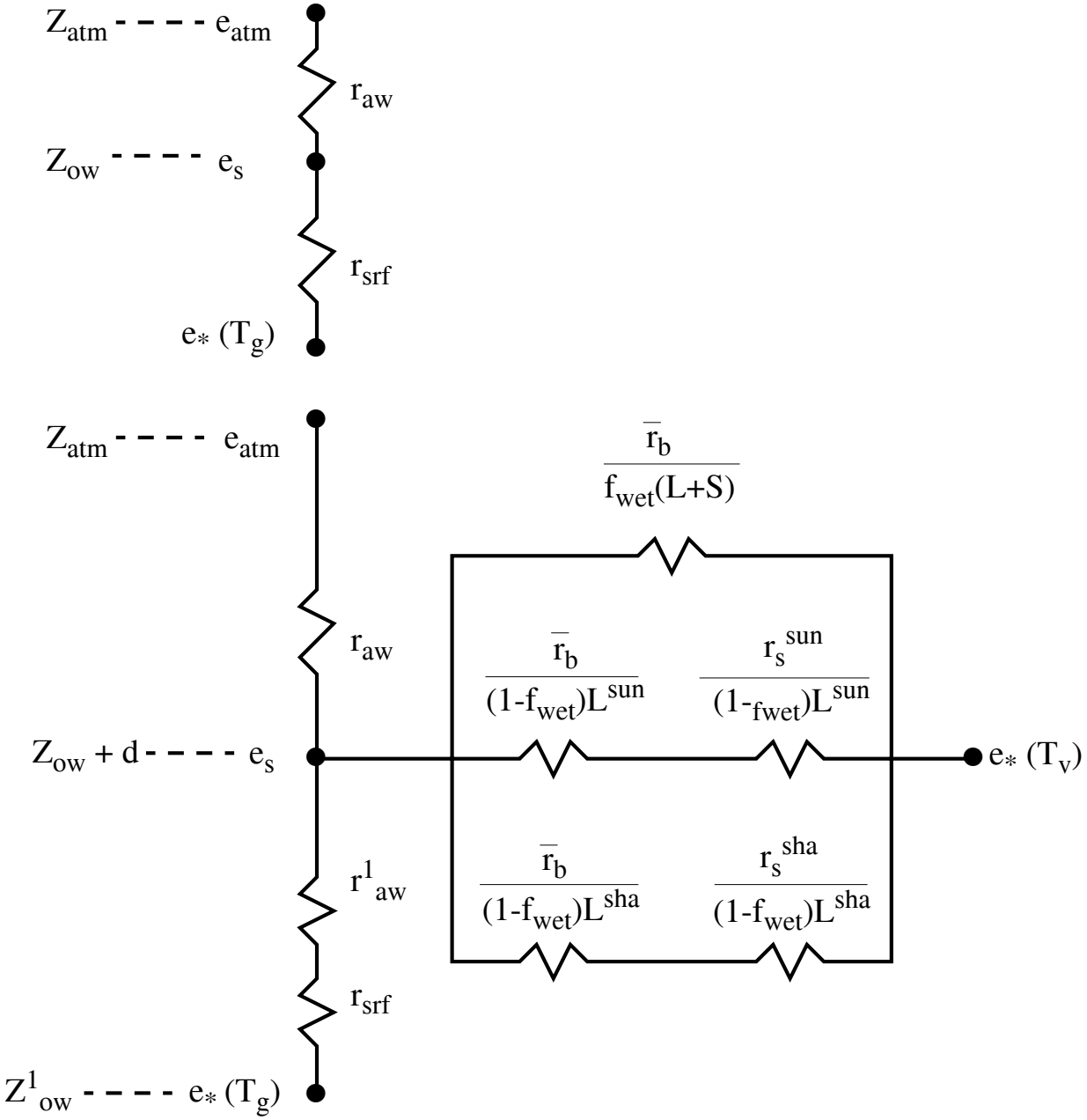
Z_{atm} - - - - e_{atm}
r_{aw}
Z_{ow} - - - - e_s
r_{srf}
e_* (T_g)
Z_{atm} - - - - e_{atm}
$\frac{\bar{r}_b}{f_{wet}(L+S)}$
r_{aw}
$\frac{\bar{r}_b}{(1-f_{wet})L^{sun}}$
$\frac{r_s^{sun}}{(1-f_{wet})L^{sun}}$
Z_{ow} + d - - - - e_s
e_* (T_v)
r^1_{aw}
$\frac{\bar{r}_b}{(1-f_{wet})L^{sha}}$
$\frac{r_s^{sha}}{(1-f_{wet})L^{sha}}$
r_{srf}
Z^1_{ow} - - - - e_* (T_g)

Figure 17

β_e is a dimensionaless factor that ranges from one when the soil is wet to zero when the soil is dry

$$\beta_e = \left\{ \begin{array}{r} \left(\dfrac{\theta_1 - \theta_{\rm dry}}{\theta_{\rm opt} - \theta_{\rm dry}} \right) \leq 1 \text{ for } T_1 > T_f \\ 0.01 \text{ for } T_1 \leq T_f \end{array} \right\}$$

where θ_1 is the water content of the first soil layer (section 8.4), $\theta_{\rm opt}$ is the optimal water content for evapotranspiration (section 8.4.1), $\theta_{\rm dry}$ is the water content when evapotranspiration ceases (section 8.4.1), T_1 is the temperature of the first soil layer (section 6), and T_f is the freezing point (Table 4).

The roughness lengths used to calculate r_{am}, r_{ah}, and r_{aw} are z_{0m}, z_{0h}, and z_{0w}, where $z_{0m} = z_{0\ \rm soi}(1 - f_{\rm sno}) + z_{0\ \rm sno} f_{\rm sno}$ and $z_{0h} = z_{0w} = z_{0m} e^{-kB^{-1}}$, as per the definition of B^{-1}. $z_{0\ \rm soi}$ is 0.05 m for soil, glaciers, and wetlands; 0.001 m for unfrozen lakes; and 0.04 m for frozen lakes. $z_{0\ \rm sno} = 0.04$ m. Currently, $B^{-1} = 0$.

4.3 Sensible and Latent Heat Fluxes for Vegetated Surfaces

In the more complicated case of a vegetated surface, H and λE are partitioned into vegetation and ground fluxes that depend on vegetation T_v and ground T_g temperatures in addition to surface temperature T_s and vapor pressure e_s.

Assuming the canopy air has negligible capacity to store heat, the sensible heat flux H between the surface at height $z_{0h} + d$ and the atmosphere at height $z_{\rm atm}$ is partitioned into vegetation and ground fluxes as

$$H = -\rho_{\rm atm} C_p \frac{(\theta_{\rm atm} - T_s)}{r_{ah}} = H_v + H_g$$

where, with reference to Figure 16,

$$H_v = -\rho_{\rm atm} C_p (T_s - T_v) \frac{2(L+S)}{\bar{r}_b}$$

$$H_g = -\rho_{\rm atm} C_p \frac{(T_s - T_g)}{r'_{ah}} \ .$$

L and S are the leaf and stem area indices (section 1.3). $\bar{r}_b$ is the average leaf boundary layer resistance (s m^{-1}) and r'_{ah} is the aerodynamic resistance (s m^{-1}) between the ground (z'_{0h}) and $d + z_{0h}$. Defining the conductances $c_a^h = \dfrac{1}{r_{ah}}$, $c_v^h = \dfrac{2(L+S)}{\bar{r}_b}$, and $c_g^h = \dfrac{1}{r'_{ah}}$,

$$T_s = \frac{c_a^h \theta_{\rm atm} + c_g^h T_g + c_v^h T_v}{c_a^h + c_v^h + c_g^h} \ .$$

When this expression is substituted into H_v, H_v is a function of T_g and T_v

$$H_v = -\rho_{\rm atm} C_p [c_a^h \theta_{\rm atm} + c_g^h T_g - (c_a^h + c_g^h) T_v] \frac{c_v^h}{c_a^h + c_v^h + c_g^h} \ .$$

A similar expression can be found for H_g.

Assuming the canopy air has negligible capacity to store water vapor, the latent heat flux λE between the surface at height $z_{0w} + d$ and the atmosphere at height $z_{\rm atm}$ is partitioned into vegetation and ground fluxes as

$$\lambda E = -\frac{\rho_{\rm atm} C_p}{\gamma} \frac{(e_{\rm atm} - e_s)}{r_{aw}} = \lambda E_v + \lambda E_g \ .$$

This equation, which uses vapor pressure ($e_{\rm atm}$, e_s [Pa]) rather than specific humidity ($q_{\rm atm}$, q_s), is the same as that derived in section 4.1 noting that the specific humidity is approximated as $q \approx 0.622 e/P$ and defining $\gamma = \dfrac{C_p P_{\rm atm}}{0.622 \lambda}$. The latent heat flux for vegetation is, with reference to Figure 17,

$$\lambda E_v = -\frac{\rho_{\rm atm} C_p}{\gamma} [e_s - e_*(T_v)] \left[f_{\rm wet} \left(\frac{L+S}{\bar{r}_b} \right) + (1 - f_{\rm wet}) \left(\frac{L^{\rm sun}}{\bar{r}_b + r_s^{\rm sun}} + \frac{L^{\rm sha}}{\bar{r}_b + r_s^{\rm sha}} \right) \right]$$

where $e_*(T_v)$ is the saturation vapor pressure (Pa) at T_v, $L^{\rm sun}$ and $L^{\rm sha}$ are the sunlit and shaded leaf area indices (section 3.1), and $r_s^{\rm sun}$ and $r_s^{\rm sha}$ are the sunlit and

shaded stomatal resistances (s m^{-1}) (section 9.1). The terms in brackets represent evaporation of intercepted water from the wetted fraction of the canopy $f_{\rm wet}$ (section 8.1), transpiration from sunlit leaves, and transpiration from shaded leaves. The ground latent heat flux is, with reference to Figure 17,

$$\lambda E_g = -\frac{\rho_{\rm atm} C_p}{\gamma} \frac{[e_s - e_*(T_g)]}{r'_{aw} + r_{\rm srf}}$$

where $e_*(T_g)$ is the saturation vapor pressure (Pa) at T_g, r'_{aw} is the aerodynamic resistance between the ground (z'_{0w}) and $d + z_{0w}$, and $r_{\rm srf}$ is the same as in section 4.2, but using r'_{aw} instead of r_{aw}. Similar to T_s, the conductances $c_a^w = \frac{1}{r_{aw}}$, $c_e^w = \frac{f_{\rm wet}(L+S)}{\bar{r}_b}$, $c_t^w = (1 - f_{\rm wet}) \left(\frac{L^{\rm sun}}{\bar{r}_b + r_s^{\rm sun}} + \frac{L^{\rm sha}}{\bar{r}_b + r_s^{\rm sha}} \right)$, and $c_g^w = \frac{1}{r'_{aw} + r_{\rm srf}}$ are defined so that

$$e_s = \frac{c_a^w e_{\rm atm} + c_g^w e_*(T_g) + [c_e^w + c_t^w] e_*(T_v)}{c_a^w + [c_e^w + c_t^w] + c_g^w} \; .$$

Substituting in e_s, λE_v as a function of $e_*(T_g)$ and $e_*(T_v)$ is

$$\lambda E_v = -\frac{\rho_{\rm atm} C_p}{\gamma} \left[c_a^w e_{\rm atm} + c_g^w e_*(T_g) - [c_a^w + c_g^w] e_*(T_v) \right] \frac{c_e^w + c_t^w}{c_a^w + (c_e^w + c_t^w) + c_g^w} \; .$$

A similar expression can be found for λE_g.

z_{0m} and d, the roughness length for momentum and the displacement height, which are used to calculate r_{am}, r_{ah}, and r_{aw} (section 4.1), vary with leaf and stem area and canopy height (Brutsaert 1982, Raupach 1994). Currently, z_{0m} and d vary with vegetation type (Table 12) rather than vegetation structure. $z_{0h} = z_{0w} = z_{0m} e^{-kB^{-1}}$, as per the definition of B^{-1}. Currently, $B^{-1} = 0$ so $z_{0h} = z_{0w} = z_{0m}$.

Table 12. Vegetation dependent aerodynamic parameters (Bonan 1994)

Plant Type	z_{0m} (m)	d (m)	B^{-1}	a
needleleaf evergreen tree	0.94	11.39	0.	3
needleleaf deciduous tree	0.77	9.38	0.	3
broadleaf evergreen tree	2.62	23.45	0.	3
broadleaf deciduous tree	1.10	13.40	0.	3
tropical seasonal tree	0.99	12.06	0.	3
C_3 grass	0.06	0.34	0.	3
evergreen shrub	0.06	0.34	0.	3
deciduous shrub	0.06	0.34	0.	3
arctic deciduous shrub	0.06	0.34	0.	3
arctic grass	0.06	0.34	0.	3
crop	0.06	0.34	0.	3
C_4 grass	0.06	0.34	0.	3

The aerodynamic resistances to sensible heat and latent heat transfer within the canopy r'_{ah} and r'_{aw}, respectively, and the bulk leaf boundary layer resistance $\bar{r}_b$ are from Choudhury and Monteith (1988). The aerodynamic resistance to sensible heat transfer between two heights z_2 and z_1 can be derived as $\int_{z_1}^{z_2} \frac{dz}{K_h(z)}$, where $K_h(z) = ku_*(z-d)\phi_h^{-1}$ is the eddy diffusivity ($m^2\ s^{-1}$) for heat (Thom 1975). If $K_h(z)$ has an exponential profile within the canopy similar to $K_m(z)$

$$K_h(z) = K_h(z_{\rm top})e^{-a(1-z/z_{\rm top})}$$

where $z_{\rm top}$ is the top of the canopy (m) (section 1.2) and a is an empirical parameter (Table 12), then the aerodynamic resistance to sensible heat transfer in the canopy between the ground temperature T_g at height z'_{0h}, where z'_{0h} is the ground roughness

length (section 4.2), and the surface temperature T_s at height $z_{0h} + d$ is

$$r'_{ah} = \int_{z'_{0h}}^{z_{0h}+d} \frac{dz}{K_h(z)} = \frac{z_{\rm top}}{aK_h(z_{\rm top})} \left[e^{a(1-z'_{0h}/z_{\rm top})} - e^{a(1-(z_{0h}+d)/z_{\rm top})} \right] .$$

$r'_{aw} = r'_{ah}$ because the roughness lengths for sensible heat and water vapor are identical. Shuttleworth and Wallace (1985) used the same derivation for their aerodynamic resistances. The leaf boundary layer conductance g_b (m s^{-1}) depends on leaf dimension $d_{\rm leaf}$ (m) (Table 7) and wind speed $|\mathbf{u}|(z)$ (m s^{-1}) at height z as

$$g_b(z) = 0.01 \sqrt{\frac{|\mathbf{u}|(z)}{d_{\rm leaf}}} .$$

The wind profile within the canopy consistent with an exponential $K_m(z)$ profile is

$$|\mathbf{u}|(z) = |\mathbf{u}|(z_{\rm top}) e^{-a(1-z/z_{\rm top})} .$$

Integrating $g_b(z)$ over height in the canopy,

$$\frac{1}{\bar{r}_b} = \bar{g}_b = \frac{\int_0^{z_{\rm top}} g_b(z) dz}{\int_0^{z_{\rm top}} dz} = \frac{0.02}{a} \sqrt{\frac{|\mathbf{u}|(z_{\rm top})}{d_{\rm leaf}}} \left[1 - e^{-a/2} \right] .$$

The use of "K-theory" within the canopy is a major assumption that simplifies the surface flux parameterizations. Brutsaert (pp. 97-110, 1982) provides a thorough discussion of transfer processes within the canopy. He notes: an exponential profile to $|\mathbf{u}|(z)$ is widely used (p. 101); although a varies with canopy density and type a general value is $a = 3$ (p. 102); and eddy diffusivity profiles for scalars are similar to that of momentum (p. 105). Landsberg (p. 61, 1986) also notes that $a = 3$ is a general value that gives "reasonable" results. Because of these simplifications and because the atmospheric stability corrections are computationally expensive, the effects of atmospheric stability are ignored when calculating the wind $|\mathbf{u}|(z_{\rm top}) = \frac{u_*}{k} \ln \left(\frac{z_{\rm top} - d}{z_{0m}} \right)$ and eddy diffusivity $K_h(z_{\rm top}) = k u_* (z_{\rm top} - d)$ at the top of the canopy.

5. Vegetation and Ground Temperatures

In the simple case of non-vegetated surfaces, the net longwave radiative flux $\overrightarrow{L}$ (W m^{-2}) (section 3.2), the sensible heat flux H (W m^{-2}) (section 4.2), and the latent heat flux λE (W m^{-2}) (section 4.2) depend on the ground temperature T_g. With the soil heat flux G (W m^{-2}) also a function of T_g, surface fluxes and temperatures are calculated by finding T_g that balances the energy budget

$$-\overrightarrow{S}_g + \overrightarrow{L}(T_g) + H(T_g) + \lambda E(T_g) + G(T_g) + M = 0 \; .$$

$\overrightarrow{S}_g$ is the net solar radiation (W m^{-2}) at the ground (section 3.1). $\overrightarrow{L}$, H, and λE (positive towards the atmosphere) are by definition the ground surface fluxes. G (positive into the soil) is (cf. section 6)

$$G = \frac{2k_1}{\Delta z_1}\,(T_g - T_1)$$

where k_1 is the thermal conductivity (W m^{-1} K^{-1}), Δz_1 is the thickness (m), and T_1 is the temperature (K) of the first soil/lake/snow layer (section 6). M is the snow melt heat flux (W m^{-2}).

In the more complicated case of a vegetated surface, $\overrightarrow{L}$, H and λE are partitioned into vegetation and ground fluxes so that $\overrightarrow{L} = \overrightarrow{L}_v + \overrightarrow{L}_g$ (section 3.2), $H = H_v + H_g$ (section 4.3), and $\lambda E = \lambda E_v + \lambda E_g$ (section 4.3), where the subscripts "v" and "g" indicate vegetation and ground, respectively. These fluxes depend on vegetation T_v and ground T_g temperatures which are determined as the temperatures that balance the canopy and ground energy budgets

$$-\overrightarrow{S}_v + \overrightarrow{L}_v(T_v, T_g) + H_v(T_v, T_g) + \lambda E_v(T_v, T_g) = 0$$

$$-\overrightarrow{S}_g + \overrightarrow{L}_g(T_v, T_g) + H_g(T_v, T_g) + \lambda E_g(T_v, T_g) + G(T_g) + M = 0$$

where $\overrightarrow{S}_v$ and $\overrightarrow{S}_g$ are the solar radiation (W m^{-2}) absorbed by vegetation and ground (section 3.1).

After the ground temperature has been calculated, the snow melts when, as in Bonan (1994), T_g is greater than the freezing temperature T_f (Table 4). In this case, $T_g = T_f$ and the ground fluxes $\overrightarrow{L}_g$, H_g, λE_g are re-evaluated with $T_g = T_f$. If the energy inbalance is positive (i.e., there is a flux of heat into the snow and/or soil), snow melt M (W m^{-2}) is

$$M = \overrightarrow{S}_g - \overrightarrow{L}_g - H_g - \lambda E_g \leq \frac{W_{\text{sno}} h_{\text{fus}}}{\Delta t}$$

where W_{sno} is the mass of snow water (kg m^{-2}) (section 8.2), h_{fus} is the latent heat of fusion (J kg^{-1}) (Table 4), and Δt is the time step (seconds). This equation limits snow melt to be less than or equal to the amount of snow on the ground. Any excess energy is used to warm the soil.

Saturation vapor pressure $e_*(T)$ (Pa) as a function of temperature T (^{o}C) and $\frac{de_*(T)}{dT}$ are calculated using Lowe's (1977) polynomials

$$100[a_0 + T(a_1 + T(a_2 + T(a_3 + T(a_4 + T(a_5 + Ta_6)))))]$$

where the coefficients a_0 to a_6 vary for saturation vapor pressure with reference to water or ice (Tables 13 and 14). These equations are valid for $-50^oC \leq T \leq 50^oC$.

Table 13. Coefficients for $e_*(T)$

	water	ice
a_0	6.107799961	6.109177956
a_1	$4.436518521 \times 10^{-1}$	$5.034698970 \times 10^{-1}$
a_2	$1.428945805 \times 10^{-2}$	$1.886013408 \times 10^{-2}$
a_3	$2.650648471 \times 10^{-4}$	$4.176223716 \times 10^{-4}$
a_4	$3.031240396 \times 10^{-6}$	$5.824720280 \times 10^{-6}$
a_5	$2.034080948 \times 10^{-8}$	$4.838803174 \times 10^{-8}$
a_6	$6.136820929 \times 10^{-11}$	$1.838826904 \times 10^{-10}$

Table 14. Coefficients for $\frac{de_*(T)}{dT}$

	water	ice
a_0	$4.438099984 \times 10^{-1}$	$5.030305237 \times 10^{-1}$
a_1	$2.857002636 \times 10^{-2}$	$3.773255020 \times 10^{-2}$
a_2	$7.938054040 \times 10^{-4}$	$1.267995369 \times 10^{-3}$
a_3	$1.215215065 \times 10^{-5}$	$2.477563108 \times 10^{-5}$
a_4	$1.036561403 \times 10^{-7}$	$3.005693132 \times 10^{-7}$
a_5	$3.532421810 \times 10^{-10}$	$2.158542548 \times 10^{-9}$
a_6	$-7.090244804 \times 10^{-13}$	$7.131097725 \times 10^{-12}$

5.1 Non-Vegetated Surfaces

With $\overrightarrow{S}_g$ (section 3.1) a constant and $\overrightarrow{L}$ (section 3.2), H (section 4.2), λE (section 4.2), and G each a function of T_g, the ground temperature that balances the surface energy budget is found by iteratively solving the equation

$$-\overrightarrow{S}_g + \overrightarrow{L} + H + \lambda E + G + \left(\frac{\partial \overrightarrow{L}}{\partial T_g} + \frac{\partial H}{\partial T_g} + \frac{\partial \lambda E}{\partial T_g} + \frac{\partial G}{\partial T_g} \right) \Delta T_g = 0$$

where $\Delta T_g = T_g^{n+1} - T_g^n$ and the superscript "n" indicates the iteration.

The partial derivatives are

$$\frac{\partial \overrightarrow{L}}{\partial T_g} = 4\epsilon_g \sigma T_g^3$$

$$\frac{\partial H}{\partial T_g} = \frac{\rho_{\text{atm}} C_p}{r_{ah}}$$

$$\frac{\partial \lambda E}{\partial T_g} = \frac{\rho_{\text{atm}} C_p}{\gamma (r_{aw} + r_{\text{srf}})} \frac{de_*(T_g)}{dT}$$

$$\frac{\partial G}{\partial T_g} = \frac{2k_1}{\Delta z_1} \, .$$

Because the partial derivatives $\frac{\partial r_{ah}}{\partial T_g}$ and $\frac{\partial r_{aw}}{\partial T_g}$ cannot be determined analytically (section 4.1), the iterative temperature calculation begins with $\zeta = \frac{z_{\text{atm}} - d}{L}$ from the previous time step. Subsequent values for ψ_m, ψ_h, and ψ_w are one-half the values of the previous iteration and the current iteration. If ζ changes sign more than four times during the temperature iteration, $\zeta = 0$. This prevents "flip-flopping" between stable and unstable conditions.

Typical values for these partial derivatives can be compared to determine the sensitivity of the energy fluxes to changes in T_g and vice versa. At 25 ^{o}C, $\frac{\partial \overrightarrow{L}}{\partial T_g} \approx 5$.

$\frac{\partial H}{\partial T_g}$ ranges from 100 for unstable conditions ($r_{ah} = 10$) to 10 for stable conditions ($r_{ah} = 100$). $\frac{\partial \lambda E}{\partial T_g}$ varies greatly with β_e. For a wet soil ($\beta_e = 1.0$), $\frac{\partial \lambda E}{\partial T_g}$ at 25 ^{o}C ranges from 300 for unstable conditions ($r_{aw} = 10$) to 30 for stable conditions ($r_{aw} = 100$). With $\beta_e = 0.5$ (i.e., for a drier soil), $\frac{\partial \lambda E}{\partial T_g}$ ranges from 150 for unstable conditions to 15 for stable conditions. With a very dry soil ($\beta_e = 0.1$), approximate values are 30 and 3, respectively. $\frac{\partial G}{\partial T_g}$ ranges from 20 to 40 for a typical range of k_1. Thus, a unit change in T_g has the greatest effect on sensible heat flux and latent heat flux (wet soils) when the atmosphere is unstable. When the atmosphere is stable, $\frac{\partial H}{\partial T_g}$ and $\frac{\partial \lambda E}{\partial T_g}$ are reduced by an order of magnitude. Under these conditions, $\frac{\partial G}{\partial T_g}$ can be the dominant term.

5.2 Vegetated Surfaces

The fluxes and temperatures for vegetated surfaces are more complex than those of bare ground because of the inclusion of vegetation T_v and ground T_g temperatures, which are different from the surface temperature T_s, and the need to parameterize both vegetation and ground fluxes. The surface energy budgets for the canopy and the ground are nonlinear functions of T_v and T_g. Newton-Raphson iteration for nonlinear system of equations can be used to simultaneously solve for T_v and T_g that balance the energy budgets (e.g., Bonan 1994), but the convergence is poor. Instead, the temperature calculations are divided into two parts.

5.2.1 Vegetation Temperature

Using T_g from the previous time step and the fluxes $\overrightarrow{S}_v$ (section 3.1), $\overrightarrow{L}_v$ (section 3.2), H_v (section 4.3), and λE_v (section 4.3), the vegetation temperature that balances the canopy energy budget is found by iteratively solving the equation

$$-\overrightarrow{S}_v + \overrightarrow{L}_v + H_v + \lambda E_v + \left(\frac{\partial \overrightarrow{L}_v}{\partial T_v} + \frac{\partial H_v}{\partial T_v} + \frac{\partial \lambda E_v}{\partial T_v} \right) \Delta T_v = 0$$

where $\Delta T_v = T_v^{n+1} - T_v^n$ and the superscript "n" indicates the iteration. The partial derivatives are

$$\frac{\partial \overrightarrow{L}_v}{\partial T_v} = 4\epsilon_v \sigma [2 - \alpha_v (1 - \alpha_g)] T_v^3$$

$$\frac{\partial H_v}{\partial T_v} = \rho_{\mathrm{atm}} C_p (c_a^h + c_g^h) \frac{c_v^h}{c_a^h + c_v^h + c_g^h}$$

$$\frac{\partial \lambda E_v}{\partial T_v} = \frac{\rho_{\mathrm{atm}} C_p}{\gamma} (c_a^w + c_g^w) \frac{c_e^w + c_t^w}{c_a^w + (c_e^w + c_t^w) + c_g^w} \frac{de_*(T_v)}{dT} \ .$$

The partial derivatives $\frac{\partial r_{ah}}{\partial T_v}$ and $\frac{\partial r_{aw}}{\partial T_v}$, which cannot be determined analytically (section 4.1), are ignored for $\frac{\partial H_v}{\partial T_v}$ and $\frac{\partial \lambda E_v}{\partial T_v}$. Instead, the stability factors ψ_m, ψ_h, and ψ_w are weighted for previous iterations as in non-vegetated surfaces.

In calculating e_s and λE_v (section 4.3), the evaporation of intercepted water $E_v \left(\frac{c_e^w}{c_e^w + c_t^w} \right) \Delta t$ should be constrained to be less than or equal to the amount of intercepted water. However, this adds additional complexity to the iterative temperature calculation, and for convenience this constraint is not included. Rather, intercepted water is allowed to be less than zero (section 8.1).

Typical values for these partial derivatives can be compared to determine the sensitivity of the energy fluxes to T_v and vice versa. For convenience, temperature dependent fluxes are evaluated at 25 ^{o}C and the ground conductances are ignored when calculating $\frac{\partial H_v}{\partial T_v}$ and $\frac{\partial \lambda E_v}{\partial T_v}$. $\frac{\partial \overrightarrow{L}_v}{\partial T_v} \approx 10$. A typical vegetation conductance for sensible heat is $c_v^h = 0.6$, so that $\frac{\partial H_v}{\partial T_v}$ ranges from 100 for unstable conditions ($r_{ah} = 10$) to 10 for stable conditions ($r_{ah} = 100$). $\frac{\partial \lambda E_v}{\partial T_v}$ varies greatly with vegetated conductances. With a wet canopy ($f_{\mathrm{wet}} = 1$), a typical conductance is $c_e^w = 0.3$ and $\frac{\partial \lambda E_v}{\partial T_v}$ at 25 ^{o}C ranges from 200 for unstable conditions ($r_{aw} = 10$) to 30 for stable conditions ($r_{aw} = 100$). With a dry canopy ($f_{\mathrm{wet}} = 0$), typical

conductances are $c_t^w = 0.02$ for unstressed vegetation and $c_t^w = 0.002$ for stressed vegetation. For unstressed vegetation, $\frac{\partial \lambda E_v}{\partial T_v}$ at 25 ^{o}C ranges from 50 for unstable conditions to 20 for stable conditions. For stressed vegetation, $\frac{\partial \lambda E_v}{\partial T_v} \approx 5$ regardless of stability. Thus, a unit change in T_v has the greatest effect on sensible heat flux and evaporation of intercepted water when the atmosphere is unstable. When stable, evaporation of intercepted water and transpiration from unstressed vegetation are the dominant terms. However, stressed vegetation is more common, in which case all fluxes are roughly equally sensitive to a unit change in T_v.

5.2.2 Ground Temperature

With T_v known, T_s and e_s are calculated. Then, using the fluxes $\overrightarrow{S}_g$ (section 3.1), $\overrightarrow{L}_g$ (section 3.2), H_g (section 4.3), λE_g (section 4.3), and G, the ground temperature that balances the ground surface energy budget is found by iteratively solving the equation

$$-\overrightarrow{S}_g + \overrightarrow{L}_g + H_g + \lambda E_g + G + \left(\frac{\partial \overrightarrow{L}_g}{\partial T_g} + \frac{\partial H_g}{\partial T_g} + \frac{\partial \lambda E_g}{\partial T_g} + \frac{\partial G}{\partial T_g} \right) \Delta T_g = 0$$

where $\Delta T_g = T_g^{n+1} - T_g^n$ and the superscript "n" indicates the iteration. The partial derivatives are

$$\frac{\partial \overrightarrow{L}_g}{\partial T_g} = 4\epsilon_g \sigma T_g^3$$

$$\frac{\partial H_g}{\partial T_g} = \frac{\rho_{\rm atm} C_p}{r'_{ah}}$$

$$\frac{\partial \lambda E_g}{\partial T_g} = \frac{\rho_{\rm atm} C_p}{\gamma (r'_{aw} + r_{\rm srf})} \frac{de_*(T_g)}{dT}$$

$$\frac{\partial G}{\partial T_g} = \frac{2k_1}{\Delta z_1} \, .$$

6. Soil Temperatures

With the heat flux F_z (W m^{-2}) at depth z equal to

$$F_z = -k\frac{\partial T}{\partial z} ,$$

one-dimensional energy conservation requires

$$\rho c\frac{\partial T}{\partial t} = -\frac{\partial F_z}{\partial z} = \frac{\partial}{\partial z}\left[k\frac{\partial T}{\partial z}\right]$$

where ρc is the volumetric soil heat capacity (J m^{-3} K^{-1}), T is the soil temperature (K), and k is the thermal conductivity (W m^{-1} K^{-1}). This equation is solved numerically to calculate soil temperatures for a six-layer soil with the boundary conditions of G, adjusted for snow melt (section 5), as the heat flux into the soil column and zero heat flux at the bottom of the soil column.

6.1 Numerical Solution

The soil column is discretized into six layers with thickness Δz_i of 0.10, 0.20, 0.40, 0.80, 1.60, and 3.20 m. Thermal properties (i.e., temperature T_i [K]; thermal conductivity k_i [W m^{-1} K^{-1}]; volumetric heat capacity c_i [J m^{-3} K^{-1}]) are defined at the center of each layer (Figure 18).

Figure 18. Schematic diagram of the multi-layer soil profile. Thermal properties (temperature T_i, thermal conductivity k_i, volumetric heat capacity c_i) are defined at the center (depth z_i) of a layer with thickness Δz_i. The hydraulic properties (volumetric water content θ_i, hydraulic conductivity k_i, and matrix potential ψ_i) are also defined at depth z_i.

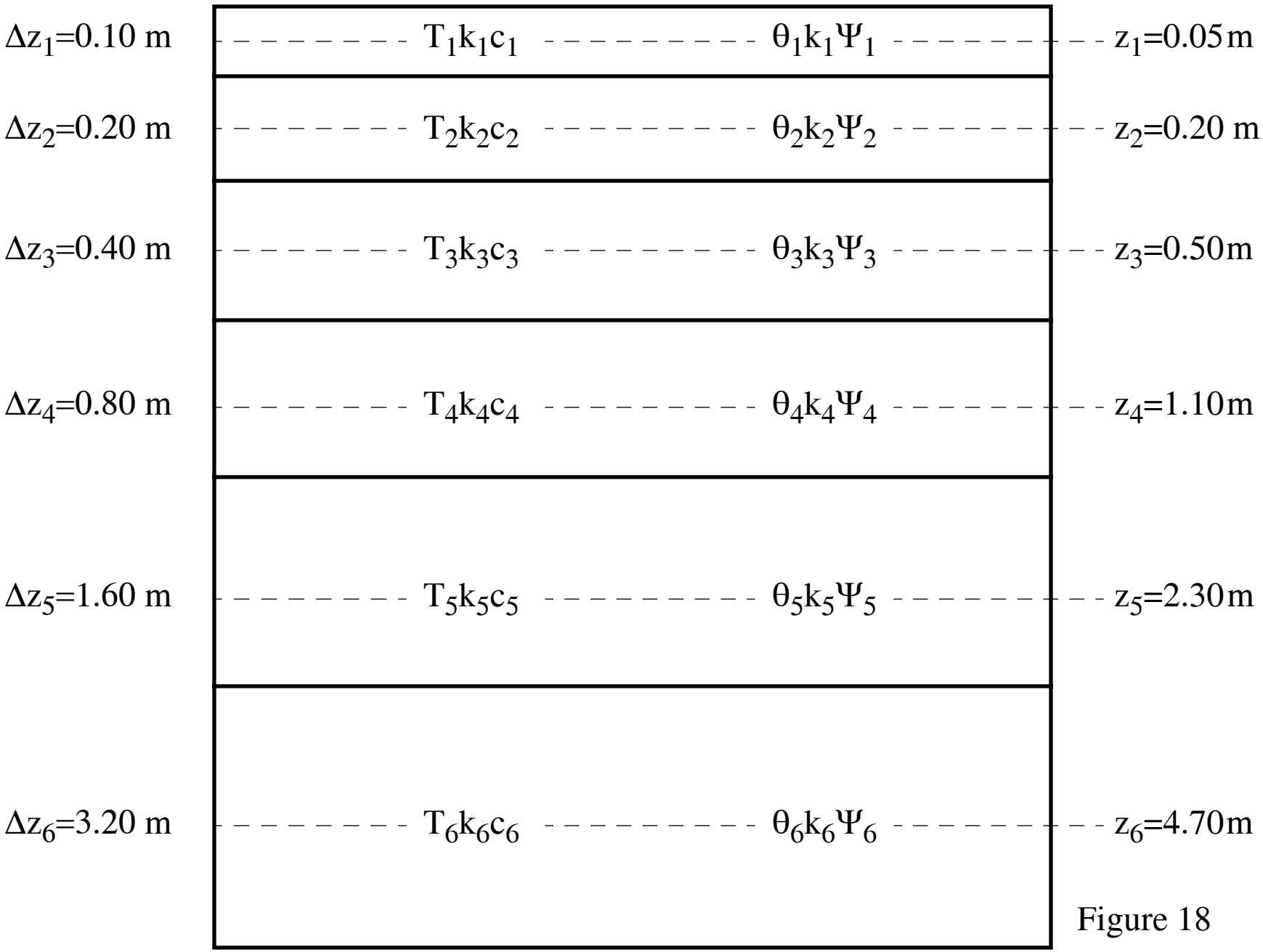
Δz_1=0.10 m
$T_1k_1c_1$
$\theta_1k_1\Psi_1$
z_1=0.05m
Δz_2=0.20 m
$T_2k_2c_2$
$\theta_2k_2\Psi_2$
z_2=0.20 m
Δz_3=0.40 m
$T_3k_3c_3$
$\theta_3k_3\Psi_3$
z_3=0.50m
Δz_4=0.80 m
$T_4k_4c_4$
$\theta_4k_4\Psi_4$
z_4=1.10m
Δz_5=1.60 m
$T_5k_5c_5$
$\theta_5k_5\Psi_5$
z_5=2.30m
Δz_6=3.20 m
$T_6k_6c_6$
$\theta_6k_6\Psi_6$
z_6=4.70m

Figure 18

The heat flux F_i (W m^{-2}) from layer i to layer $i+1$ is

$$F_i = -\left(\frac{T_i - T_{i+1}}{\frac{\Delta z_i}{2k_i} + \frac{\Delta z_{i+1}}{2k_{i+1}}}\right) ,$$

which is derived, with reference to Figure 18, assuming the heat flux from i (depth z_i) to the interface between i and $i+1$ (depth $z_i + 0.5\Delta z_i$) equals the heat flux from the interface to $i+1$ (depth z_{i+1}), i.e.,

$$-k_i\left(\frac{T_i - T_m}{\frac{1}{2}\Delta z_i}\right) = -k_{i+1}\left(\frac{T_m - T_{i+1}}{\frac{1}{2}\Delta z_{i+1}}\right)$$

where T_m is the interface temperature.

The energy balance for the i^{th} layer is

$$\frac{c_i \Delta z_i}{\Delta t}(T_i^{n+1} - T_i^n) = -F_{i-1} + F_i$$

where the superscripts n and $n+1$ indicate values at the beginning and end of the time step, respectively, and Δt is the time step (seconds). This equation is solved using the Crank-Nicholson method, which combines the explicit method with fluxes evaluated at n (F_{i-1}^n, F_i^n) and the implict method with fluxes evaluated at $n+1$ $(F_{i-1}^{n+1}, F_i^{n+1})$

$$\frac{c_i \Delta z_i}{\Delta t}(T_i^{n+1} - T_i^n) = \frac{1}{2}\left(-F_{i-1}^n + F_i^n - F_{i-1}^{n+1} + F_i^{n+1}\right) ,$$

resulting in a tridiagonal system of equations

$$r_i = a_i T_{i-1}^{n+1} + b_i T_i^{n+1} + c_i T_{i+1}^{n+1} .$$

In the following derivation of r_i, a_i, b_i, and c_i, the variables m_1, m_2, and m_3 are defined as

$$m_1 = \frac{\Delta z_{i-1}}{k_{i-1}} + \frac{\Delta z_i}{k_i}$$

$$m_2 = \frac{\Delta z_i}{k_i} + \frac{\Delta z_{i+1}}{k_{i+1}}$$

$$m_3 = \frac{\Delta t}{\Delta z_i c_i} \, .$$

For the first soil layer $i = 1$, $F_{i-1} = -G$, where G is the heat flux into the soil (positive into the soil). The resulting equations are

$$\frac{c_i \Delta z_i}{\Delta t}(T_i^{n+1} - T_i^n) = G - \left(\frac{T_i^n - T_{i+1}^n + T_i^{n+1} - T_{i+1}^{n+1}}{\frac{\Delta z_i}{k_i} + \frac{\Delta z_{i+1}}{k_{i+1}}} \right)$$

$$r_i = T_i^n + G m_3 - (T_i^n - T_{i+1}^n)\frac{m_3}{m_2}$$

$$a_i = 0$$

$$b_i = 1 + \frac{m_3}{m_2}$$

$$c_i = -\frac{m_3}{m_2} \, .$$

The boundary condition at the bottom of the soil column is zero heat flux, $F_i = 0$, resulting in for $i = 6$

$$\frac{c_i \Delta z_i}{\Delta t}(T_i^{n+1} - T_i^n) = \frac{T_{i-1}^n - T_i^n + T_{i-1}^{n+1} - T_i^{n+1}}{\frac{\Delta z_{i-1}}{k_{i-1}} + \frac{\Delta z_i}{k_i}}$$

$$r_i = T_i^n + (T_{i-1}^n - T_i^n)\frac{m_3}{m_1}$$

$$a_i = -\frac{m_3}{m_1}$$

$$b_i = 1 + \frac{m_3}{m_1}$$

$$c_i = 0 \ .$$

For the other soil layers, $1 < i < 5$,

$$\frac{c_i \Delta z_i}{\Delta t}(T_i^{n+1} - T_i^n) = \frac{(T_{i-1}^n - T_i^n + T_{i-1}^{n+1} - T_i^{n+1})}{\frac{\Delta z_{i-1}}{k_{i-1}} + \frac{\Delta z_i}{k_i}} - \frac{(T_i^n - T_{i+1}^n + T_i^{n+1} - T_{i+1}^{n+1})}{\frac{\Delta z_i}{k_i} + \frac{\Delta z_{i+1}}{k_{i+1}}}$$

$$r_i = T_i^n + (T_{i-1}^n - T_i^n)\frac{m_3}{m_1} - (T_i^n - T_{i+1}^n)\frac{m_3}{m_2}$$

$$a_i = -\frac{m_3}{m_1}$$

$$b_i = 1 + \frac{m_3}{m_1} + \frac{m_3}{m_2}$$

$$c_i = -\frac{m_3}{m_2} \ .$$

This solution conserves energy as $\sum_i \frac{c_i \Delta z_i}{\Delta t} \left(T_i^{n+1} - T_i^n\right) = G$.

6.2 Thermal Properties

An apparent heat capacity, in which the latent heat of freezing and thawing is added to the heat capacity over the temperature range $T_f \pm 0.5K$, is used to account for phase change (pp. 503-505, Lunardini 1981). The apparent heat capacity c (J m^{-3} K^{-1}) over the temperature range $T_f \pm 0.5K$ is

$$2c\Delta T = \int_{T_f - \Delta T}^{T_f} c_f dT + L + \int_{T_f}^{T_f + \Delta T} c_u dT$$

where $\Delta T = 0.5K$, T_f is the freezing point (Table 4), c_f and c_u are the frozen and unfrozen volumetric heat capacities (J m^{-3} K^{-1}), respectively, and L is the volumetric latent heat (J m^{-3}).

The soil heat capacity for the i$^{\text{th}}$ layer is therefore

$$c_i = \left\{ \begin{array}{c} c_u \text{ for } T_i > T_f + \Delta T \\ \frac{c_f + c_u}{2} + \frac{L_i}{2\Delta T} \text{ for } T_f - \Delta T \leq T_i \leq T_f + \Delta T \\ c_f \text{ for } T_i < T_f - \Delta T \end{array} \right\} .$$

$L_i = \theta_i h_{\text{fus}} \rho_w$ where θ_i is the volumetric soil water content (mm^3 mm^{-3}) of the i^{th} soil layer (section 8.4), h_{fus} is the latent heat of fusion of water (J kg^{-1}) (Table 4), and ρ_w is the density of water (kg m^{-3}) (Table 4). The unfrozen and frozen soil heat capacities vary linearly with soil water

$$c_u = (1 - \theta_{\text{sat}}) c_s + c_w \theta_i$$

$$c_f = (1 - \theta_{\text{sat}}) c_s + c_i \theta_i$$

where c_w and c_i are the heat capacities of water and ice, respectively, (Table 4), c_s is the heat capacity of soil solids, θ_i is the volumetric water content of the i^{th} soil layer (section 8.4), and θ_{sat} is the volumetric water content at saturation (porosity) (section 8.4.1). For glaciers and wetlands, $\theta_i = \theta_{\text{sat}} = 1$ so that $c_u = c_w$ and $c_f = c_i$.

Thermal conductivity is a blend of frozen and unfrozen values over the temperature range $T_f \pm 0.5K$, as recommended by Lunardini (1981)

$$k_i = \left\{ \begin{array}{c} k_u \text{ for } T_i > T_f + \Delta T \\ k_f + \frac{k_u - k_f}{2\Delta T} \left[T_i - T_f + \Delta T \right] \text{ for } T_f - \Delta T \leq T_i \leq T_f + \Delta T \\ k_f \text{ for } T_i < T_f - \Delta T \end{array} \right\} .$$

The unfrozen k_u and frozen k_f thermal conductivities (W m^{-1} K^{-1}) are calculated from Farouki (1981)

$$k_u = \left[k_s^{(1-\theta_{\rm sat})} k_w^{\theta_i} - 0.15\right] \frac{\theta_i}{\theta_{\rm sat}} + 0.15$$

$$k_f = \left[k_s^{(1-\theta_{\rm sat})} k_i^{\theta_i} - 0.15\right] \frac{\theta_i}{\theta_{\rm sat}} + 0.15$$

where k_w and k_i are the thermal conductivities of water and ice, respectively, (Table 4) and k_s is the thermal conductivity of soil solids. For glaciers and wetlands, where $\theta_i = \theta_{\rm sat} = 1$, $k_u = k_w$ and $k_f = k_i$.

The heat capacity and thermal conductivity of soil solids vary with soil texture

$$c_s = \left(\frac{2.128\ \%\text{sand} + 2.385\ \%\text{clay}}{\%\text{sand} + \%\text{clay}}\right) 10^6$$

$$k_s = \frac{8.80\ \%\text{sand} + 2.92\ \%\text{clay}}{\%\text{sand} + \%\text{clay}}\ .$$

Thermal properties for sand, loam, and clay soils are shown in Table 15. These are similar to those used by Bonan (1994, 1995a, 1995b) in earlier model versions.

When snow is on the ground, it's thermal properties are blended with the first soil layer to create a snow/soil layer with a thickness $\Delta z_1 + z_{\rm sno}$, where $z_{\rm sno}$ is the depth (m) of snow on the ground (section 8.2). The thermal conductivity and heat capacity of this layer are

$$k_1 = \frac{k_{\rm sno} k_{\rm soi} (\Delta z_1 + z_{\rm sno})}{k_{\rm sno} \Delta z_1 + k_{\rm soi} z_{\rm sno}}$$

$$c_1 = \frac{c_{\rm sno} c_{\rm soi} (\Delta z_1 + z_{\rm sno})}{c_{\rm sno} \Delta z_1 + c_{\rm soi} z_{\rm sno}}$$

where the subscripts "sno" and "soi" indicate values for snow and soil respectively. Rather than allowing for changes with bulk density and depth, $k_{\rm sno} = 0.34$ W m^{-1} K^{-1} and $c_{\rm sno} = 0.525 \times 10^6$ J m^{-3} K^{-1} are constants. The snow height used for this blended layer is constrained to ≤ 1 m. This blended snow and soil layer is also used

to calculate the soil heat flux for the surface temperature calculations (section 5). This avoids the problem of multi-layer heat transfer in snow (e.g., Goodrich 1982) while accounting for the insulating effects of snow on soil temperature (Figure 19).

Figure 19. Soil temperature as a function of depth for five soil columns with snow depths of 0, 25, 50, 75, and 100 cm. Soil temperatures were initialized to 2 ^{o}C. Thermal properties of the soil were k_f = 2.326 W m^{-1} K^{-1}, k_u = 1.861 W m^{-1} K^{-1}, c_f = 1.967 MJ m^{-3} K^{-1}, c_u = 2.862 MJ m^{-3} K^{-1}, and L = 110.5 MJ m^{-3}. Results are for a 100 day simulation with the surface temperature set to -10 ^{o}C. Deeper snow resulted in warmer soil temperatures, which is consistent with results from Goodrich (1982). Conversely, in the spring as air temperature warms, the presence of snow inhibits soil warming.

Table 15. Thermal and hydraulic properties for sand, loam, and clay soils

	Texture		
Parameter	Sand	Loam	Clay
sand (%)	92	43	22
clay (%)	3	18	58
k_s (W m^{-1} K^{-1})	8.61	7.06	4.54
c_s (MJ m^{-3} K^{-1})	2.14	2.20	2.31
b	3.39	5.77	12.13
k_{sat} (mm s^{-1})	0.0236	0.0042	0.0020
ψ_{sat} (mm)	-47	-207	-391
θ_{sat}	0.373	0.435	0.461
θ_{opt}	0.034	0.138	0.281
θ_{dry}	0.028	0.122	0.266

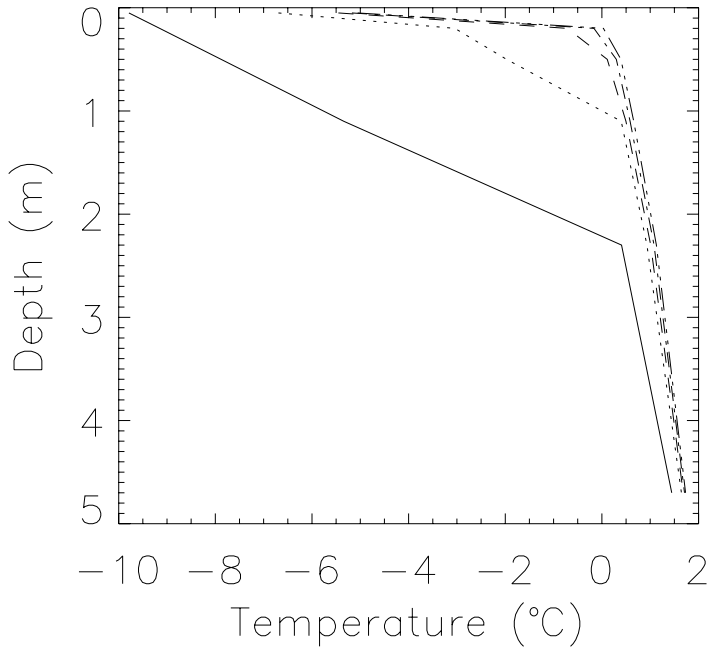
Depth (m)
0
1
2
3
4
5
−10
−8
−6
−4
−2
0
2
Temperature (°C)
z_{sno} = 0 cm
z_{sno} = 25 cm
z_{sno} = 50 cm
z_{sno} = 75 cm
z_{sno} = 100 cm

Figure 19

6.3 Accuracy of Solution

The accuracy of this numerical method was evaluated by comparing the numerical solution to Neumann's analytical solution for the following problem:

initial soil temperatures = 2^oC

surface temperature = -10^{o}C

$c_u = 2.862$ MJ m^{-3} K^{-1}

$c_f = 1.967$ MJ m^{-3} K^{-1}

$k_u = 1.861$ W m^{-1} K^{-1}

$k_f = 2.326$ W m^{-1} K^{-1}

$L = 110.5$ MJ m^{-3}.

Temperatures $T(z)$ (^{o}C) at depth z (cm) after t hours are (Jumikis 1966)

$$T(z) = T_s \left(1 - \frac{\text{erf}\left[\frac{z}{2\sqrt{\alpha_f t}}\right]}{\text{erf}\left[\frac{m}{2\sqrt{\alpha_f}}\right]} \right)$$

for $z \leq z_f$ and

$$T(z) = T_0 \left(1 - \frac{1 - \text{erf}\left[\frac{z}{2\sqrt{\alpha_u t}}\right]}{1 - \text{erf}\left[\frac{m}{2\sqrt{\alpha_u}}\right]} \right)$$

for $z > z_f$, where $z_f = m\sqrt{t}$ is the frost penetration depth (cm) after t hours, $m = 3.6$, α_u and α_f are the unfrozen and frozen thermal diffusivities $\left(\frac{k}{c}\right)$ in units of cm^2 hr^{-1}, and T_0 and T_s are the initial soil temperature and surface temperature, respectively. The error function is $\text{erf(x)} = \frac{2}{\sqrt{\pi}} \int_0^{\text{x}} \text{e}^{-\text{t}^2} \text{dt}$.

The numerical solution using the apparent heat capacity method to account for phase change compares favorably with the Neumann solution for a 63-layer soil with $\Delta z_i = 0.10$ m (Figure 20). Without phase change (i.e., $L = 0$), the soil temperatures cool too much. For the six-layer soil, the numerical solution captures the general features of the Neumann solution (Figure 21). However, soil

temperatures for a given layer decrease rapidly after the layer or deeper layers have undergone phase change and remain constant while deeper layers undergo phase change (i.e., $T_i = \pm 0.5^o C$). This results in a "blocky" temperature time-series. This problem diminishes as the soil layers become thinner, but is still apparent for $\Delta z_i = 0.10$ m (Figure 20). Bonan (1991b) found that a 25-layer soil produces results similar to those found with the 63-layer soil. In practice, a 14-layer soil is also reasonable. However, these are computationally expensive because the soil hydrology uses the same soil layers. Although the apparent heat capacity method is deficient for the 6-layer soil, the solution is better than ignoring phase change (Figure 21) and avoids the costly iteration required of other methods (Goodrich 1978, Lunardini 1981).

Figure 20. Soil temperatures at six depths for a 63-layer soil column with $\Delta z_i = 10$ cm. Results are for the numerical method with phase change and without phase change ($L = 0$) and for the Neumann solution. Soil temperatures were initialized to 2 ^{o}C. Thermal properties of the soil were $k_f = 2.326$ W m^{-1} K^{-1}, $k_u = 1.861$ W m^{-1} K^{-1}, $c_f = 1.967$ MJ m^{-3} K^{-1}, $c_u = 2.862$ MJ m^{-3} K^{-1}, and $L = 110.5$ MJ m^{-3}. Results are for 200 days with the surface temperature set to -10 ^{o}C.

Figure 21. As in Figure 20, but for the six-layer soil column.

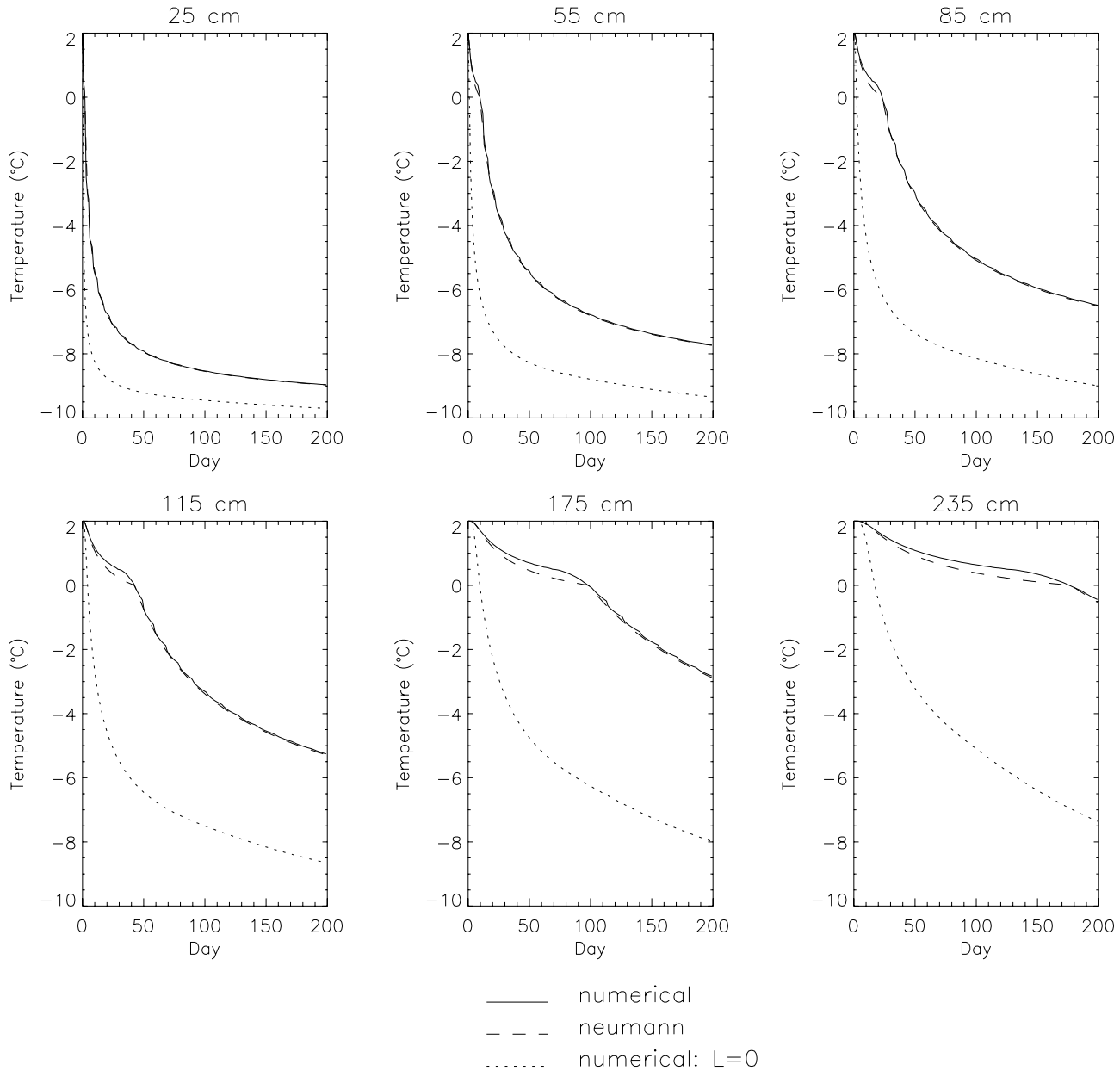
25 cm
55 cm
85 cm
115 cm
175 cm
235 cm
Temperature (°C)
Day
2
0
−2
−4
−6
−8
−10
0
50
100
150
200
numerical
neumann
numerical: L=0

Figure 20

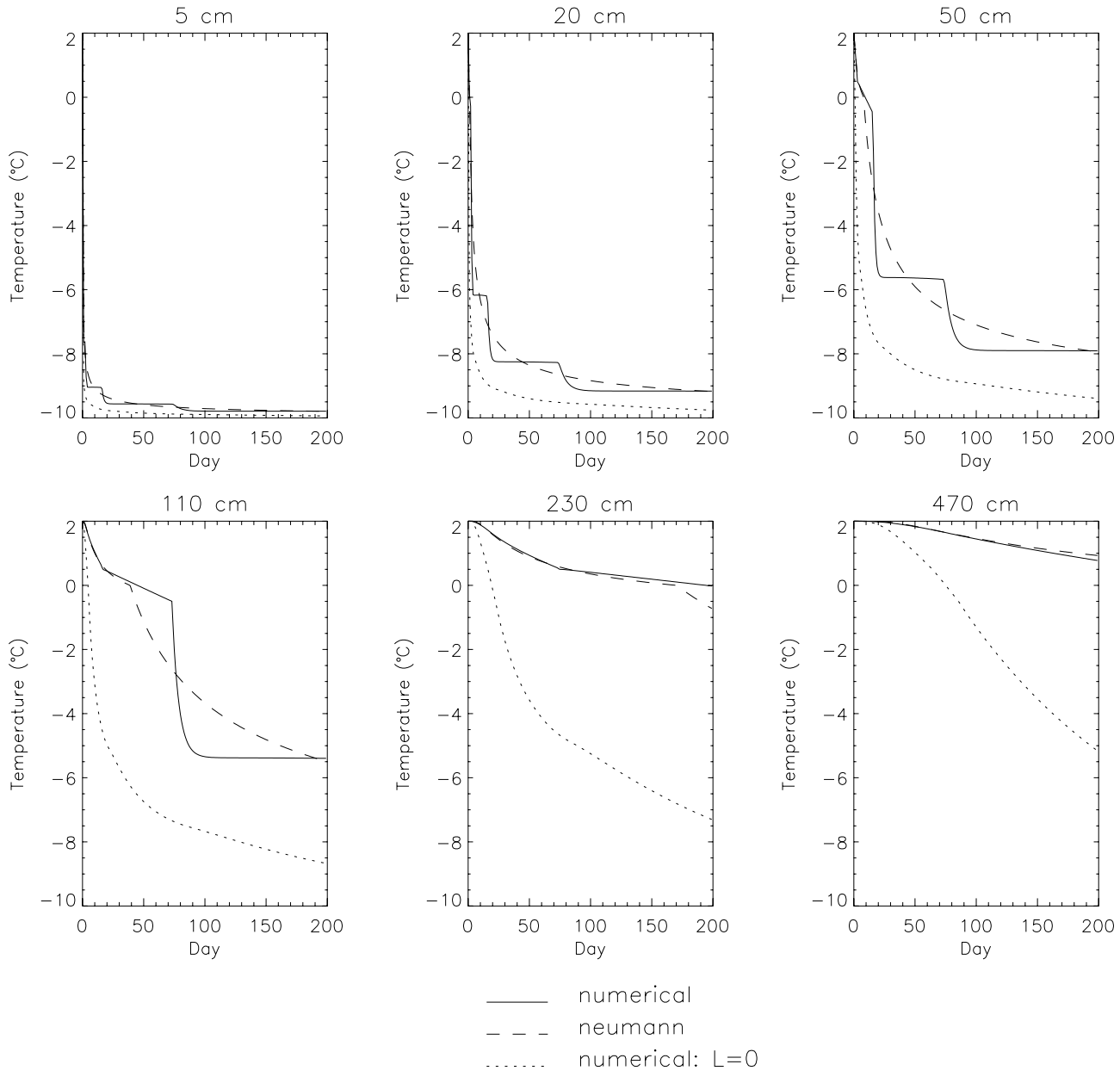
5 cm
20 cm
50 cm
110 cm
230 cm
470 cm
Temperature (°C)
Day
numerical
neumann
numerical: L=0

Figure 21

7. Lake Temperatures

Lake temperatures are calculated from a one-dimensional thermal stratification model, based on the lake models of Henderson-Sellers (1985, 1986) and Hostetler and Bartlein (1990) and the coupled lake-atmosphere model of Hostetler et al. (1993, 1994). Bonan (1995b) provides justification for many of the assumptions and documents the effects of lakes on climate. Assuming constant cross-sectional area with depth,

$$\frac{\partial T}{\partial t} = \frac{\partial}{\partial z}\left[(\kappa_m + \kappa_e)\frac{\partial T}{\partial z}\right] + \frac{1}{c_w}\frac{d\phi}{dz}$$

where T is lake temperature (K), $\kappa_m = k_w/c_w$ and κ_e are the molecular and eddy diffusion coefficients ($m^2\ s^{-1}$), k_w is the thermal conductivity of water (W m^{-1} K^{-1}) (Table 4), c_w is the heat capacity of water (J m^{-3} K^{-1}) (Table 4), and ϕ is a solar radiation heat source term (W m^{-2}). Similar to soils, this equation is solved numerically to calculate temperatures for six-layer deep and shallow lakes with the boundary conditions of zero heat flux at the bottom and the net flux of energy at the surface F_0 (W m^{-2})

$$F_0 = \beta \overrightarrow{S}_g - (\overrightarrow{L}_g + H_g + \lambda E_g + M)$$

where $\overrightarrow{S}_g$ is the solar radiation absorbed by the lake (W m^{-2}) (section 3.1), $\overrightarrow{L}_g$ is the net longwave radiation (W m^{-2}) (section 3.2), H_g is the sensible heat flux (W m^{-2}) (section 4.2), λE_g is the latent heat flux (W m^{-2}) (section 4.2), and M is snow melt (W m^{-2}) (section 5). β is the fraction of $\overrightarrow{S}_g$ absorbed in the surface layer.

Deep and shallow lakes differ in total depth. Deep lakes are 50 m deep, with layer thicknesses Δz_i of 1, 2, 4, 8, 15, and 20 m. Shallow lakes are 10 m deep, with layer thicknesses Δz_i of 0.5, 1.0, 1.5, 2.0, 2.5, and 2.5 m. Shallow lakes also differ

from deep lakes in that $\kappa_e = 0$ and there is no convective mixing. This means that shallow lake temperatures are the same as that for soil using thermal conductivity and heat capacity of water (k_w, c_w) and allowing for absorption of solar radiation with depth.

The numerical implementation of the lake model is similar to that for soil. The energy conservation equation for layers $1 < i < 5$ is

$$T_i^{n+1} - T_i^n =$$
$$m_3 \left(\frac{T_{i-1}^n - T_i^n + T_{i-1}^{n+1} - T_i^{n+1}}{m_1} - \frac{T_i^n - T_{i+1}^n + T_i^{n+1} - T_{i+1}^{n+1}}{m_2} + \frac{\phi_{i-\frac{1}{2}} - \phi_{i+\frac{1}{2}}}{c_w} \right)$$

where

$$m_1 = \frac{\Delta z_{i-1}}{\kappa_m + \kappa_{e,i-1}} + \frac{\Delta z_i}{\kappa_m + \kappa_{e,i}}$$

$$m_2 = \frac{\Delta z_i}{\kappa_m + \kappa_{e,i}} + \frac{\Delta z_{i+1}}{\kappa_m + \kappa_{e,i+1}}$$

$$m_3 = \frac{\Delta t}{\Delta z_i} .$$

For the first layer $i = 1$,

$$T_i^{n+1} - T_i^n = m_3 \left(\frac{F_0}{c_w} - \frac{T_i^n - T_{i+1}^n + T_i^{n+1} - T_{i+1}^{n+1}}{m_2} + \frac{\phi_{i-\frac{1}{2}} - \phi_{i+\frac{1}{2}}}{c_w} \right) .$$

For bottom layer $i = 6$,

$$T_i^{n+1} - T_i^n = m_3 \left(\frac{T_{i-1}^n - T_i^n + T_{i-1}^{n+1} - T_i^{n+1}}{m_1} + \frac{\phi_{i-\frac{1}{2}} - \phi_{i+\frac{1}{2}}}{c_w} \right) .$$

a_i, b_i, and c_i for the tridiagonal system of equations are defined as for soil (section 6.1), but

$$r_i = T_i^n + \frac{\phi_{i-\frac{1}{2}} - \phi_{i+\frac{1}{2}}}{c_w} m_3 + \left\{ \begin{array}{r} \frac{F_0}{c_w} m_3 - (T_i^n - T_{i+1}^n)\frac{m_3}{m_2} \text{ for } i = 1 \\ (T_{i-1}^n - T_i^n)\frac{m_3}{m_1} - (T_i^n - T_{i+1}^n)\frac{m_3}{m_2} \text{ for } 1 < i < 5 \\ (T_{i-1}^n - T_i^n)\frac{m_3}{m_1} \text{ for } i = 6 \end{array} \right\} .$$

The eddy diffusion coefficient $k_{e,i}$ (m^2 s^{-1}) for shallow lakes is zero. For deep lakes,

$$\kappa_{e,i} = \frac{k w^* z_i}{P_0(1 + 37R_i^2)} e^{-k^* z_i}$$

where k is the von Karman constant (Table 4), $P_0 = 1$ is the neutral value of the turbulent Prandtl number, z_i is depth (m), the surface friction velocity (m s^{-1}) is $w^* = 0.0012 u_2$, and k^* varies with latitude ϕ as $k^* = 6.6\sqrt{|\sin\phi|}u_2^{-1.84}$. As in Hostetler and Bartlein (1990), 2 m wind speed u_2 (m s^{-1}) is used to evaluate w^* and k^* rather than the 10 m wind used by Henderson-Sellers (1985). $u_2 = \frac{u_*}{k}\ln\left(\frac{2}{z_{0m}}\right) \geq 1$, where z_{0m} is the roughness length for momentum (m) (section 4.2) and u_* is the friction velocity (m s^{-1}) (section 4.1). The Richardson number is

$$R_i = \frac{-1 + \sqrt{1 + \frac{40 N^2 k^2 z_i^2}{w^{*2} \exp(-2k^* z_i)}}}{20} .$$

$N^2 = \frac{-g}{\rho_i}\frac{\partial \rho}{\partial z}$, where g is the acceleration due to gravity (m s^{-2}) (Table 4), ρ_i is the density of water (kg m^{-3}), and $\frac{\partial \rho}{\partial z}$ is approximated as $\frac{\rho_{i+1} - \rho_i}{z_{i+1} - z_i}$. The density of water is, as in Hostetler and Bartlein (1990),

$$\rho_i = (1 - 1.9549 \times 10^{-5}|T_i - 277|^{1.68})1000 .$$

$k_{e,i} = 0$ if the lake is frozen.

$\phi_{i-\frac{1}{2}}$ and $\phi_{i+\frac{1}{2}}$ are the solar radiation fluxes (W m^{-2}) at the top ($z = z_i - \frac{1}{2}\Delta z_i$) and bottom ($z = z_i + \frac{1}{2}\Delta z_i$) of the i^{th} layer. For $z > z_a$, where z_a is the base of the surface absorption layer, the solar radiation at depth z is (Henderson-Sellers 1986)

$$\phi(z) = (1 - \beta)\,\overrightarrow{S}_g e^{-\eta(z - z_a)}$$

where η is the light extinction coefficient for water and z_a is the base of the surface absorption layer. Henderson-Sellers (1986) noted that $z_a \approx 0.6$ m and that η ranges from 0.05 for clear water to 1.0 for turbid water. For this version of the land surface model, these parameters are globally uniform, depending only on whether the lake is deep or shallow. For deep lakes, $z_a = 0.6$ m, 40% of the solar radiation is absorbed in the surface layer ($\beta = 0.4$), and $\eta = 0.1$ so that the lakes absorb 99% of $\overrightarrow{S}_g$. For shallow lakes, $z_a = 0.5$ m (i.e., the bottom of the first layer), $\beta = 0.4$, and $\eta = 0.5$ so that the lakes absorb 99% of $\overrightarrow{S}_g$. This heat source term is applied only to unfrozen lakes. When the lake is frozen, all the solar radiation is absorbed in the surface layer.

Convective mixing in deep lakes occurs using the same scheme as in Hostetler et al.'s (1993, 1994) coupled lake-atmosphere model. Unfrozen lakes overturn when $\rho_i > \rho_{i+1}$, in which case the average temperature for layers 1 to $i + 1$ is applied to layers 1 to i+1 and the densities are updated. This scheme is applied iteratively to layers 1 through 5.

This solution conserves energy as

$$\sum_i \frac{c_w \Delta z_i}{\Delta t}\left(T_i^{n+1} - T_i^n\right) = F_0 + \sum_i \phi_{i-\frac{1}{2}} - \phi_{i+\frac{1}{2}}\,.$$

8. Hydrology

The model parameterizes interception, throughfall, snow accumulation and melt, infiltration, surface runoff, sub-surface drainage, and redistribution within the soil column to simulate canopy water W_{can}, snow water W_{sno}, and soil water $\sum_i \theta_i \Delta z_i$, where θ_i is the volumetric soil water content ($\text{mm}^3\ \text{mm}^{-3}$) and Δz_i is the soil thickness (mm) (Figure 22). All fluxes and pools of water are in units of kg $H_2O\ m^{-2}$ = mm H_2O. Fluxes are positive towards the atmosphere.

For non-irrigated soils, the total water balance of the system is

$$\Delta W_{\text{can}} + \Delta W_{\text{sno}} + \sum_i \Delta\theta_i \Delta z_i = (q_{\text{prcl}} + q_{\text{prcc}} - E_v - E_g - q_{\text{over}} - q_{\text{drai}})\Delta t$$

where Δt is the time step (seconds) and q_{prcl} is large-scale precipitation, q_{prcc} is convective precipitation, E_v is vegetation evapotranspiration (section 4), E_g is ground evaporation (section 4), q_{over} is surface runoff, i.e., overland flow (section 8.3), and q_{drai} is sub-surface drainage (section 8.4), all in units of mm s^{-1}. "Soils" are kept "saturated" (i.e., $\frac{\theta}{\theta_{\text{sat}}} = 1$) for glaciers, lakes, and wetlands. For these surfaces, q_{drai} and q_{over} equal zero. Also, some crops are "irrigated" during the growing season. Consequently, total water is conserved only for non-irrigated soils.

Figure 22. Schematic diagram of the water fluxes.

Latent heat fluxes ($W\ m^{-2}$) are converted to water fluxes (mm s^{-1}) using the latent heat of vaporization ($J\ kg^{-1}$) (Table 4) for vegetation T_v or ground T_g temperatures greater than freezing T_f (Table 4) and the latent heat of sublimation ($J\ kg^{-1}$) (Table 4) for T_v or $T_g \leq T_f$.

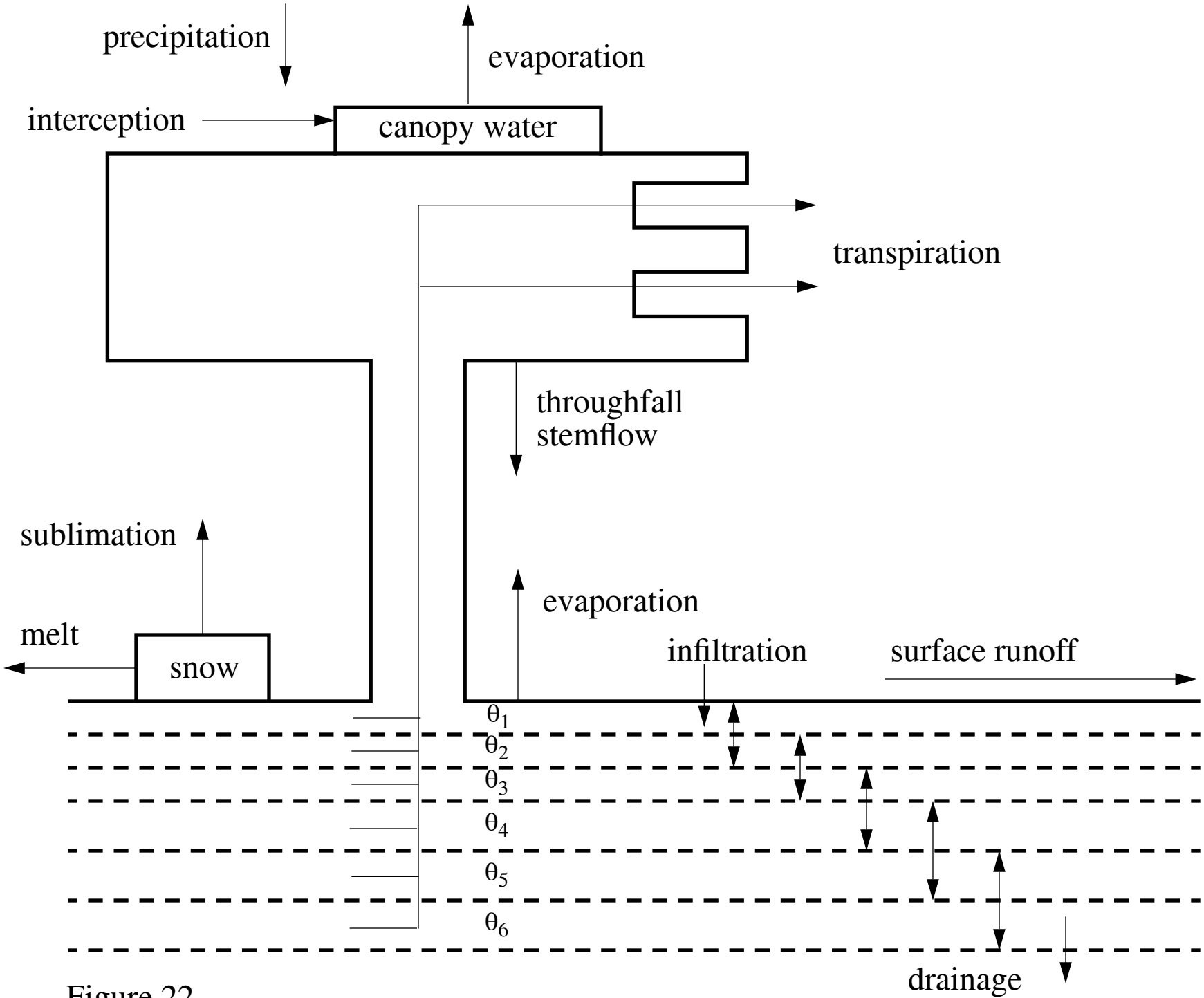
precipitation
evaporation
interception
canopy water
transpiration
throughfall
stemflow
sublimation
evaporation
melt
snow
infiltration
surface runoff
θ1
θ2
θ3
θ4
θ5
θ6
drainage

Figure 22

The total vegetation flux E_v is partitioned into canopy evaporation $q_{\rm ceva}$ (mm s^{-1}), transpiration $q_{\rm tran}$ (mm s^{-1}), and canopy dew $q_{\rm cdew}$ (mm s^{-1})

$$\begin{aligned} q_{\rm ceva} &= E_v \left(\frac{c_e^w}{c_e^w + c_t^w} \right) \text{ for } E_v > 0 \\ q_{\rm tran} &= E_v \left(\frac{c_t^w}{c_e^w + c_t^w} \right) \text{ for } E_v > 0 \\ q_{\rm cdew} &= |E_v| \text{ for } E_v < 0 \end{aligned}$$

where c_e^w and c_t^w are the evaporation and transpiration conductances (section 4.3).

The ground flux E_g is partitioned into soil evaporation $q_{\rm seva}$ (mm s^{-1}) and ground surface dew $q_{\rm sdew}$ (mm s^{-1})

$$\begin{aligned} q_{\rm seva} &= E_g \text{ for } E_g > 0 \\ q_{\rm sdew} &= |E_g| \text{ for } E_g < 0 \; . \end{aligned}$$

$q_{\rm seva}$ is adjusted for sublimation from the snow pack $q_{\rm subl}$ (mm s^{-1}) if appropriate (section 8.2). Likewise, $q_{\rm sdew}$ is added as frost to the snow pack if appropriate (section 8.2).

Three important features of the surface hydrology are (Bonan 1996): (a) Spatial heterogeneity in precipitation is included by assuming some fraction of the surface, $1 - k_c = 0.4$, receives only large-scale precipitation at a mean rate $q_{\rm prcl}$ and the remainder, $k_c = 0.6$, receives both convective and large-scale precipitation at a mean rate $q_{\rm prcl} + \frac{q_{\rm prcc}}{k_c}$. Interception and throughfall differ for these two regions based on the precipitation rate; (b) In both precipitation regions, throughfall and soil water have spatial heterogeneity (exponential distributions), which affects surface runoff and infiltration by determing the net flux of water at the surface and the infiltration capacity; and (c) Canopy, snow, and soil water pools are updated using the surface averaged fluxes (interception, throughfall, infiltration) so that there is no distinction of water pools between the two precipitation regions.

8.1 Canopy Water

Precipitation is either intercepted by the canopy or falls to the ground as throughfall and stemflow. Interception is the smaller of either 20% of precipitation or $\frac{p(L+S) - W_{\rm can}}{\Delta t}$, where L and S are the one-sided leaf and stem area indices (section 1.3) and $p(L+S)$ is the maximum water than can be held by the canopy. $p = 0.1$ mm. Any remaining precipitation falls to the ground as rain if the atmospheric temperature $T_{\rm atm} > 2.2\ ^o$C or snow if $T_{\rm atm} \leq 2.2\ ^o$C, as in BATS (Dickinson et al. 1993).

Interception and throughfall are solved for two surface regions: convective and large-scale precipitation fall over the region k_c at a mean rate $q_{\rm prcl} + \frac{q_{\rm prcc}}{k_c}$; only large-scale precipitation falls over the region $1 - k_c$ at a mean rate $q_{\rm prcl}$. Total interception $q_{\rm intr}$ and total throughfall $q_{\rm drip}$ are the weighted sums of the two regions.

Canopy water is a simple mass balance determined by gains from interception and dew and loss from evaporation

$$\frac{\Delta W_{\rm can}}{\Delta t} = q_{\rm intr} + q_{\rm cdew} - q_{\rm ceva} = q_{\rm prcc} + q_{\rm prcl} + q_{\rm cdew} - q_{\rm drip} - q_{\rm ceva}\ .$$

The wetted fraction of the canopy is, as in BATS (Dickinson et al. 1993), $f_{\rm wet} = \left[\frac{W_{\rm can}}{p(L+S)}\right]^{2/3} \leq 1$. Intercepted water is assumed to be snow, for the surface radiation calculations (section 2.1), if the vegetation temperature $T_v \leq T_f$, i.e., freezing. The energy needed to freeze and thaw intercepted water is not considered.

8.2 Snow

Snow is a simple mass balance determined by gains from the flux of snow at the ground surface and surface dew and losses from snow melt and sublimation

$$\frac{\Delta W_{\rm sno}}{\Delta t} = q_{\rm drip} + q_{\rm sdew} - q_{\rm melt} - q_{\rm subl}\ .$$

Water is added to the snowpack from throughfall, based on the temperature criterion $T_{\rm atm} \leq 2.2\ ^o$C. Water is also added as frost from surface dew if the ground temperature $T_g < T_f$. Snow melt is $q_{\rm melt} = \dfrac{M}{h_{\rm fus}}$, where M is the flux of energy (W m^{-2}) used in melting snow (section 5) and h$_{\rm fus}$ is the latent heat of fusion (J kg^{-1}) (Table 4). Water is also sublimated from the snowpack $q_{\rm subl}$, determined as the smaller of the ground evaporation $q_{\rm seva}$ or the mass of snow after melt $\dfrac{W_{\rm snow}}{\Delta t} - q_{\rm melt}$ (i.e., can not sublimate more snow than is on the ground after snow melt). Snow depth (m) is $z_{\rm sno} = \dfrac{W_{\rm sno}}{\rho_{\rm sno}}$ where $\rho_{\rm sno} = 250$ kg m^{-3} is the bulk density of snow, which is treated as a constant rather than accounting for compaction with depth. The fraction of the ground covered with snow is $f_{\rm sno} = \dfrac{z_{\rm sno}}{0.05} \leq 1$.

8.3 Infiltration and Surface Runoff

The liquid water at the soil surface (i.e., throughfall, snow melt, dew) either infiltrates into the soil column $q_{\rm infl}$ (mm s^{-1}) or is lost as surface runoff $q_{\rm over}$ (mm s^{-1}). Ignoring, for the moment, spatial heterogeneity, surface runoff (mm s^{-1}) is

$$R = \left\{ \begin{array}{c} P+Q, \text{ for } s \geq 1 \text{ and } P > 0 \\ P+Q-f^*, \text{ for } s < 1, Q \geq f^*, \text{ and } P > 0 \\ P+Q-f^*, \text{ for } s < 1, Q < f^*, \text{ and } P > f^* - Q \end{array} \right\}$$

where P is throughfall (mm s^{-1}), $Q = q_{\rm melt} + q_{\rm sdew}$ (mm s^{-1}), $s = \dfrac{\theta_1}{\theta_{\rm sat}}$ is the water content of the first soil layer relative to saturation, and f^* is the infiltration capacity (mm s^{-1}) which depends on s. All the surface water $(P+Q)$ is lost as Dunne runoff when the soil is saturated ($s \geq 1$). Horton runoff occurs when the soil is not saturated ($s < 1$) and when $P + Q > f^*$. This happens for two reasons: when $Q \geq f^*$, $P + Q > f^*$ for all $P > 0$; and when $Q < f^*$, $P + Q > f^*$ when $P > f^* - Q$. For non-soil surfaces, $R = 0$. Infiltration is $I = P + Q - R$.

Spatial heterogeneity is introduced in two ways (see also Bonan 1996). First, the mean rate of throughfall differs between the regions k_c and $1 - k_c$ (cf. section

8.1). Second, P and s have stochastic spatial distributions similar to Entekhabi and Eagleson's (1989), Pitman et al.'s (1990, 1993), Dolman and Gregory's (1992), and Johnson et al.'s (1993) work with precipitation and Entekhabi and Eagleson's (1989) and Johnson et al.'s (1993) work with soil water

$$f_P(P) = \frac{1}{\bar{P}} \exp\left(-\frac{P}{\bar{P}}\right)$$

$$f_s(s) = \frac{1}{\bar{s}} \exp\left(-\frac{s}{\bar{s}}\right)$$

where $\bar{P}$ is the average throughfall (mm s^{-1}) for the region k_c or $1 - k_c$ and $\bar{s}$ is the average s. Consequently I and R are solved separately for each region assuming an exponential distribution of throughfall and soil water within the region and a constant rate of snow melt and surface dew. Total surface runoff q_{over} and infiltration q_{infl} are the weighted sums of the two regions.

Runoff for each region is given by

$$\begin{aligned} R = & \int_1^\infty \int_0^\infty (P + Q)\, f_P(P)\, dP\, f_s(s)\, ds + \\ & \int_{s_Q}^1 \int_0^\infty (P + Q - f^*)\, f_P(P)\, dP\, f_s(s)\, ds + \\ & \int_0^{s_Q} \int_{f^* - Q}^\infty (P + Q - f^*)\, f_P(P)\, dP\, f_s(s)\, ds \end{aligned}$$

where s_Q is the value of s at which $Q \geq f^*$. The first term is the Dunne runoff for the area $s \geq 1$. The next two terms are the Horton runoff for the area $0 \leq s < 1$.

The solution to R requires a physically realistic infiltration capacity that is easily integrated with respect to s. As in Entekhabi and Eagleson (1989)

$$f^* = k_{\text{sat}} v s + k_{\text{sat}}(1 - v)$$

where k_{sat} is the saturated hydraulic conductivity (mm s^{-1}), $v = \dfrac{-(d\psi/ds)}{0.5\Delta z_1}$ evaluated for $s = 1$, ψ is the soil matrix potential (mm), and $\Delta z_1 = 100$ mm is the

thickness of the first soil layer, with hydraulic properties defined at depth $0.5\Delta z_1$. Expressions for $k_{\rm sat}$ and ψ are given in section 8.4.1. The value of s at which $Q \geq f^*$ is $s_Q = \dfrac{Q - k_{\rm sat}(1-v)}{k_{\rm sat} v}$.

The solution to R is $R = f_1 + f_2 + f_3$, where f_1 is the Dunne runoff from the area with $s \geq 1$ and $P > 0$

$$f_1 = (\bar{P} + Q)\exp\left(-\frac{1}{\bar{s}}\right) ,$$

f_2 is the Horton runoff from the area $s_Q \leq s < 1$ (i.e., $s < 1$, $Q \geq f^*$) and $P > 0$

$$f_2 = [\bar{P} + Q - k_{\rm sat}(1-v)]\left[\exp\left(-\frac{s_Q}{\bar{s}}\right) - \exp\left(-\frac{1}{\bar{s}}\right)\right] + k_{\rm sat} v \left[(1+\bar{s})\exp\left(-\frac{1}{\bar{s}}\right) - (s_Q + \bar{s})\exp\left(-\frac{s_Q}{\bar{s}}\right)\right] ,$$

and f_3 is the Horton runoff from the area $0 \leq s < s_Q$ (i.e., $s < 1$, $Q < f^*$) and $P > f^* - Q$

$$f_3 = \frac{\bar{P}^2}{\bar{P} + k_{\rm sat} v \bar{s}} \exp\left[\frac{Q - k_{\rm sat}(1-v)}{\bar{P}}\right]\left[1 - \exp\left(-\frac{s_Q}{\bar{s}} - \frac{s_Q k_{\rm sat} v}{\bar{P}}\right)\right] .$$

With $Q = 0$, $s_Q = 1$ and this equation reduces to Equation (15) in Entekhabi and Eagleson (1989). This runoff parameterization differs from Entekhabi and Eagleson (1989) in that it allows for a constant rate of snow melt and surface dew. It differs from Pitman et al. (1990, 1993) in that only throughfall, not the net flux of water at the surface, has an exponential distribution.

This runoff parameterization was found to give too much surface runoff, resulting in dry soils, when coupled to a GCM (Bonan 1996). The Dunne runoff was adjusted as $P + Q - k_{\rm sat}$ for $s \geq 1$ and $P > k_{\rm sat} - Q$, resulting in

$$f_1 = \int_1^\infty \int_{k_{\rm sat}-Q}^\infty (P + Q - k_{\rm sat})\, f_P(P)\, dP\, f_s(s)\, ds = \bar{P}\exp\left(\frac{Q - k_{\rm sat}}{\bar{P}} - \frac{1}{\bar{s}}\right)$$

for $Q < k_{\rm sat}$ and

Figure 23. Surface runoff in relation to precipitation for an unvegetated surface (i.e., throughfall = precipitation). Data are for sand (92% sand, 3% clay), loam (43% sand, 18% clay), and clay (22% sand, 58% clay) soils, with the hydraulic properties listed in Table 15, using the standard and adjusted Dunne runoff and with q_{melt} equal to 0 and 9 mm hr^{-1}. a) Saturated soil, $\theta_1 = \theta_{\mathrm{sat}}$. b) Dry soil, $\theta_1 = 0.75\theta_{\mathrm{sat}}$.

$$f_1 = (\bar{P} + Q - k_{\mathrm{sat}})\exp\left(-\frac{1}{\bar{s}}\right)$$

for $Q > k_{\mathrm{sat}}$. This adjusted Dunne runoff greatly reduces surface runoff compared to the standard method (Figure 23).

8.4 Soil Water

Soil water is calculated from the conservation equation

$$\frac{\Delta\theta\Delta z}{\Delta t} = -q_i + q_o - e$$

where θ is the volumetric soil water content (mm^3 mm^{-3}), Δz is the soil thickness (mm), Δt is the time step (seconds), e is the evapotranspiration loss (mm s^{-1}), and q_i and q_o are the fluxes of water (mm s^{-1}) into and out of the soil (positive in the upwards direction). Vertical water flow in an unsaturated porous media is described by Darcy's law

$$q = -k\left[\frac{\partial(\psi + z)}{\partial z}\right] = -k\left(\frac{\partial\psi}{\partial z} + 1\right) = -k\left(\frac{\partial\theta}{\partial z}\frac{\partial\psi}{\partial\theta} + 1\right)$$

where k is the hydraulic conductivity (mm s^{-1}), ψ is the soil matrix potential (mm), and z is height (mm) above some datum in the soil column. Setting $e = 0$, so that $\frac{\Delta\theta}{\Delta t} = -\left(\frac{q_i - q_o}{\Delta z}\right)$, i.e. $\frac{\partial\theta}{\partial t} = -\frac{\partial q}{\partial z}$, results in the Richards equation

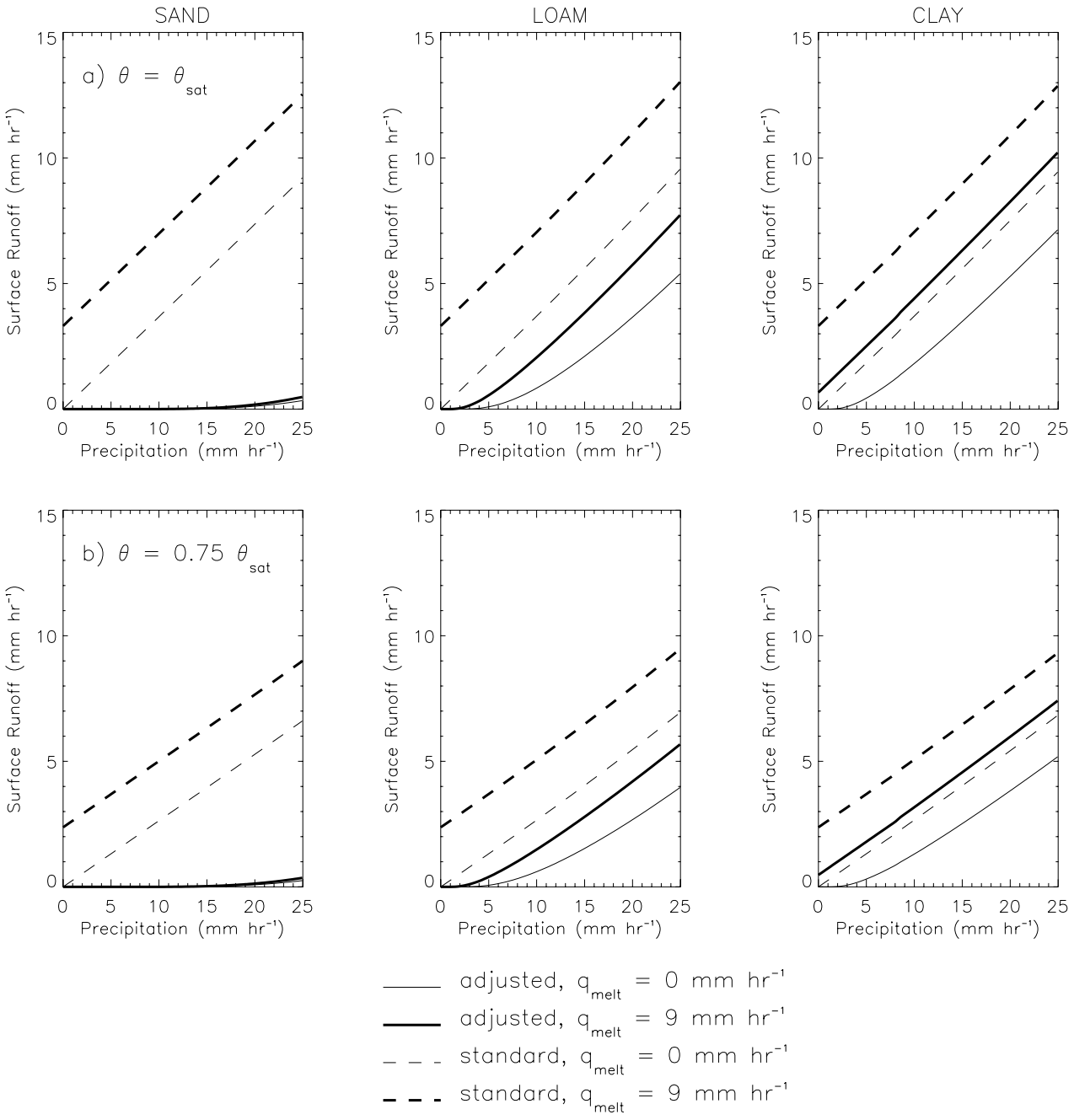
SAND
LOAM
CLAY
a) θ = θsat
b) θ = 0.75 θsat
Surface Runoff (mm hr-1)
Precipitation (mm hr-1)
0
5
10
15
20
25
adjusted, qmelt = 0 mm hr-1
adjusted, qmelt = 9 mm hr-1
standard, qmelt = 0 mm hr-1
standard, qmelt = 9 mm hr-1

Figure 23

$$\frac{\partial \theta}{\partial t} = \frac{\partial}{\partial z}\left[k\left(\frac{\partial \theta}{\partial z}\frac{\partial \psi}{\partial \theta} + 1\right)\right] .$$

This equation, with $e = q_{\text{seva}} + q_{\text{tran}}$ (i.e., soil evaporation and transpiration) and with the boundary conditions of q_{infl} as the flux of water into the soil and gravitational drainage $q_{\text{drai}} = k$ as the flux of water at the bottom of the soil column, is numerically implemented for a six-layer soil to calculate soil water. For irrigated crops, soil layers to a depth of 1 m are kept saturated during the growing season (i.e., when leaf area index is greater than zero). Consequently, soil water is conserved only for non-irrigated soils, where

$$\sum_i \Delta\theta_i \Delta z_i = (q_{\text{infl}} - q_{\text{seva}} - q_{\text{tran}} - q_{\text{drai}})\Delta t .$$

8.4.1 Hydraulic Properties

The hydraulic conductivity k and the soil matrix potential ψ vary with θ and soil texture based on the work of Clapp and Hornberger (1978) and Cosby et al. (1984). For the i^{th} layer,

$$k_i = k_{\text{sat}} s_i^{2b+3}$$

$$\psi_i = \psi_{\text{sat}} s_i^{-b}$$

where $s_i = \dfrac{\theta_i}{\theta_{\text{sat}}}$. Cosby et al. (1984) empirically related the hydraulic conductivity at saturation k_{sat} (mm s^{-1}), the matrix potential at saturation ψ_{sat} (mm), the water content at saturation θ_{sat} (i.e., porosity), and b to %sand and %clay

$$k_{\text{sat}} = 0.0070556 \times 10^{-0.884+0.0153(\%\text{sand})}$$

$$\psi_{\text{sat}} = -10.0 \times 10^{1.88-0.0131(\%\text{sand})}$$

$$\theta_{\text{sat}} = 0.489 - 0.00126(\%\text{sand})$$

$$b = 2.91 + 0.159(\%\text{clay}) \ .$$

From the definition of ψ, the water content when the soil is dry θ_{dry} and the optimal water content for evapotranspiration θ_{opt}, which are used to calculate β_e (section 4.2) and β_t (section 9.1), are

$$\theta_{\text{dry}} = \theta_{\text{sat}} \left(\frac{-316230}{\psi_{\text{sat}}} \right)^{-\frac{1}{b}}$$

$$\theta_{\text{opt}} = \theta_{\text{sat}} \left(\frac{-158490}{\psi_{\text{sat}}} \right)^{-\frac{1}{b}} \ .$$

Typical values for sand, loam, and clay soils are listed in Table 15. The small differences between θ_{opt} and θ_{dry} result in a "step" response of evapotranspiration to soil water, in which the β factors are for the most part either zero or one.

8.4.2 Numerical Solution

As with soil temperatures, the soil column is discretized into six layers with thickness Δz_i of 100, 200, 400, 800, 1600, and 3200 mm. Hydraulic properties (i.e., water content θ_i [mm^3 mm^{-3}]; hydraulic conductivity k_i [mm s^{-1}]; matrix potential ψ_i [mm]) are defined at the center of each layer with depth z_i (mm) (Figure 18).

Analogous to the soil heat flux (section 6.1), the flux of water q_i (mm s^{-1}) between layers i and $i+1$ is

$$q_i = -\left[\frac{(\psi_i + z_i) - (\psi_{i+1} + z_{i+1})}{\frac{\Delta z_i}{2k_i} + \frac{\Delta z_{i+1}}{2k_{i+1}}} \right]$$

where with $z_i - z_{i+1} = (\Delta z_i + \Delta z_{i+1})/2$,

$$q_i = - \left[\frac{2(\psi_i - \psi_{i+1}) + (\Delta z_i + \Delta z_{i+1})}{\frac{\Delta z_i}{k_i} + \frac{\Delta z_{i+1}}{k_{i+1}}} \right] .$$

These equations are derived, with reference to Figure 18, assuming the water flux from i (depth z_i) to the interface between i and $i+1$ (depth $z_i + 0.5\Delta z_i$) equals the water flux from the interface to $i+1$ (depth z_{i+1}), i.e.,

$$-k_i \left[\frac{(\psi_i + z_i) - (\psi_m + z_m)}{\frac{1}{2}\Delta z_i} \right] = -k_{i+1} \left[\frac{(\psi_m + z_m) - (\psi_{i+1} + z_{i+1})}{\frac{1}{2}\Delta z_{i+1}} \right]$$

where ψ_m is the interface matrix potential and z_m is the interface depth.

The water balance for the i^{th} layer is

$$\frac{\Delta\theta_i \Delta z_i}{\Delta t} = -q_{i-i} + q_i - e_i \ .$$

ψ and k are non-linear functions of θ (section 8.4.1) so that $q_i = f(\theta_i, \theta_{i+1})$. With q_i approximated as

$$q_i = q_i^n + \frac{\partial q_i}{\partial \theta_i}\Delta\theta_i + \frac{\partial q_i}{\partial \theta_{i+1}}\Delta\theta_{i+1} \ ,$$

where q_i^n is the water flux evaluated at the beginning of the time step, the water balance for the i^{th} layer is

$$e_i + q_{i-1}^n - q_i^n = - \left[\frac{\partial q_{i-1}}{\partial \theta_{i-1}} \right] \Delta\theta_{i-1} + \left[\frac{\partial q_i}{\partial \theta_i} - \frac{\partial q_{i-1}}{\partial \theta_i} - \frac{\Delta z_i}{\Delta t} \right] \Delta\theta_i + \left[\frac{\partial q_i}{\partial \theta_{i+1}} \right] \Delta\theta_{i+1} \ ,$$

which is a tridiagonal system of equations for $\Delta\theta$.

Defining $u = -2(\psi_i - \psi_{i+1}) - (\Delta z_i + \Delta z_{i+1})$ and $v = \Delta z_i k_i^{-1} + \Delta z_{i+1} k_{i+1}^{-1}$,

$$\frac{\partial q_i}{\partial \theta_i} = \left[-2v \frac{d\psi_i}{d\theta_i} + u \frac{\Delta z_i}{k_i^2} \frac{d\ k_i}{d\theta_i} \right] v^{-2}$$

$$\frac{\partial q_i}{\partial \theta_{i+1}} = \left[2v \frac{d\psi_{i+1}}{d\theta_{i+1}} + u \frac{\Delta z_{i+1}}{k_{i+1}^2} \frac{d\ k_{i+1}}{d\theta_{i+1}} \right] v^{-2}$$

where from section (8.4.1),

$$\frac{d\ k_i}{d\theta_i} = \left(\frac{2b+3}{\theta_i} \right) k_i$$

$$\frac{d\psi_i}{d\theta_i} = - \left(\frac{b}{\theta_i} \right) \psi_i \ .$$

The boundary conditions are $q_{i-1} = -q_{\rm infl}$ for the first soil layer (i=1) and $q_i = -k_i$ for the bottom soil layer (i=6). Surface evaporation is removed from the first soil layer and transpiration is removed from each soil layer in proportion to the relative root abundance r_i (section 1.2) so that $e_i = q_{\rm seva} + q_{\rm tran} r_i$ for the first soil layer and $e_i = q_{\rm tran} r_i$ for the other layers. The water balance for the first soil layer (i=1) is, therefore,

$$\frac{\Delta\theta_i \Delta z_i}{\Delta t} = q_{\rm infl} + q_i - e_i$$

and

$$e_i - q_{\rm infl} - q_i^n = \left[\frac{\partial q_i}{\partial \theta_i} - \frac{\Delta z_i}{\Delta t} \right] \Delta\theta_i + \left[\frac{\partial q_i}{\partial \theta_{i+1}} \right] \Delta\theta_{i+1} \ .$$

For the bottom layer (i=6), $q_i = -k_i = -k_i^n - \dfrac{d\ k_i}{d\theta_i} \Delta\theta_i$ so that the water balance is

$$e_i + q_{i-1}^n + k_i^n = - \left[\frac{\partial q_{i-1}}{\partial \theta_{i-1}} \right] \Delta\theta_{i-1} - \left[\frac{d\ k_i}{d\theta_i} + \frac{\partial q_{i-1}}{\partial \theta_i} + \frac{\Delta z_i}{\Delta t} \right] \Delta\theta_i \ .$$

The sub-surface drainage is $q_{\rm drai} = -q_i$.

From physical constraints, $0 \le \theta_i \le \theta_{\rm sat}$. To help prevent negative θ_i or $\theta_i > \theta_{\rm sat}$, a partial time step $< \Delta t$ is used for the soil water calculations when $\Delta t > 600$

s (10 min). This partial time step is 600 s (10 min) for $\Delta t = 1200$ s (20 min) and $\Delta t = 1800$ s (30 min). Otherwise, the time step is $0.5\Delta t$. Partial time steps > 600 s are not recommended. Despite this small time step, soil water may still exceed the physical constraints. Any soil water in excess of saturation $\sum_i (\theta_i - \theta_{\rm sat})\Delta z_i$ is added back to the soil, starting at the top, to bring each successive soil layer to saturation. Any remaining excess water is added to the sub-surface drainage $q_{\rm drai}$. Likewise, if $\theta_i < 0.01$, water is removed from layer $i+1$ (i.e., the immediately lower layer) to bring $\theta_i = 0.01$. These two "fixes" are rarely needed.

The validity of this numerical scheme is illustrated in Figure 24 for drainage and infiltration problems. In Figure 24a, sand, loam, and clay soil columns were initialized at saturation and allowed to drain, with no evapotranspiration loss, for 48 hours. The sand drained fastest, followed by the loam, and then the clay. Drainage for the upper soil layers essentially ceased after 24 hours, with soil water contents close to field capacity. This is consistent with the definition of field capacity (i.e., soil water after more than 24 hours of drainage). In Figure 24b, the soils were initialized to dry values and water was allowed to infiltrate at the rate $k_{\rm sat}$, again with no evapotranspiration loss. All soils showed the classic wetting front, with the sand becoming saturated within 30 hours and the loam and clay having slower wetting.

Figure 24. Soil water profiles for sand (92% sand, 3% clay), loam (43% sand, 18% clay), and clay (22% sand, 58% clay) soils, with the hydraulic properties listed in Table 15, over a 48 hour period. a) Drainage from saturated soils. b) Wetting of dry soils with infiltration equal to the saturated hydraulic conductivity.

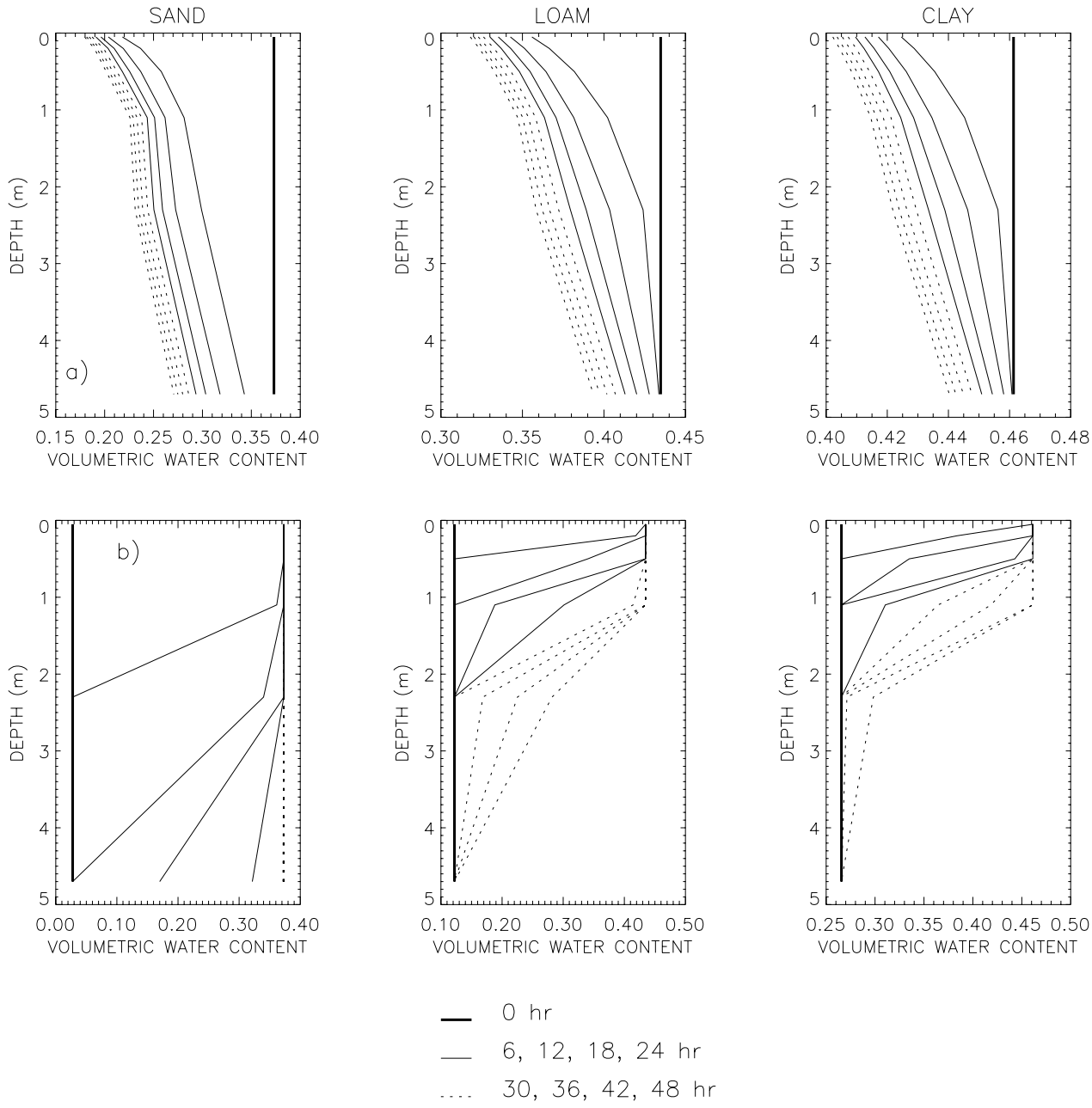
SAND
LOAM
CLAY
DEPTH (m)
VOLUMETRIC WATER CONTENT
a)
b)
0 hr
6, 12, 18, 24 hr
30, 36, 42, 48 hr

Figure 24

9. Surface CO_2 Fluxes

Building upon the work of Bonan (1991a, 1993a, 1993b, 1995a), the model simulates land-atmosphere exchange of CO_2 from plant growth (photosynthetic CO_2 uptake; maintenance and growth respiration CO_2 loss) and CO_2 loss from microbial respiration (i.e., decomposition) (Figure 25). Photosynthesis is coupled to the stomatal resistance parameterization and hence is an integral part of the surface energy fluxes. Maintenance, growth, and microbial respiration are biogeochemical fluxes that do not affect the biophysical fluxes.

Figure 25. Schematic diagram of the CO_2 fluxes. Plant respiration has two components: maintenance R_m and growth R_g respiration for foliage, stem, and root biomass.

9.1 Photosynthesis and Stomatal Resistance

Leaf stomatal resistance, which is needed for the latent heat flux (section 4.3), is coupled to leaf photosynthesis in a manner similar to Collatz et al. (1991) (see also Sellers et al. 1992)

$$\frac{1}{r_s} = m\frac{A}{c_s}\frac{e_s}{e_i}P_{\text{atm}} + b$$

where r_s is leaf stomatal resistance (s m^2 μmol^{-1}), m is an empirical parameter, A is leaf photosynthesis (μmol CO_2 m^{-2} s^{-1}), c_s is the CO_2 concentration at the leaf surface (Pa), e_s is the vapor pressure at the leaf surface (Pa), e_i is the saturation vapor pressure (Pa) inside the leaf at the vegetation temperature T_v, P_{atm} is the atmospheric pressure (Pa), and b is the minimum stomatal conductance (μmol m^{-2} s^{-1}) when $A = 0$. The difference between this equation and that used by Collatz

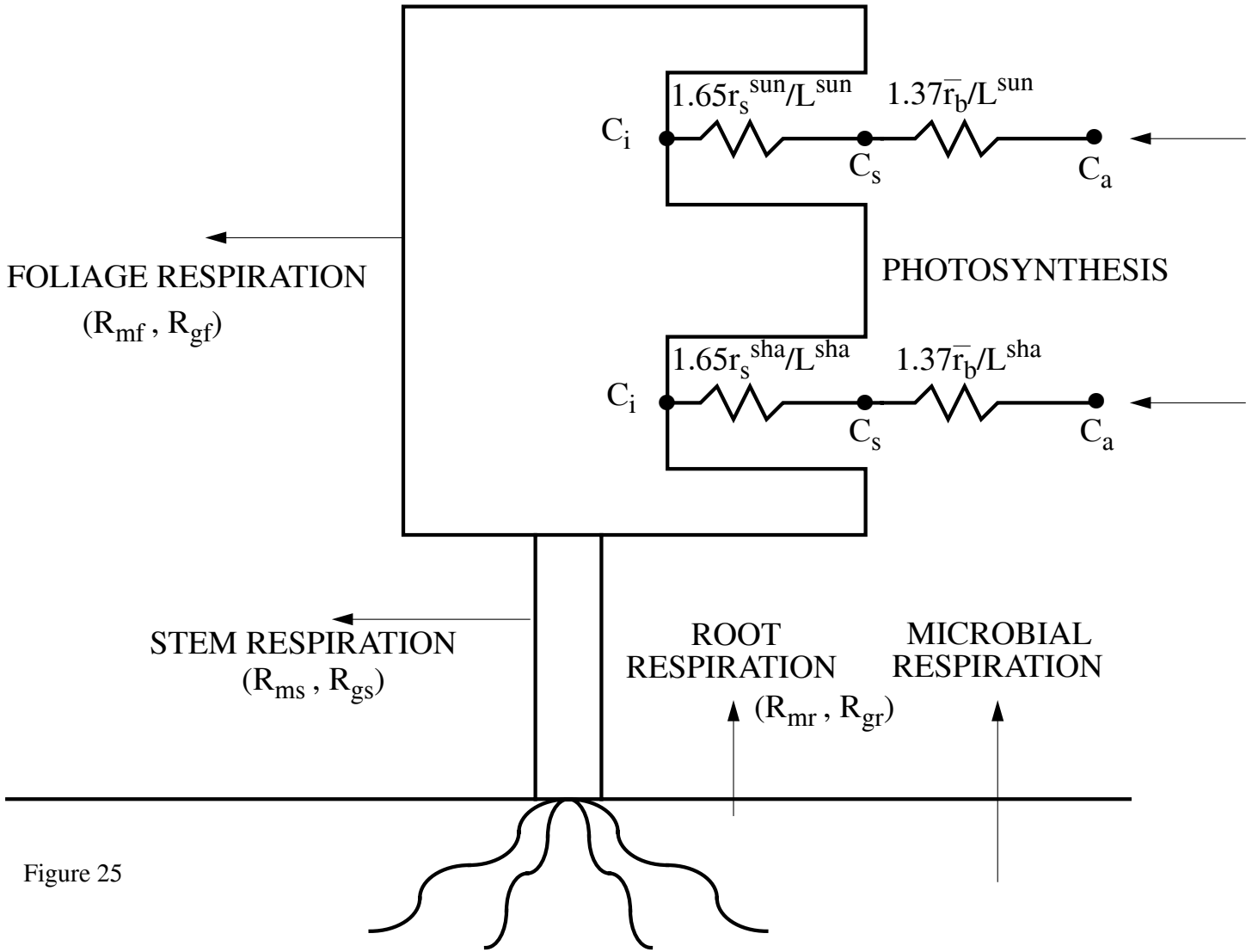
$1.65r_s^{sun}/L^{sun}$
$1.37\bar{r}_b/L^{sun}$
C_i
C_s
C_a
FOLIAGE RESPIRATION
(R_{mf} , R_{gf})
PHOTOSYNTHESIS
$1.65r_s^{sha}/L^{sha}$
$1.37\bar{r}_b/L^{sha}$
C_i
C_s
C_a
STEM RESPIRATION
(R_{ms} , R_{gs})
ROOT
RESPIRATION
(R_{mr} , R_{gr})
MICROBIAL
RESPIRATION

Figure 25

$\frac{\text{s m}^2}{\text{mol}} \times \frac{\text{mol}}{\text{m}^3} = \frac{\text{s}}{\text{m}}$. The volume ($\text{m}^3$) of 1 mol of gas at a temperature T (K) and pressure P (Pa) is $V = \frac{nRT}{P}$, where $n = 1$, R=8.314 m^3 Pa mol^{-1} K^{-1}. Consequently, 1 s m^{-1} = $8.314 \times 10^{-6} \frac{T}{P}$ s m^2 μmol^{-1}.

et al. (1991) is that they used net photosynthesis (i.e., photosynthesis minus respiration) instead of photosynthesis. Collatz et al.'s (1991) derivation of this equation is empirical, using net photosynthesis. However, use of net photosynthesis causes stomatal conductance to be less than the minimum conductance b at night or in the winter, when plants do not photosynthesize but still respire. In contrast, using photosynthesis ensures that stomatal conductance equals b when there is no photosynthesis.

Leaf photosynthesis is $A = \min(w_c, w_j, w_e)$. $A = 0$ when the vegetation temperature T_v (section 5.2) $\leq T_{\min}$. Photosynthesis in C_3 plants is based on the models of Farquhar et al. (1980) and Collatz et al. (1991). Photosynthesis in C_4 plants is based on the models of Collatz et al. (1992) and Dougherty et al. (1994). The RuBP carboxylase (Rubisco) limited rate of carboxylation is

$$w_c = \left\{ \begin{array}{r} \frac{(c_i - \Gamma_*)V_{\max}}{c_i + K_c\,(1 + o_i/K_o)} \quad \text{for } C_3 \text{ plants} \\ V_{\max} \quad \text{for } C_4 \text{ plants} \end{array} \right\} .$$

The maximum rate of carboxylation allowed by the capacity to regenerate RuBP (i.e., the light limited rate) is

$$w_j = \left\{ \begin{array}{r} \frac{(c_i - \Gamma_*)4.6\phi\alpha}{c_i + 2\Gamma_*} \quad \text{for } C_3 \text{ plants} \\ 4.6\phi\alpha \quad \text{for } C_4 \text{ plants} \end{array} \right\} .$$

The export limited rate of carboxylation for C_3 plants and the PEP carboxylase limited rate of carboxylation for C_4 plants is

$$w_e = \left\{ \begin{array}{r} 0.5V_{\max} \text{ for C}_3 \text{ plants} \\ 4000V_{\max}\dfrac{c_i}{P_{\text{atm}}} \text{ for C}_4 \text{ plants} \end{array} \right\} .$$

Collatz et al. (1992) used the term $18000V_{\max}$ (their k) for C_4 w_e. However, when this value was used, photosynthesis saturated at extremely low values of ambient CO_2. The term $4000V_{\max}$ resulted in saturation at about 400 ppm, which is more consistent with observations.

In these equations, c_i is the internal leaf CO_2 concentration (Pa) and $o_i = 0.209P_{\text{atm}}$ is the O_2 concentration (Pa). K_c and K_o, the Michaelis-Menten constants (Pa) for CO_2 and O_2, vary with vegetation temperature T_v (^{o}C) as in Collatz et al. (1991) $K_c = K_{c25}a_{kc}^{\frac{T_v-25}{10}}$ and $K_o = K_{o25}a_{ko}^{\frac{T_v-25}{10}}$, where K_{c25} and K_{o25} are values (Pa) at 25^{o}C and a_{kc} and a_{ko} are temperature sensitivity parameters. $\Gamma_* = \dfrac{1}{2}\dfrac{K_c}{K_o}0.21o_i$ is the CO_2 compensation point (Pa). The term 0.21 represents the ratio of maximum rates of oxygenation to carboxylation, which is virtually constant with temperature (Farquhar and von Caemmerer 1982). α is the quantum efficiency (μmol CO_2 per μmol photon), and ϕ is the absorbed photosynthetically active radiation (W m^{-2}) (section 3.1), which is converted to photosynthetic photon flux assuming 4.6 μmol photons per Joule.

The maximum rate of carboxylation varies with temperature, foliage nitrogen, and soil water

$$V_{\max} = V_{\max 25}a_{\text{vmax}}^{\frac{T_v-25}{10}}f(N)f(T_v)\beta_t$$

where $V_{\max 25}$ is the value at 25^{o}C (μmol CO_2 m^{-2} s^{-1}) and a_{vmax} is a temperature sensitivity parameter. $f(T_v)$ is a function that mimics thermal breakdown of metabolic processes (Farquhar et al. 1980, Collatz et al. 1991)

$$f(T_v) = \left[1 + \exp\left(\frac{-220000 + 710(T_v + 273.16)}{8.314(T_v + 273.16)}\right)\right]^{-1} .$$

$f(N) = \dfrac{N}{N_{\max}} \leq 1$ adjusts the rate of photosynthesis for foliage nitrogen N (section 1.2). Currently, $f(N) = 1$ so that values of $V_{\max 25}$ already include nitrogen limitation. β_t is a heuristic function, ranging from one when the soil is wet to zero when the soil is dry, that decreases photosynthesis and increases stomatal resistance as the soil drys

$$\beta_t = \sum_i w_i r_i$$

where w_i is the available water in the ith soil layer relative to an optimal water content and r_i is the relative root abundance in the ith soil layer (section 1.2).

$$w_i = \left\{ \begin{array}{ll} \left(\dfrac{\theta_i - \theta_{\rm dry}}{\theta_{\rm opt} - \theta_{\rm dry}} \right)^{v_w} & \leq 1 \text{ for } T_i > T_f \\ & \\ & 0.01 \text{ for } T_i \leq T_f \end{array} \right\}$$

where θ_i is the water content of the i^{th} soil layer (section 8.4), $\theta_{\rm opt}$ is the optimal water content for evapotranspiration (section 8.4.1), $\theta_{\rm dry}$ is the water content when evapotranspiration ceases (section 8.4.1), and T_i is the temperature of the i^{th} soil layer (section 6). v_w is a vegetation-dependent parameter that allows for different plant responses to soil water. Currently, $v_w = 1$. These equations limit transpiration to periods with soil temperatures greater than freezing T_f (Table 4).

The CO_2 concentration at the leaf surface c_s (Pa), the internal leaf CO_2 concentration c_i (Pa), and the vapor pressure at the leaf surface e_s (Pa) are calculated assuming there is negligible capacity to store CO_2 and water vapor at the leaf surface so that, with reference to Figure 25,

$$A = \frac{c_a - c_i}{(1.37\bar{r}_b + 1.65 r_s) P_{\rm atm}} = \frac{c_a - c_s}{1.37\bar{r}_b P_{\rm atm}} = \frac{c_s - c_i}{1.65 r_s P_{\rm atm}}$$

and the transpiration fluxes are related as

$$\frac{e'_a - e_i}{(\bar{r}_b + r_s)} = \frac{e'_a - e_s}{\bar{r}_b} = \frac{e_s - e_i}{r_s}$$

where $\bar{r}_b$ is leaf boundary layer resistance (s m^2 μmol^{-1}) (section 4.3), the terms 1.37 and 1.65 are the ratios of diffusivity of CO_2-to-H_2O for the leaf boundary layer resistance and stomatal resistance (Landsberg 1986), $c_a = 355\text{x}10^{-6} P_{\text{atm}}$ is the atmospheric CO_2 concentration (Pa), and the vapor pressure of air (Pa) is $e'_a = \max(e_a, 0.25e_i)$. The vapor pressure of air in the plant canopy e_a is described in section 4.3 (note that in section 4.3 e_a is referred to as e_s). The lower limit $0.25e_i$ is used to prevent numerical instability in the iterative stomatal resistance calculation. For C_4 plants, this lower limit is $0.40e_i$ because C_4 plants are not as sensitive to vapor pressure as C_3 plants.

With $c_s = c_a - 1.37\bar{r}_b P_{\text{atm}} A$ and $e_s = \dfrac{e'_a r_s + e_i \bar{r}_b}{\bar{r}_b + r_s}$, stomatal resistance is the larger of the two roots that satisfy the quadratic equation

$$\left(\frac{mAP_{\text{atm}} e'_a}{c_s e_i} + b\right) r_s^2 + \left(\frac{mAP_{\text{atm}} \bar{r}_b}{c_s} + b\bar{r}_b - 1\right) r_s - \bar{r}_b = 0 \ .$$

This equation is iterated three times with an initial arbitrary value of $c_i = 0.7c_a$ for C_3 plants and $c_i = 0.4c_a$ for C_4 plants used to calculate A. Subsequent values for c_i are given by $c_i = c_s - 1.65 r_s P_{\text{atm}} A$.

These equations are solved for sunlit and shaded leaves using average absorbed photosynthetically active radiation for sunlit and shaded leaves (ϕ^{sun}, ϕ^{sha} [section 3.1]) to give sunlit and shaded stomatal resistance (r_s^{sun}, r_s^{sha}) and photosynthesis (A^{sun}, A^{sha}). Canopy photosynthesis is $A^{\text{sun}} L^{\text{sun}} + A^{\text{sha}} L^{\text{sha}}$, where L^{sun} and L^{sha} are the sunlit and shaded leaf area indices (section 3.1). Canopy conductance is $\dfrac{1}{r_s^{\text{sun}}} L^{\text{sun}} + \dfrac{1}{r_s^{\text{sha}}} L^{\text{sha}}$. This canopy integration of photosynthesis and stomatal resistance using sunlit and shaded portions of the canopy is very similar to that used in Sellers et al. (1992). Their canopy scaling factor Π (eq. 31), which is

used to scale the "single leaf" net photosynthesis over the canopy (eq. 34), is the sunlit leaf area index. Consequently, their canopy conductance (eq. 35) is based on the assumption that the sunlit portion of the canopy photosynthesizes at the rate $A_{\rm net}\Pi$ whereas the shaded portion of the canopy has no photosynthesis and has a conductance equal to b. In contrast, the canopy integration technique used here allows both sunlit and shaded leaves to photosynthesize, although at different rates depending on the amount of absorbed photosynthetically active radiation.

Photosynthetic parameters, based on Bonan (1995a), are listed in Table 16 for each plant type. K_{c25}, K_{o25}, a_{kc}, a_{ko}, $a_{\rm vmax}$, and m are from Collatz et al. (1991). α is based on typical values given in Landsberg (1986). b was chosen to give a maximum stomatal resistance of 20000 s m^{-1}. $T_{\rm min}$ is a typical value of when plants photosynthesize with respect to temperature. $V_{\rm max25}$ for C_3 plants was chosen to give maximum photosynthetic rates of 5, 10, and 15 μmol CO_2 m^{-2} s^{-1}, which are consistent with values reported by Woodward and Smith (1994) and Schulze et al. (1994). C_4 parameters were chosen to give reasonable photosynthetic responses to light, temperature, and CO_2. Photosynthetic and stomatal responses to light, temperature, CO_2 concentration, soil water, vapor pressure, and foliage nitrogen are illustrated in Figures 26 and 27. The C_4 plant has the expected response to

Figure 26. Photosynthetic response to light, temperature, CO_2 concentration, soil water content, vapor pressure, and foliage nitrogen for three values of $V_{\rm max25}$. For these simulations, $\beta_t = \dfrac{\theta - \theta_{\rm dry}}{\theta_{\rm opt} - \theta_{\rm dry}} \leq 1$ with $\theta_{\rm dry} = 0.122$ and $\theta_{\rm opt} = 0.138$ (i.e., a loamy soil). Standard values are $P_{\rm atm} = 101300$ Pa, $o_i = 0.209 P_{\rm atm}$, $c_a = 355\text{x}10^{-6} P_{\rm atm}$, $\phi = 272$ W m^{-2}, $T_v = 25$ ^{o}C, $e_a = 3167$ Pa, N=2%, $\theta = 0.2$, and $\bar{r}_b = 20$ s m^{-1}.

Figure 27. As in Figure 26, but for stomatal resistance.

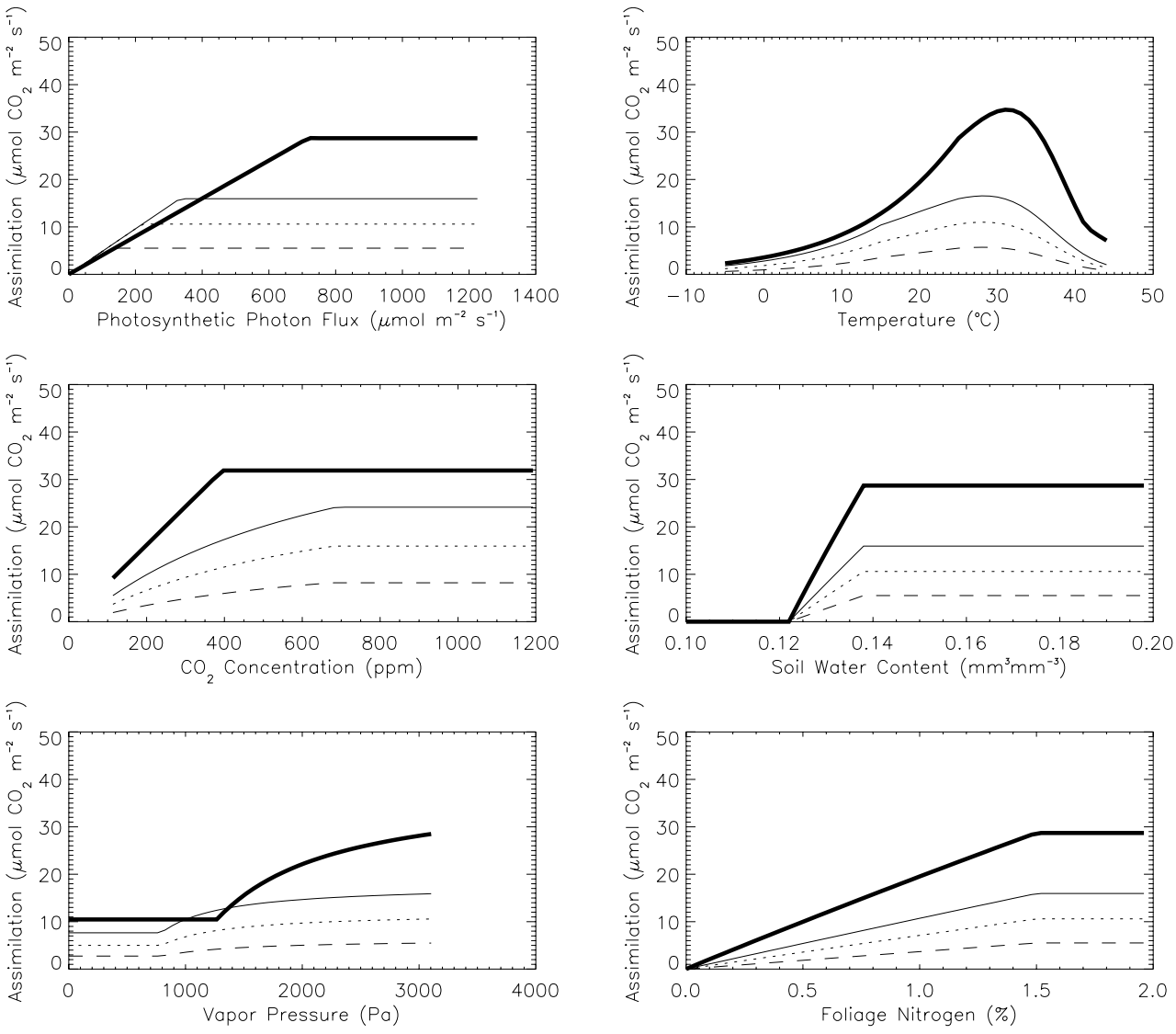
Assimilation (μmol CO2 m-2 s-1)
Photosynthetic Photon Flux (μmol m-2 s-1)
Temperature (°C)
CO2 Concentration (ppm)
Soil Water Content (mm3mm-3)
Vapor Pressure (Pa)
Foliage Nitrogen (%)
C3: Vmax25 = 50 μmol CO2 m-2 s-1
C3: Vmax25 = 33 μmol CO2 m-2 s-1
C3: Vmax25 = 17 μmol CO2 m-2 s-1
C4: Vmax25 = 33 μmol CO2 m-2 s-1

Figure 26

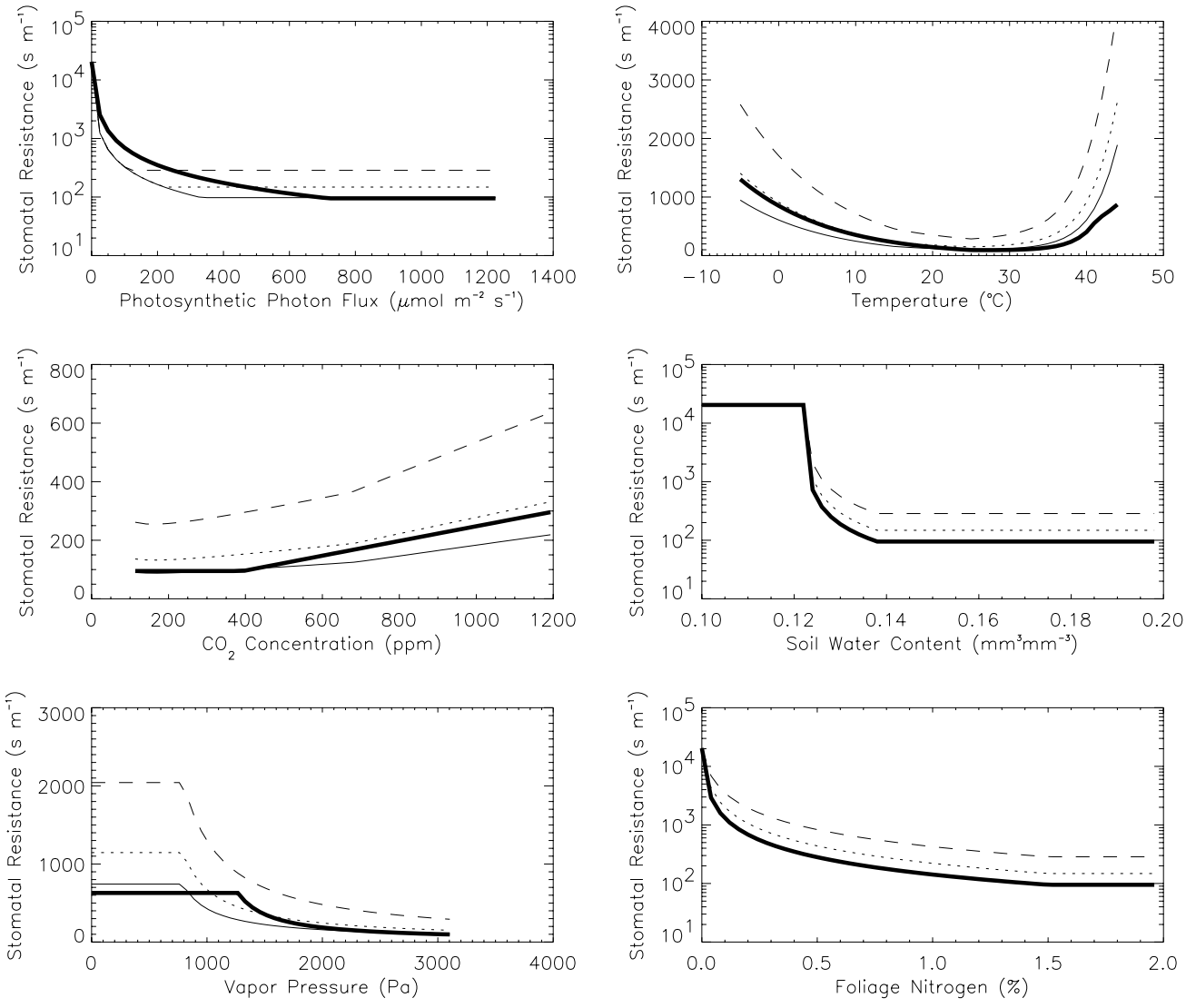
Stomatal Resistance (s m⁻¹)
Photosynthetic Photon Flux (μmol m⁻² s⁻¹)
Temperature (°C)
CO2 Concentration (ppm)
Soil Water Content (mm³mm⁻³)
Vapor Pressure (Pa)
Foliage Nitrogen (%)
C3: Vmax25 = 50 μmol CO2 m⁻² s⁻¹
C3: Vmax25 = 33 μmol CO2 m⁻² s⁻¹
C3: Vmax25 = 17 μmol CO2 m⁻² s⁻¹
C4: Vmax25 = 33 μmol CO2 m⁻² s⁻¹

Figure 27

environmental conditions relative to the comparable C_3 plant: higher light saturation point; higher light saturated rate of photosynthesis; warmer optimal temperature for photosynthesis; and smaller response to increasing CO_2 with saturation at about 400 ppm (Figure 26).

Table 16. Photosynthetic parameters

Plant Type	K_{c25}	a_{kc}	K_{o25}	a_{ko}	$V_{\max 25}$	a_{vmax}	α	b	m	$T_{\min}$	$N_{\max}$
needle. evergreen tree	30	2.1	30000	1.2	33	2.4	0.06	2000	6	-5	-
needle. deciduous tree	30	2.1	30000	1.2	33	2.4	0.06	2000	6	-5	-
broad. evergreen tree	30	2.1	30000	1.2	50	2.4	0.06	2000	9	5	-
broad. deciduous tree	30	2.1	30000	1.2	33	2.4	0.06	2000	9	0	-
tropical seas. tree	30	2.1	30000	1.2	50	2.4	0.06	2000	9	5	-
C_3 grass	30	2.1	30000	1.2	33	2.4	0.06	2000	9	0	-
evergreen shrub	30	2.1	30000	1.2	17	2.4	0.06	2000	9	-5	-
deciduous shrub	30	2.1	30000	1.2	17	2.4	0.06	2000	9	0	-
arctic decid. shrub	30	2.1	30000	1.2	33	2.4	0.06	2000	9	0	-
arctic grass	30	2.1	30000	1.2	33	2.4	0.06	2000	9	0	-
crop	30	2.1	30000	1.2	50	2.4	0.06	2000	9	0	-
C_4 grass	-	-	-	-	33	2.4	0.04	2000	5	0	-

K_{c25}, Pa. K_{o25}, Pa. $V_{\max 25}$, μmol m^{-2} s^{-1}. α, μmol μmol^{-1}. b, μmol m^{-2} s^{-1}. $T_{\min}$, ^{o}C. $N_{\max}$, %.

9.2 Plant and Microbial Respiration

CO_2 loss during plant respiration is broken into maintenance respiration, which depends on temperature, and growth respiration, which is independent of temperature. Total maintenance respiration R_m (μmol CO_2 m^{-2} s^{-1}) from foliage, stem, and root tissues is

$$R_m = [L\ R_{f25} f(N) \beta_t + V_b^s\ R_{s25} + V_b^r\ R_{r25}] a_{rm}^{\frac{T_v - 25}{10}}$$

where L is leaf area index (m^2 m^{-2}) (section 1.3), R_{f25} is foliage respiration at 25^{o}C (μmol CO_2 m^{-2} s^{-1}), V_b^s is stem biomass (kg m^{-2}) (section 1.2), R_{s25} is stem respiration at 25^{o}C (μmol CO_2 kg^{-1} s^{-1}), V_b^r is root biomass (kg m^{-2}) (section 1.2), R_{r25} is root respiration at 25^{o}C (μmol CO_2 kg^{-1} s^{-1}), T_v is the vegetation temperature (^{o}C) (section 5.2), and a_{rm} is a temperature sensitivity parameter. The terms in this equation represent foliage, stem, and root maintenance respiration, respectively. The foliage nitrogen f(N) and soil water β_t factors are applied to leaf respiration because these factors are applied to $V_{\max}$ and R_{f25} is proportional to $V_{\max}$ (Farquhar et al. 1980). Maintenance respiration is reduced by one-half outside of the growing season (Bonan 1991a, 1993a, 1993b, 1995a). Growth respiration R_g (μmol CO_2 m^{-2} s^{-1}) is proportional to photosynthesis (Jones 1992)

$$R_g = 0.25(A^{\text{sun}} L^{\text{sun}} + A^{\text{sha}} L^{\text{sha}})$$

where A^{sun} and A^{sha} are the sunlit and shaded leaf photosynthesis (section 9.1) and L^{sun} and L^{sha} are the sunlit and shaded leaf area indices (section 3.1). Net primary production ΔM (μg m^{-2}) is

$$\gamma(A^{\text{sun}} L^{\text{sun}} + A^{\text{sha}} L^{\text{sha}} - R_m - R_g)\Delta t$$

where $\gamma = 28.5$ μg dry biomass per μmol CO_2 (Landsberg 1986) and Δt is the time

step (seconds).

Microbial respiration R_s (μmol CO_2 m^{-2} s^{-1}) is

$$R_s = \frac{\bar{\theta}}{a_1 + \bar{\theta}} \frac{a_2}{a_2 + \bar{\theta}} a_3 S_c a_4^{\frac{T_s - 10}{10}}$$

where $\bar{\theta}$ is the volumetric soil water content to a depth of 1 m (section 8.4), a_1 is one-half field capacity, a_2 is one-half saturation, S_c is soil carbon (kg C m^{-2}) (section 1.2), a_3 is the respiration rate (μmol CO_2 kg C^{-1} s^{-1}) at 10^oC, a_4 is a temperature sensitivity parameter, and T_s is the temperature (^{o}C) of the first soil layer (section 6). Typical values are $a_1 = 0.20$, $a_2 = 0.23$, and a_4=2.0 (Bonan 1995a).

Respiration parameters are listed in Table 17. R_{f25} is $0.015 V_{\max 25}$ for C_3 plants (Farquhar et al. 1980) and $0.025 V_{\max 25}$ for C_4 plants (Collatz et al. 1992). $a_3 \times S_c$ replaces the a_3 parameter in Bonan (1995a). $R_{s25} \times V_b^s$ and $R_{r25} \times V_b^r$ replace the p parameter in Bonan (1995a). Values of R_{s25} and R_{r25} were chosen to give reasonable respiration rates, similar to Bonan (1995a).

Table 17. Respiration parameters

Plant Type	R_{f25}	R_{s25}	R_{r25}	a_{rm}	a_3
needleleaf evergreen tree	0.50	0.94	0.36	2.0	0.37
needleleaf deciduous tree	0.50	0.14	0.05	2.0	0.37
broadleaf evergreen tree	0.75	0.16	0.05	2.0	0.23
broadleaf deciduous tree	0.50	0.02	0.01	2.0	0.40
tropical seasonal tree	0.75	0.02	0.21	2.0	0.12
C_3 grass	0.50	0.00	0.59	2.0	0.17
evergreen shrub	0.26	0.00	0.00	2.0	0.19
deciduous shrub	0.26	0.00	0.00	2.0	0.19
arctic deciduous shrub	0.50	1.02	2.11	2.0	0.05
arctic grass	0.50	1.02	2.11	2.0	0.05
crop	0.75	0.00	0.00	2.0	0.23
C_4 grass	0.82	0.00	2.27	2.0	0.17

R_{f25}, μmol CO_2 m^{-2} s^{-1}. R_{s25}, μmol CO_2 kg^{-1} s^{-1}. R_{r25}, μmol CO_2 kg^{-1} s^{-1}. a_3, μmol CO_2 kg^{-1} C s^{-1}.

10. References

Arya, S.P. 1988. Introduction to Micrometeorology. Academic Press, San Diegeo.

Beljaars, A.C.M., and Holtslag, A.A.M. 1991. Flux parameterization over land surfaces for atmospheric models. J. Appl. Meteor. 30:327-341.

Beljaars, A.C.M., and Viterbo, P. 1994. The sensitivity of winter evaporation to the formulation of aerodynamic resistance in the ECMWF model. Bound.-Layer Meteor. 71:135-149.

Bonan, G.B. 1991a. Atmosphere-biosphere exchange of carbon dioxide in boreal forests. J. Geophys. Res. 96D:7301-7312.

Bonan, G.B. 1991b. A biophysical surface energy budget analysis of soil temperature in the boreal forests of interior Alaska. Water Resour. Res. 27:767-781.

Bonan, G.B. 1993a. Physiological controls of the carbon balance of boreal forest ecosystems. Can. J. For. Res. 23:1453-1471.

Bonan, G.B. 1993b. Physiological derivation of the observed relationship between net primary production and mean annual air temperature. Tellus 45B:397-408.

Bonan, G.B. 1993c. Do biophysics and physiology matter in ecosystem models? Climatic Change 24:281-285.

Bonan, G.B. 1994. Comparision of two land surface process models using prescribed forcings. J. Geophys. Res. 99D:25803-25818.

Bonan, G.B. 1995a. Land-atmosphere CO_2 exchange simulated by a land surface process model coupled to an atmospheric general circulation model. J. Geophys. Res. 100D:2817-2831.

Bonan, G.B. 1995b. Sensitivity of a GCM simulation to inclusion of inland water surfaces. J. Climate 8:2691-2704.

Bonan, G.B. 1995c. Land-atmosphere interactions for climate system models: coupling biophysical, biogeochemical, and ecosystem dynamical processes. Remote Sens. Environ. 51:57-73.

Bonan, G.B. 1996. Sensitivity of a GCM simulation to subgrid infiltration and surface runoff. Climate Dyn., in press.

Brutsaert, W. 1982. Evaporation into the Atmosphere: Theory, History, and Applications. D. Reidel Publ. Co., Dordrecht.

Campbell, G.S. 1977. An Introduction to Environmental Biophysics. Springer-Verlag, New York.

Choudhury, B.J., and Monteith, J.L. 1988. A four-layer model for the heat budget of homogeneous land surfaces. Quart. J. Roy. Meteor. Soc. 114:373-398.

Clapp, R.B., and Hornberger, G.M. 1978. Empirical equations for some soil hydraulic properties. Water Resour. Res. 14:601-604.

Cogley, J.G. 1991. GGHYDRO - Global Hydrographic Data Release 2.0. Trent Climate Note 91-1, Dept. Geography, Trent University, Peterborough, Ontario.

Collatz, G.J., Ball, J.T., Grivet, C., and Berry, J.A. 1991. Physiological and environmental regulation of stomatal conductance, photosynthesis, and transpiration: a model that includes a laminar boundary layer. Agric. For. Meteorol. 54:107-136.

Collatz, G.J., Ribas-Carbo, M., and Berry, J.A. 1992. Coupled photosynthesis-stomatal conductance model for leaves of C_4 plants. Aust. J. Plant Physiol. 19:519-538.

Cosby, B.J., Hornberger, G.M., Clapp, R.B., and Ginn, T.R. 1984. A statistical exploration of the relationships of soil moisture characteristics to the physical properties of soils. Water Resour. Res. 20:682-690.

Dickinson, R.E. 1983. Land surface processes and climate-surface albedos and energy balance. Adv. Geophys. 25:305-353.

Dickinson, R.E., Henderson-Sellers, A., and Kennedy, P.J. 1993. Biosphere-Atmosphere Transfer Scheme (BATS) version 1e as coupled to the NCAR Community Climate Model. NCAR Technical Note NCAR/TN-387+STR, National Center for Atmospheric Research, Boulder, CO.

Dolman, A.J., and Gregory, D. 1992. The parametrization of rainfall interception in GCMs. Quart. J. Roy. Meteor. Soc. 118:455-467.

Dorman, J.L., and Sellers, P.J. 1989. A global climatology of albedo, roughness length and stomatal resistance for atmospheric general circulation models as represented by the simple biosphere model (SiB). J. Appl. Meteor. 28:833-855.

Dougherty, R.L., Bradford, J.A., Coyne, P.I., and Sims, P.L. 1994. Applying an empirical model of stomatal conductance to three C-4 grasses. Agric. For. Meteor. 67:269-290.

Entekhabi, D., and Eagleson, P.S. 1989. Land surface hydrology parameterization for atmospheric general circulation models including subgrid scale spatial variability. J. Climate 2:816-831.

Farouki, O.T. 1981. The thermal properties of soils in cold regions. Cold Regions Sci. Tech. 5:67-75.

Farquhar, G.D., and von Caemmerer, S. 1982. Modeling of photosynthetic response to environmental conditions. pp. 549-587. In: O.L. Lange, P.S. Nobel, C.B. Osmond, and H. Ziegler (eds) Encyclopedia of Plant Physiology. Vol. 12B. Physiological Plant Ecology. II. Water Relations and Carbon Assimilation. Springer-Verlag, New York.

Farquhar, G.D., von Caemmerer, S., and Berry, J.A. 1980. A biochemical model of

photosynthetic CO_2 assimilation in leaves of C_3 species. Planta 149:78-90.

Gale, M.R., and Grigal, D.F. 1987. Vertical root distributions of northern tree species in relation to successional status. Can. J. For. Res. 17:829-834.

Goodrich, L.E. 1978. Efficient numerical technique for one-dimensional thermal problems with phase change. Int. J. Heat Mass Transfer 21:615-621.

Goodrich, L.E. 1982. The influence of snow cover on the ground thermal regime. Can. Geotech. J. 19:421-432.

Henderson-Sellers, B. 1985. New formulation of eddy diffusion thermocline models. Appl. Math. Modelling 9:441-446.

Henderson-Sellers, B. 1986. Calculating the surface energy balance for lake a reservoir modeling: a review. Rev. Geophys. 24:625-649.

Hostetler, S.W., and Bartlein, P.J. 1990. Simulation of lake evaporation with application to modeling lake level variations of Harney-Malheur Lake, Oregon. Wat. Resour. Res. 26:2603-2612.

Hostetler, S.W., Bates, G.T., and Giorgi, F. 1993. Interactive coupling of a lake thermal model with a regional climate model. J. Geophys. Res. 98D:5045-5057.

Hostetler, S.W., Giorgi, F., Bates, G.T., and Bartlein, P.J. 1994. Lake-atmosphere feedbacks associated with paleolakes Bonneville and Lahontan. Science 263:665-668.

Jones, H.G. 1992. Plants and Microclimate: A Quantitative Approach to Environmental Plant Physiology. 2nd Edition. Cambridge Univ. Press, Cambridge.

Johnson, K.D., Entekhabi, D., and Eagleson, P.S. 1993. The implementation and validation of improved land-surface hydrology in an atmospheric general circulation model. J. Climate 6:1009-1026.

Jumikis, A.R. 1966. Thermal Soil Mechanics. Rutgers University Press, New Brunswick, New Jersey.

Landsberg, J.J. 1986. Physiological Ecology of Forest Production. Academic Press, London.

Lowe, P.R. 1977. An approximating polynomial for the computation of saturation vapor pressure. J. Appl. Meteor. 16:100-103.

Lunardini, V.J. 1981. Heat Transfer in Cold Climates. Van Nostrand Reinhold, New York.

Marshall, S.E. 1989. A physical parameterization of snow albedo for use in climate models. NCAR Cooperative Thesis NCAR/CT-123, National Center for Atmospheric Research, Boulder, CO.

McGuire, A.D., Melillo, J.M., Joyce, L.A., Kicklighter, D.W., Grace, A.L., Moore, B. III., and Vorosmarty, C.J. 1992. Interactions between carbon and nitrogen dynamics in estimating net primary productivity for potential vegetation in North America. Global Biogeochemical Cycles 6:101-124.

Monteith, J.L., and Unsworth, M.H. 1990. Principles of Environmental Physics. 2nd edition. Edward Arnold, London.

Olson, J.S., Watts, J.A., and Allison, L.J. 1983. Carbon in live vegetation of major world ecosystems. ORNL-5862. Oak Ridge National Laboratory, Oak Ridge, TN.

Pitman, A.J., Henderson-Sellers, A., and Yang, Z.-L. 1990. Sensitivity of regional climates to localized precipitation in global models. Nature 346:734-737.

Pitman, A.J., Yang, Z.-L., and Henderson-Sellers, A. 1993. Sub-grid scale precipitation in AGCMs: re-assessing the land surface sensitivity using a single column model. Climate Dyn.9:33-41

Press, W.H., Flannery, B.P., Teukolsky, S.A., and Vetterling, W.T. 1986. Numerical Recipes: The Art of Scientific Computing. Cambridge Univ. Press, Cambridge.

Raupach, M.R. 1994. Simplified expressions for vegetation roughness length and zero-plane displacement as functions of canopy height and area index. Bound.-Layer Meteor. 71:211-216.

Running, S.W., Nemani, R.R., Peterson, D.L., Band, L.E., Potts, D.F., Pierce, L.L., and Spanner, M.A. 1989. Mapping regional forest evapotranspiration and photosynthesis by coupling satellite data with ecosystem simulation. Ecology 70:1090-1101.

Schulze, E.-D., Kelliher, F.M., Körner, C., Lloyd, J., and Leuning, R. 1994. Relationships among maximum stomatal conductance, ecosystem surface conductance, carbon assimilation rate, and plant nitrogen nutrition: a global ecology scaling exercise. Ann. Rev. Ecol. Syst. 25:629-660.

Sellers, P.J. 1985. Canopy reflectance, photosynthesis and transpiration. Int. J. Remote Sensing 6:1335-1372.

Sellers, P.J., Mintz, Y., Sud, Y.C., and Dalcher, A. 1986. A simple biosphere model (SiB) for use within general circulation models. J. Atmos. Sci. 43:505-531.

Sellers, P.J., Berry, J.A., Collatz, G.J., Field, C.B., and Hall, F.G. 1992. Canopy reflectance, photosynthesis, and transpiration. III. A reanalysis using improved leaf models and a new canopy integration scheme. Remote Sens. Environ. 42:187-216.

Shuttleworth, W.J., and Wallace, J.S. 1985. Evaporation from sparse crops - an energy combination theory. Quart. J. Roy. Meteor. Soc. 111:839-855.

Stull, R.B. 1988. An Introduction to Boundary Layer Meteorology. Kluwer Academic Publ., Dordrecht.

Thom, A.S. 1975. Momentum, mass and heat exchange of plant communities. pp. 57-109. In: J.L. Monteith (ed) Vegetation and the Atmosphere. Vol. I. Academic Press, San Diego.

Webb, R.S., Rosenzweig, C.E., and Levine, E.R. 1993. Specifying land surface characteristics in general circulation models: soil profile data set and derived water-holding capacities. Global Biogeochemical Cycles 7:97-108.

Woodward, F.I., and Smith, T.M. 1994. Predictions and measurements of the maximum photosynthetic rate, A_{max}, at the global scale. pp. 491-509. In: E.-D. Schulze and M.M. Caldwell (eds) Ecophysiology of Photosynthesis. Springer-Verlag, New York.

PART II: USER'S GUIDE

This section is a brief introduction to the overall design of the land surface model, information about running the model, and a description of the code. The source code, with detailed comments throughout, is the definitive description.

11. Model Architecture

The model consists of two main subroutines. Subroutine **lsmini** initializes the land surface model. It also returns as two-dimensional (longitude $\times$ latitude) arrays any land surface variables (e.g., surface temperature) required by the atmospheric model. Non-land values are undefined. Subroutine **lsmdrv** calculates surface fluxes and updates the ecological, hydrologic, and thermal state of the land.

The processing of each land grid point by subroutine **lsmdrv** begins by gathering the **lpt** land points on the **lsmlon** by **lsmlat** grid into a "big" vector of **kpt** points, allowing for up to **msub** subgrid points per land point. The **kpt** points are processed by subroutine **lsm** as **numlv** "little" vectors of **numkpt** points. The processing of these "little" vectors can be multi-tasked if desired. Figure 28 illustrates this architecture for a 3 $\times$ 2 grid with 4 land points and a total of 10 LSM points, allowing for subgrid points.

Figure 28. Illustration of model architecture. The 3 $\times$ 2 grid has four land points (non-hatched boxes), which consist of one, two, three, and four subgrid points. The 3 $\times$ 2 atmospheric temperature field T is expanded to a "big" vector T' of length ten, assigning subgrid points the grid value. These ten points are processed in three calls to subroutine **lsm**, as "little" vectors of four, three, and three points. As output, **lsm** fills in a "big" vector of sensible heat flux H', with length 10, in strips of four, three, and three points. When all ten points have been processed, the vector H' is mapped to a 3 $\times$ 2 sensible heat flux field H, filling in land points only by weighting subgrid fluxes for appropriate subgrid fractional areas.

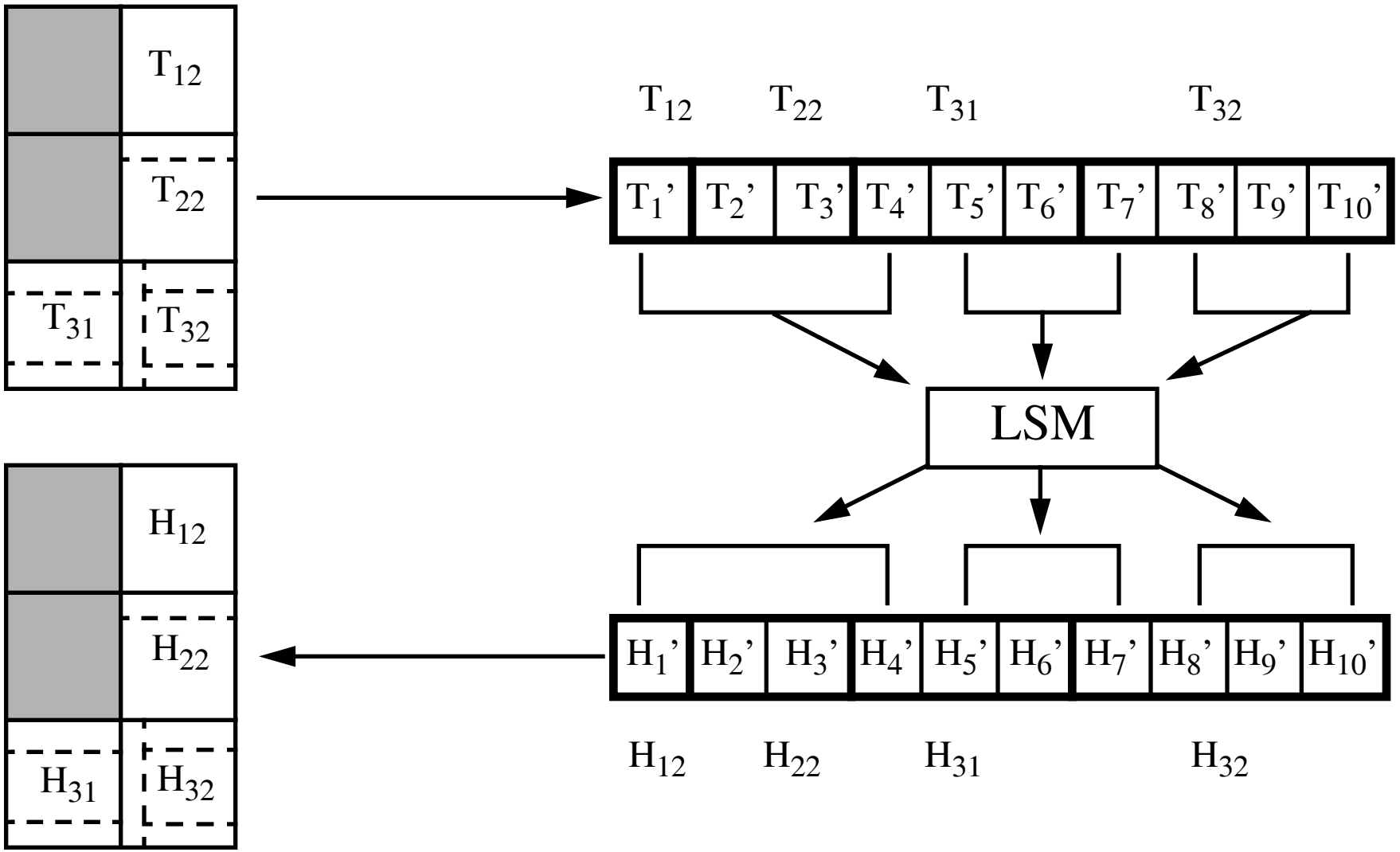
T12
T22
T31
T32
T1' T2' T3' T4' T5' T6' T7' T8' T9' T10'
LSM
H12
H22
H31
H32
H1' H2' H3' H4' H5' H6' H7' H8' H9' H10'
H12 H22 H31 H32

Figure 28

This architecture has the following advantages: (a) only land points are processed; (b) local arrays within subroutine **lsm** are dimensioned by the number of points processed in each call to **lsm** rather than by **kpt**, resulting in small memory requirements when using multiple processors; and (c) multi-tasking many processes (e.g., 30) results in reasonable load balancing among processors. The number of points to process in each call to **lsm** should be large enough to take advantage of vectorization yet small enough to have a sufficient number of processes to multi-task.

Input and output between the atmosphere and land models are in terms of two-dimensional (**lsmlon** $\times$ **lsmlat**) fields. Currently, this grid must be the same as the atmospheric model. That is, the model expects atmospheric fields for the entire **lsmlon** $\times$ **lsmlat** domain to force the model and returns as output two-dimensional **lsmlon** $\times$ **lsmlat** fields, setting only the land points in the domain.

The source code **lsmmain.F**, which is the main driver program for "off-line" stand-alone or uncoupled simulations, illustrates this coupling using the atmospheric forcing in **atm.F**. There is one call to **lsmini** during initialization, one call per time step to **lsmdrv**, and **numlv** calls to **lsm** per call to **lsmdrv**. The calling diagrams for these subroutines are shown in Figures 29 and 30.

Figure 29. Calling diagram for subroutine **lsmini**. Routines in grey indicate code that is called **numlv** times to process the **kpt** points as "little" vectors. This code is not multi-tasked. **getenv**, **unlink**, **msread**, and **mswrite** are Fortran library routines required when using the NCAR Mass Store.

Figure 30. Calling diagram for subroutine **lsmdrv**. Routines in grey indicate code that is called **numlv** times to process the **kpt** points as "little" vectors. This code is multi-tasked. **getenv**, **unlink**, **msread**, and **mswrite** are Fortran library routines required when using the NCAR Mass Store.

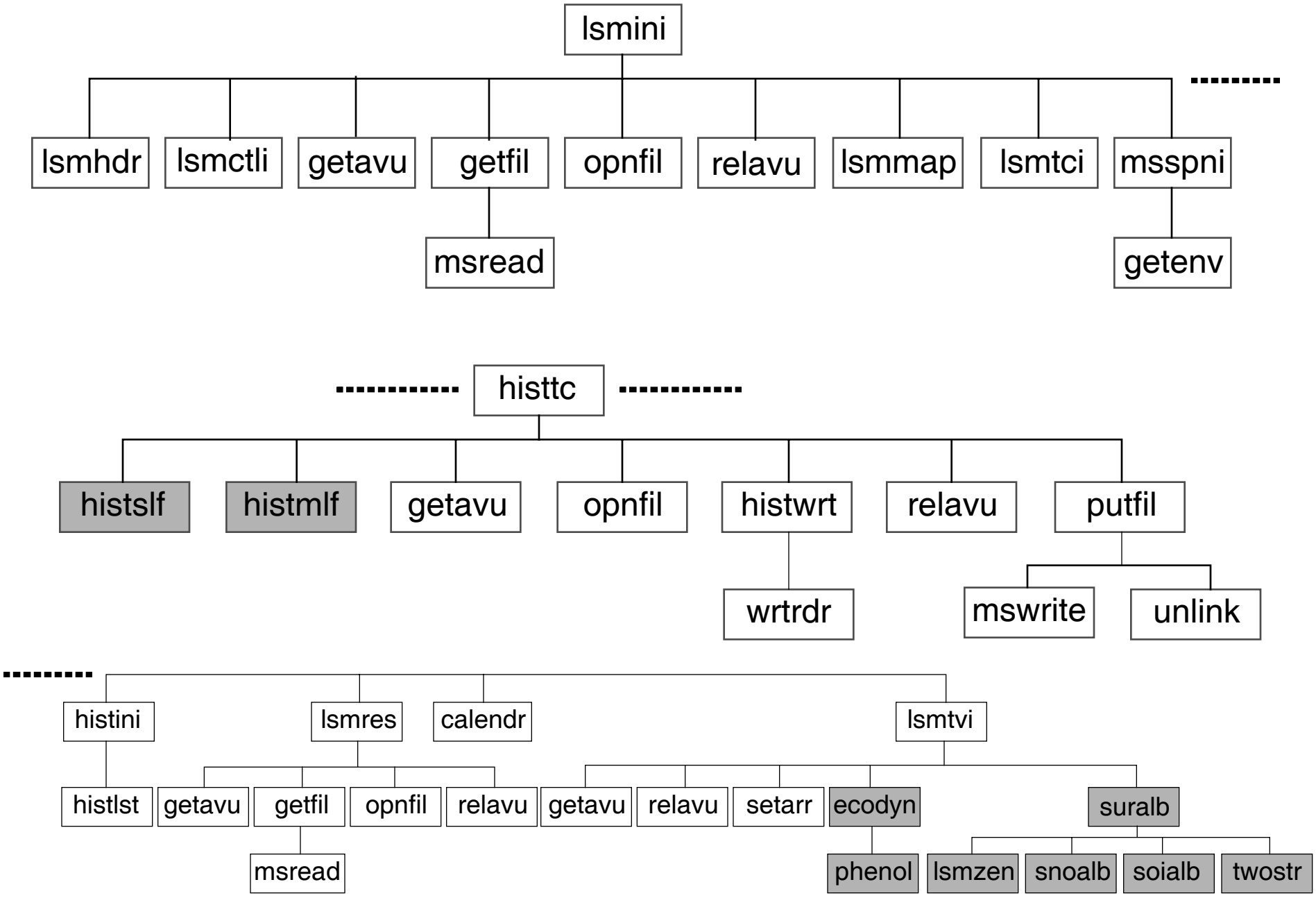
lsmini
lsmhdr
lsmctli
getavu
getfil
opnfil
relavu
lsmmap
lsmtci
msspni
msread
getenv
histtc
histslf
histmlf
getavu
opnfil
histwrt
relavu
putfil
wrtrdr
mswrite
unlink
histini
lsmres
calendr
lsmtvi
histlst
getavu
getfil
opnfil
relavu
getavu
relavu
setarr
ecodyn
suralb
msread
phenol
lsmzen
snoalb
soialb
twostr

Figure 29

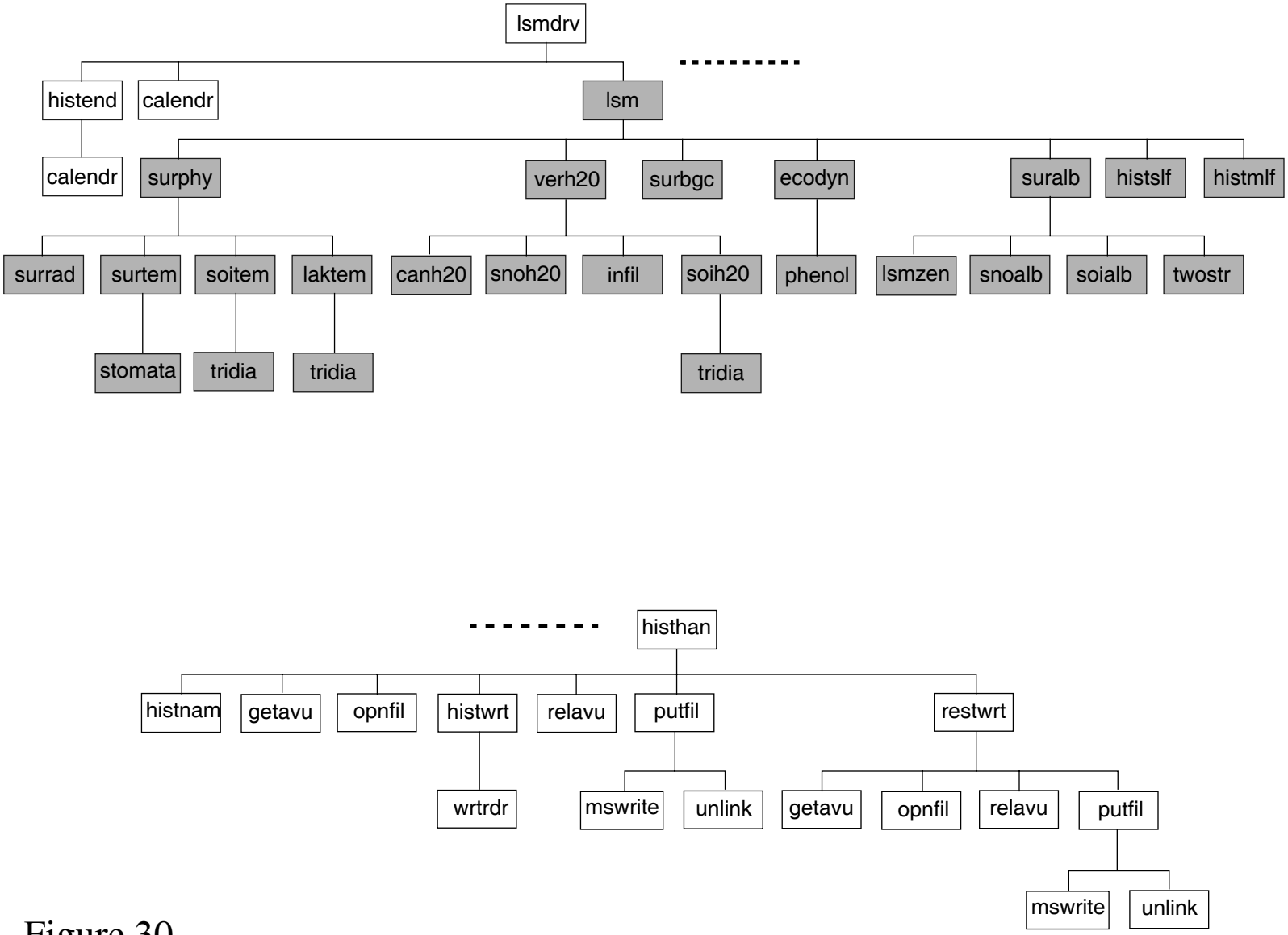
lsmdrv
histend
calendr
lsm
calendr
surphy
verh20
surbgc
ecodyn
suralb
histslf
histmlf
surrad
surtem
soitem
laktem
canh20
snoh20
infil
soih20
phenol
lsmzen
snoalb
soialb
twostr
stomata
tridia
tridia
tridia
histhan
histnam
getavu
opnfil
histwrt
relavu
putfil
restwrt
wrtrdr
mswrite
unlink
getavu
opnfil
relavu
putfil
mswrite
unlink

Figure 30

12. Input Data Sets

The model requires two input data sets. The surface boundary data set, defined by the **fsurdat** namelist parameter (section 14.3), defines time-invariant surface properties. Currently, the grid dimensions and indexing of this data set must be the same as the atmospheric model. For the NCAR CCM3, this means that data sets are oriented from the South Pole to the North Pole, starting at Greenwich and proceeding eastwards. Surface data for each grid cell are: latitude and longitude at the center of the grid cell; integer surface type (Table 5); integer color class for soil albedos (Table 10); %sand, %silt, and %clay for thermal and hydraulic properties (sections 6.2, 8.4.1); and % of grid cell covered by (a) lake and (b) wetlands, for use as multiple subgrid points. The first few lines in the data set are the number of longitude points for each latitude strip, allowing for variable longitudinal resolution with latitude. An example data set can be found in the file "fsurdat_t42". See subroutine **lsmini** for more details.

The initial conditions data set, defined by the **finidat** namelist parameter (section 14.3), contains contains initial water (snow, vegetation, soil) and temperature (vegetation, ground surface, soil) for the **kpt** subgrid points. The remaining variables needed for initialization are either calculated based on these variables or set to arbitrary values because their exact value is not too important. The one exception is the soot content of snow, which currently is time-invariant. By default, water and temperatures are initialized to arbitrary conditions so that no initial data is required. See subroutine **lsmtvi** for more details.

13. History and Restart Files

If **LSM_HIST** is defined in **preproc.h** (section 14.1) and if the namelist variable **lsmhrh** is true (section 14.3), the model writes its own history and restart files. These files can be used to analyze model output and to restart previous simulations. The primary code needed to process history and restart files is (Figures 29, 30): **histtc** to create a history file of time constant fields; **histini** to initialize the primary history files of time varying fields; **histslf** and **histmlf** to accumulate single-level and multi-level field values over the history interval; **histend** to determine the end of a history interval; **histhan** to open, write, and close history and restart files; and **lsmres** to restart the model for continuation runs.

13.1 Model Output

History and restart files are in the directories defined by the **locpnh** and **locpnr** namelist variables. These files have the names "lsmh_xxxxx" and "lsmr_xxxxx", respectively, where "xxxxx" is unique text determined by the file number, e.g. 00001 to 99999. When using the monthly average option this text is in the form "mm-yyy", e.g. 09-001 is data for September of year 1. If using the NCAR Mass Store, these local history and restart files are copied to the Mass Store using the name "/LOGID/lsmv1/caseid/hist/lsmh_xxxxx" for history files and using the name "/LOGID/lsmv1/caseid/rest/lsmr_xxxxx" for restart files. Logid is set by default, but the caseid must be set using the setenv command.

The active list of fields for history files is set in subroutine **histlst**. This subroutine sets the default field list (i.e., the name, units, and description of the fields) and the field type. Field type is: the average over a history interval, the maximum value in the history interval, the minimum value in the history interval, or the instantaneous value at the end of the history interval. The default field type can be overridden by setting the paired (field name, field type) **chntyp** namelist

variable (section 14.3) to the appropriate field names and field types. The default fields set in **histlst** can be made inactive by setting the **excl** namelist variable (section 14.3) to the appropriate field names. Fields are segregated by single-level or multi-level. Multi-level refers to the number of soil layers so that soil temperature and soil water are multi-level fields.

New fields can be added to the history files by modifying the code in subroutine **histlst**. The **nflds** variable needs to be incremented by one for each new field. The eight character field name **fldnam**, units **flduni**, level **fldlev**, and type **fldtyp** variables need to be set to appropriate values. The 40 character field description **flddes** also needs to be set. These are set using the current value for **nflds**. **nflds** is then incremented for the next field, and this process is repeated for however many new active fields are added. The array dimensions **mslflds** and **mmlflds**, set in **lsmpar.h**, may have to be increased depending on the number of single- and multi-level fields, respectively, added to the history files. The model will stop if these array dimensions are exceeded. Subroutines **histslf** and/or **histmlf** will have to be called from subroutine **lsm** to accumulate the new single- and/or multi-level fields over the history interval (see subroutine **lsm** for examples).

Field values for the current iteration are accumulated by subroutines **histslf** and **histmlf** for single-level and multi-level fields, respectively, based on the field type (average, maximum, minimum, or instantaneous). The "little" vectors processed by these subroutines are mapped into "big" vectors of **kpt** points. These "big" vectors are actually multi-dimensional arrays that contain the accumulated value of each field and each level for the **kpt** points. There are two arrays (**slfval**, **mlfval**), one for single-level fields and one for multi-level fields. Fields that are averaged are normalized by the length of the history interval before being written to the history file.

A time sample is written to the current history file every **nhtfrq** iterations

or at the end of the month (if using the monthly average option). Up to **mfilt** time samples are written to a history file unless using the monthly average option, in which case only one time sample (the monthly average) is written. This time sample, written by subroutine **histwrt**, includes: an integer header record, a real header record, a character header record, and real data records for each field. Data for each field are written as a vector of **kpt** points. Multi-level fields have **msl** vectors (i.e., a vector for each soil layer). The integer and real header records contain the variables needed to map the **kpt** subgrid points into a two-dimensional (**lsmlon** $\times$ **lsmlat**) field. The character header record contains information on the simulation, the start and end of the history interval, the names, units, types, and descriptions of the single-level fields, and the names, units, types, and descriptions of multi-level fields. All data are written as binary output. The code in **hist_read.s** shows how to read a LSM history file, extract a particular field, and map the field onto the 2-d grid.

The history file is closed and disposed to the Mass Store, if desired, when the file is full or if the end of the run coincides with the end of a history interval. At the same time, the restart files are written. That is, the restart file "lsmr_00090" is written at the same iteration that the history file "lsmh_00090" is closed. If using the monthly average option, the restart file is written at the end of the month. Consequently, the model can be restarted only at the end of a history interval.

Restart files are written by subroutine **restwrt**. The main restart file (e.g, lsmr_00001, lsmr_12-002), is a binary file containing the variables needed to restart the simulation. The file "lsmr_rstrt" is an ASCII file that contains the names of the current history and restart files (Mass Store names if using the Mass Store).

Subroutine **histtc** is code that creates, during initialization, a history file for the time constant vegetation and soil variables. This file, with the name "lsmh_timcon", is written in the same directory as the time-varying history files.

13.2 Model Input for Continuation Runs

Two types of continuation runs are possible:

1. A restart run continues an earlier run using the most recent restart file. Run control variables set in the namelist must be the same as in the run that is being restarted. The model does not check for consistency. The appropriate restart file (e.g., lsmr_00100) is read from the file "lsmr_rstrt", located in either the local directory **locpnr** or the Mass Store directory "/LOGID/lsmv1/caseid/rest/". If the associated history file (e.g., lsmh_00100), located in the directory **locpnh** or the Mass Store directory "/LOGID/lsmv1/caseid/hist/", is not full this history file is opened and positioned to the end of the file so that subsequent time samples are added until the file is full.

2. A branch run allows the user to begin a new simulation by "branching" from an existing control run. In this case, the model restarts from a specified restart file set by the **nrevsn** namelist variable (section 14.3). This can be either a local or Mass Store file name. Because a branch run is a new case, the length of the history interval and the active field list do not have to be the same as in the control simulation. Thus, one can use the branching option to "repeat" a specified time interval of a previous run in which daily-average history files were written as a new run in which selected fields are written to a history file every iteration, thereby resolving the diurnal cycle. History and restart files are written in the directories **locpnh** and **locpnr** as defined for the current run or to the Mass Store using the current setting for "caseid". A new time constant history file is also created.

14. Run Control Parameters

Three files set the control parameters for the model: pre-processor directives are set in **preproc.h**; grid dimensions, array sizes, and the number of "little" vectors are defined in **lsmpar.h**; and logical run control parameters and input/output data set names are set in the **lsmexp** namelist.

14.1 Pre-Processor Directives

The model utilizes the following C pre-processor "cpp" directives:

#include <file>: reads in contents of "file" at this location.

#define variable: defines "variable".

#undef variable: undefines "variable".

#ifdef variable: subsequent lines up to a matching #else or #endif directive appear in output if "variable" is defined.

#ifndef variable: subsequent lines up to a matching #else or #endif directive appear in output if "variable" is undefined.

The following #define and #undef directives are set in the file **preproc.h**:

LSMLAT defines the number of latitudes on the LSM grid by setting the comparable parameter in **lsmpar.h**.

LSMLON defines the number of longitudes on the LSM grid by setting the comparable parameter in **lsmpar.h**.

LPT defines the number of land points on the LSM grid by setting the comparable parameter in **lsmpar.h**.

KPT defines the total number of land points on the LSM grid, allowing for subgrid points, by setting the comparable parameter in **lsmpar.h**. This is the length of the "big" vectors.

NUMLV defines the number of "little" vectors used to process the **kpt** points by setting the comparable parameter in **lsmpar.h**. The length of the "little" vectors is determined by **numlv**.

ATM_HIST defines residual developmental code that returns selected 2-d land surface fields to the atmospheric model for output on the atmospheric history files.

COUP_CCM is defined only when coupling to the NCAR CCM3. In this case, CCM3 code is used to get the next available Fortran unit number and to close and release a Fortran unit no longer in use. In addition, base calendar information, the current time, run type (initial, restart, branch), and model time step are input from the CCM3.

LSM_HIST defines code for LSM history and restart files. See also **lsmsrc.h**

MSS is defined when using the NCAR Mass Store to get input files and save output files. If this is defined, the model requires the Fortran library routines **getenv**, **unlink**, **msread**, and **mswrite**.

OFFLINE_LSM is defined when using the "off-line" code (i.e., when running the model in a stand-alone or uncoupled mode). In this case, the source files **lsmmain.F** and **atm.F** must be compiled (see **lsmsrc.h**). **ATMLAT** and **ATMLON** define the "atmospheric" grid in **lsmmain.F**.

SUN_FORT is defined when using the f77 compiler on Sun workstations. This is needed only because the Sun and Cray Fortran compilers differ in their open statements. When appending data to an existing

file, the Sun compiler uses the "access" keyword; the Cray compiler uses the "position" keyword.

14.2 Grid Dimensions and Array Sizes

Parameters that set the grid dimensions (**lsmlon**, **lsmlat**), the number of land points on the grid (**lpt**), the maximum number of subgrid points (**msub**), the length of the "big" vectors (**kpt**), the number of "little" vectors (**numlv**), and their length are defined in **lsmpar.h**. This file also defines the number of solar radiation wavebands, the number of soil layers, the number of plant types, the number of soil color classes, and the number of "soil" types. It sets the number of single-level equivalent variables that need to be saved for restart (i.e., the land surface variables that need to be saved from one time step to the next). It sets the maximum number of single- and multi-level variables for output on history files.

The number of longitude and latitude points on the land surface model grid are defined by **lsmlon** and **lsmlat**. Currently, these must be the same as the atmospheric model so that there is a one-to-one correspondence between the atmosphere and land grids.

The land surface model works by gathering the **lpt** land points on the **lsmlon** by **lsmlat** grid into a "big" vector of **kpt** subgrid points, allowing for up to **msub** subgrid points per land point. The **kpt** subgrid points are processed as **numlv**-1 "little" vectors of **lvec** points and 1 "little" vector of **mpt** points. These **numlv** calls to the "little vector" land surface code can be multi-tasked if desired. **mpt** is needed because **kpt** may not be evenly divisible by **numlv**. Hence, **mpt** is the maximum number of points to be processed by the "little vector" code and is the array dimension of variables in the "little vector" code.

The mapping of atmospheric and surface fields between the 2-d (longitude by latitude) and "big" subgrid vector versions and the partitioning of the "big" vectors

into "little" vectors require that:

lpt equal the number of land points on the 2-d grid; and

kpt equal the number of total LSM points, including subgrid points.

Consequently, if the grid is changed (e.g., adding or deleting land) both **lpt** and **kpt** must be modified accordingly. If subgrid points (e.g., lakes) are added or removed, **kpt** must be updated. Or if a surface type is changed (e.g., tropical forest with two subgrid surface types to desert with one subgrid surface type), **kpt** must be updated. During initialization, the model calculates the values for **lpt** and **kpt** given the current data sets being used. If these values do not equal those values defined in **lsmpar.h**, as set by **preproc.h**, the model prints out the values and stops. Hence, the model can be used to determine the appropriate values for **lpt** and **kpt**.

14.3 Run Options lsmexp Namelist

Logical variables that control run options and input/output data set names are set through the **lsmexp** namelist. This namelist is read in from standard input (unit 5). Run definition variables are:

ctitle is an 80 character case title for use with history files. Default: blank

nsrest is an integer variable that equals 0 for an initial run, 1 for a restart, and 3 for a branch run. Default: undefined

nestep is the integer end of the run in iterations (positive) or days (negative). Default: undefined

nelapse is the integer elapsed time of the run in iterations (positive) or days (negative). It is superceded by **nestep**. Default: undefined

Input data sets are defined by:

fsurdat is an 80 character variable defining the time-invariant surface data. Default: blank

finidat is an 80 character variable defining the name of the initial conditions data set. By default, the model is initialized to arbitrary conditions so that no initial data is required.

nrevsn is an 80 character LSM restart file name for use with a branch run. In a branch run, the model will use this file to restart. Default: blank

Mass Store variables are:

nswrps is an 8 character Mass Store write password. Default: blank

irt is the integer Mass Store retention period (days). Default: 0

History and restart file variables are:

lsmhrh is true if using the LSM history and restart handler. Default: false

nhtfrq is the integer history interval in hours (negative) or iterations (positive). Default: -24

ninavg equals "q" or "Q" if using the monthly average history option. In this case, history files will be monthly average output with one time sample (the month) per file (i.e., overriding **nhtfrq** and **mfilt**). Default: blank

mfilt integer number of time samples per history file. Default: 1

excl is an 8 character array of the names of variables to exclude from the history files. For example, setting **excl** = 'TV', 'TAM' deletes the fields TV and TAM from the history files. Default: blank

chntyp is a paired 8 character array of field names and field types to override the default settings. Valid field types are "average", "maximum", "minimum", or "instant". For example, setting **chntyp** = 'FPSN', 'maximum' results in the maximum value over the history interval of the field FPSN being written to the history file. Default: blank

locpnh is an 80 character variable that sets the directory for local history files. Default: the current working directory

locpnr is an 80 character variable that sets the directory for local restart files. Default: the current working directory

The following variables control the model time and calendar:

nnbdat is the integer base date of the run in yymmdd format (e.g., 010625 is June 25 of year 1). Default: undefined

nnbsec is the integer base seconds of the base date (e.g., 0). Default: undefined

nndbas is the integer base day of the run (e.g., 0). Default: undefined

nnsbas is the integer base seconds of the base day (e.g., 0). Default: undefined

dtime is a real variable that sets the model time step (seconds). Default: undefined

Variables that control model physics are:

hydro is false if the prognostic hydrology is not used. In this case, canopy, snow, and soil water pools will not change from the initial conditions. Default: true

pergro is true for random perturbation growth tests. A perturbation growth test, in which initial conditions are randomly perturbed by some small amount, is a useful means to ensure the model is working correctly when using different compilers, operating systems, or other changes that result in a small perturbation (e.g., changing optimization, order of operations). However, when compared to a control run, the land surface model generally has large, rapid solution separation (Figure 31) due to the following reasons: (a) the large sensitivity of the vegetated latent heat flux to small changes in the wetted fraction of the canopy and (b) the strong non-linearity of the latent and sensible heat fluxes to atmospheric stability. This option reduces the solution separation due to a small random perturbation in initial conditions by setting the wetted fraction of the canopy to zero (i.e., $f_{\rm wet} = 0$) and setting atmospheric stability to neutral (i.e., $\zeta = 0$). **pergro** should be set to false unless a perturbation growth test is being performed. Default: false

conchk is true if the various energy and water conservation checks discussed in the technical description are performed. In this case, error messages will be printed to standard output (unit 6) if the conservation check is not satisfied. These conservations checks require a high internal data precision. On some computers, real variables may have to be treated as double precision to satisfy these checks. Default: false

irad is the frequency for solar radiation calculations in hours (negative) or iterations (positive). Default: -1

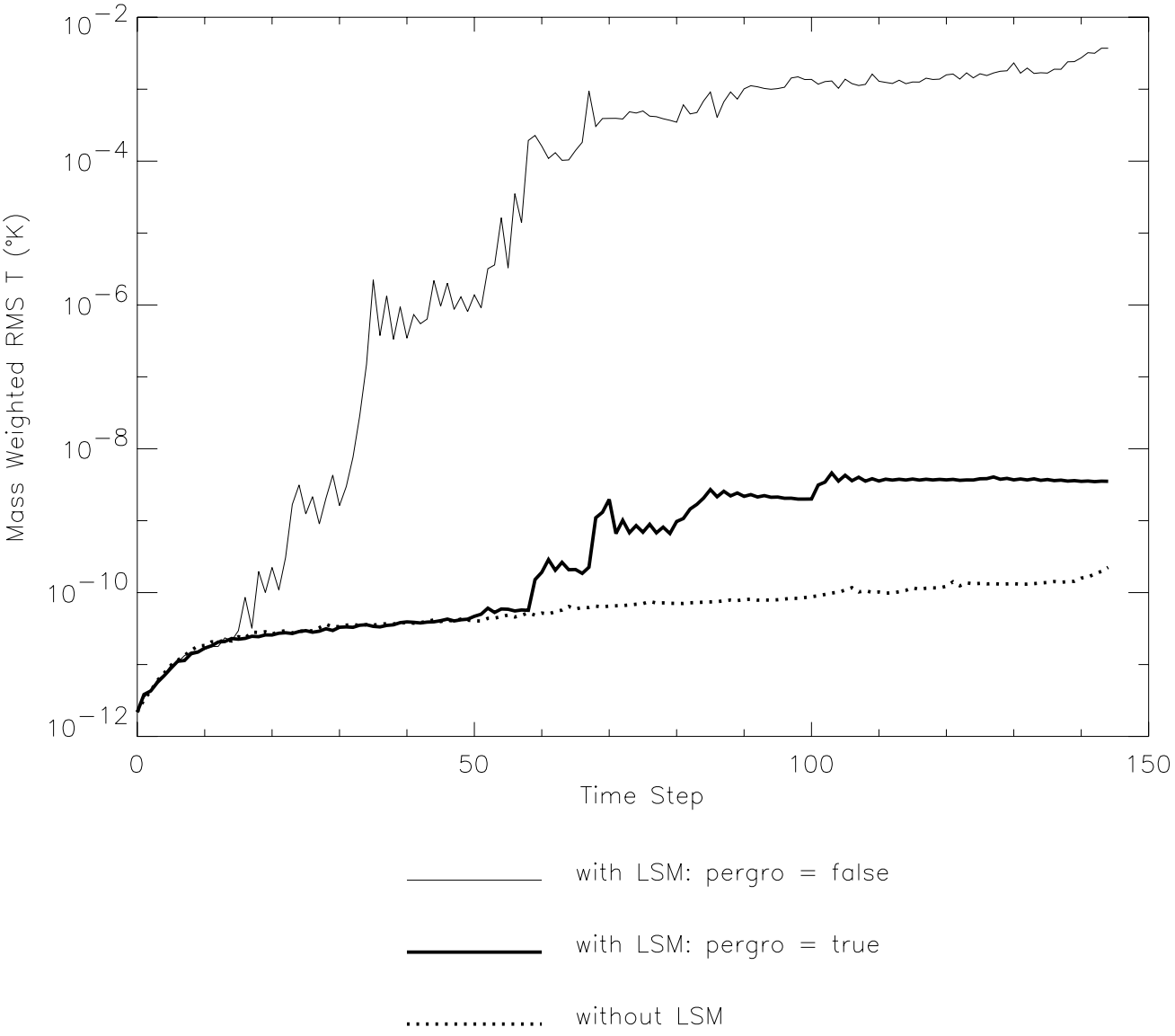
10^{-2}
10^{-4}
10^{-6}
10^{-8}
10^{-10}
10^{-12}
Mass Weighted RMS T (°K)
0
50
100
150
Time Step
with LSM: pergro = false
with LSM: pergro = true
without LSM

Figure 31

Figure 31. Mass weighted root mean square difference in atmospheric temperature, averaged for all grid points and all levels, between control and perturbation simulations of LSM coupled to a version of the CCM. The perturbation simulations differed from the appropriate non-perturbed controls only in that initial atmospheric temperatures were randomly perturbed. Each simulation was for two days (144 time steps).

Most of these variables are set to default values (see subroutine **lsmctli**). When coupling to the NCAR CCM3, the base calendar information, the current time, the ending time, the run type (initial, restart, branch), and the model time step are input from the CCM3. In this case, the minimum namelist parameters are **fsurdat** and **finidat** (if using the initial conditions data set), assuming no LSM history files are desired.

When uncoupled to the CCM3, the minimum namelist parameters are: **nsrest**; **nestep** or **nelapse**; **fsurdat** and **finidat**; **lsmhrh** (to turn on the history and restart file handler using default values); the base calendar variables; and the time step. An example namelist can be found in the file "run_lsmv1.s".

15. LSM Code Description

The land surface model consists of two main routines: **lsmini**, which initializes the model (Figure 29), and **lsmdrv**, which is the main time-stepping call to the model (Figure 30). The code consists of two types of files: *.h files are included through the #include pre-processor directive. *.F files are the main Fortran source files. An example surface data set is given in the file "fsurdat_t42". "run_lsmv1.s" is a UNIX script to run the model. "hist_read.s" is a UNIX script to read a history file and extract particular fields.

*15.1 LSM Code: *.h Files*

lakcon.h. This file contains the **lakcon** common block of constants for the lake temperature model.

lsmctl.h. This file contains the **lsmctl** common block of run control variables.

lsmhis.h. This file contains the **lsmhis** common block of history file variables.

lsmio.h. This file contains the **lsmio** common block, which flags Fortran unit numbers in use for input or output.

lsmpar.h. This file sets array dimensions. (cf. section 14.2)

lsmsrc.h. This file contains a list of all the *.F files. It can be used as input to the C pre-processor cpp to create an output file that has all the source code.

lsmtc.h. This file contains the **lsmtc** common block, which passes time-invariant variables initialized in **lsmini** to **lsmdrv**. These variables include the following: (a) the subgrid to grid mapping indices and weights, (b) the starting location (1 to **kpt**) and the number of points for each "little" vector, (c) time-invariant surface

types, soil hydraulic properties, and soil thermal properties, and (d) latitudes and longitudes.

lsmtv.h. This file contains the **lsmtv** common block. This common block contains the time-varying variables, for the **kpt** subgrid points, that need to be saved from one time step to the next and which need to be written to a restart file. For convenience, these variables are equivalenced with the **lsf** array, which is dimensioned by **mlsf** single-level equivalent fields $\times$ **kpt** points. Consequently, only **lsf** needs to be written to and read from the restart file. The **lsf** array is local to code where this file is included. Hence, this file needs to be included in the code that reads/writes **lsf** from/to the restart files.

phycon.h. This file contains the **phycon** common block of physical constants.

preproc.h. This file sets pre-processor #define and #undef directives. (cf. section 14.1)

radcon.h. This file contains the **radcon** common block of miscellaneous albedo-related radiation constants.

snocon.h. This file contains the **snocon** common block of miscellaneous snow parameters.

soicon.h. This file contains the **soicon** common block of parameters that vary with soil "type".

vartyp.h. This file sets no implicit Fortran variable type.

vegcon.h. This file contains the **vegcon** common block of vegetation-dependent parameters.

vegtyp.h. This file contains the **vegtyp** common block of multiple plant types and fractional areas for each surface type.

*15.2 LSM Code: *.F Files*

atm.F. This code, called by **lsmmain.F**, mimics the atmospheric forcing required by the land model. It is used only if **OFFLINE_LSM** is defined in **preproc.h**.

calendr.F. This subroutine generates calendar day from time step.

canh2o.F. This subroutine calculates canopy water.

ecodyn.F. This subroutine sets vegetation phenology (growing season, leaf area index, stem area index), vegetation biomass, and soil carbon *for the next time step* (i.e., the next call to the land surface model). Although vegetation and soil do not vary from year-to-year, they are included here so that they can change over time based on current surface conditions. Leaf and stem areas are only updated every albedo time step (i.e., if albedos are not calculated every time step) so that there is no inconsistency in the leaf and stem areas used to calculate albedos and those used in the rest of the model. The wetted fraction of canopy is also calculated here based on the current canopy water and leaf and stem areas.

getavu.F. This function gets the next available Fortran unit number.

getfil.F. This subroutine gets the local copy of a desired file. It first looks in the current working directory for the file. If the file is not found there, it uses the full permanent file name. If this is not found, it then copies the file from the Mass Store.

histend.F. This subroutine determines if the current time is the end of a history interval and saves appropriate calendar information.

histhan.F. This subroutine is the main history and restart file handler. It opens new history files as needed, writes data to the current history file, closes the file, and disposes it to the Mass Store if desired. It also writes and disposes restart files. Restart files are written only if the history file is full or if the end of the run coincides with the end of a history write interval.

histini.F. This subroutine initializes variables for history files.

histlst.F. This subroutine initializes the active field list for history files.

histmlf.F. This subroutine accumulates a multi-level field over the history time interval.

histnam.F. This subroutine creates a unique history or restart file name from the current file number or from the month and year of the simulation (if using the monthly average option).

histslf.F. This subroutine accumulates a single-level field over the history time interval.

histtc.F. This subroutine creates a history file of the time constant data in the **lsmtc** common block.

histwrt.F. This subroutine writes to a history file the current time sample's integer, real, and character headers and real data records.

infil.F. This subroutine calculates surface runoff and infiltration.

lakconi.F. This block data subprogram initializes the **lakcon** common block of constants for the lake temperature model.

laktem.F. This subroutine calculates lake temperatures.

lencs.F. This function returns the position of the right-most non-blank, non-null character in a character variable.

lsm.F. This subroutine calculates surface fluxes and updates the ecological, hydrologic, and thermal state of the land for a "little" vector on **npt** points. Local arrays are dimensioned by **mpt** because only up to **mpt** points are processed in each call to **lsm**. However, only **npt** points are actually processed. This discrepancy between **npt** and **mpt** arises because the "big" vector of **kpt** points may not be divided into **numlv** "little" vectors of equal length.

lsmctli.F. This subroutine initializes run control variables in the **lsmctl** and **lsmhis** common blocks. These variables are set using the **lsmexp** namelist. (cf. section 14.3)

lsmdrv.F. This subroutine is the 2-d driver for the model. Input/output from/to the atmospheric model are 2-dimensional (longitude $\times$ latitude) arrays. Local arrays are "big" vectors of **kpt** points. These points are processed as "little" vectors of **numkpt** points in **numlv** calls to subroutine **lsm**.

lsmhdr.F. This subroutine writes header information about the current version of the model to standard output.

lsmini.F. This subroutine initializes the land surface model. For an initial run, this subroutine also initializes required land surface variables as 2-dimensional (longitude $\times$ latitude) arrays for the atmosphere model.

lsmmain.F. This is the main program for "off-line" simulations. It mimics the coupling of the land model with an atmospheric model. It is used only if **OFFLINE_LSM** is defined in **preproc.h**.

lsmmap.F. This subroutine builds the subgrid to grid mapping indices and weights and vice versa.

lsmres.F. This subroutine restarts the model for continuation runs.

lsmtci.F. This subroutine initializes vegetation and soil types, soil properties, and other miscellaneous variables for all **kpt** subgrid points. These are part of the **lsmtc** common block of time-invariant variables.

lsmtvi.F. This subroutine initializes time varying variables for the **lsmtv** common block. There are six main variables: snow, canopy, and soil water; vegetation, ground, and soil temperatures. Most of the remaining variables are set from these variables. Some variables are set to arbitrary constants because their exact value is not too important for initialization. Vegetation structure and soil carbon (**ecodyn**) and albedos (**suralb**) are initialized for the first call to **lsmdrv**. Although soot is currently time-invariant, it is included here so that snow can age over time.

lsmzen.F. This subroutine uses calendar day, latitude, and longitude to calculate the cosine of the solar zenith angle.

msspni.F. This subroutine sets the pathnames for history and restart files disposed to the Mass Store.

opnfil.F. This subroutine opens a local file.

phenol.F. This subroutine sets leaf and stem areas from prescribed monthly values.

phyconi.F. This block data subprogram sets physical constants for the **phycon** common block.

putfil.F. This subroutine copies a local file to the Mass Store.

radconi.F. This block data subprogram sets miscellaneous albedo-related radiation constants for the **radcon** common block.

relavu.F. This subroutine closes and releases a Fortran unit number.

restwrt.F. This subroutine writes the main restart file and the pointer file to the main restart file, disposing these to the Mass Store if desired.

setarr.F. This subroutine sets an array to a constant value.

snoalb.F. This subroutine calculates snow albedos.

snoconi.F. This block data subprogram sets miscellaneous snow parameters for the **snocon** common block.

snoh2o.F. This subroutine calculates snow water.

soialb.F. This subroutine calculates albedos for soil, lakes, wetlands, and glaciers, accounting for snow.

soiconi.F. This block data subprogram sets soil "type" dependent variables for the **soicon** common block.

soih2o.F. This subroutine calculates soil water and sub-surface drainage.

soitem.F. This subroutine calculates soil temperatures.

stomata.F. This subroutine calculates leaf stomatal resistance and leaf photosynthesis for sunlit or shaded leaves.

stoprun.F. This subroutine stops the run.

suralb.F. This subroutine calculates albedos *for the next time step* using the current state of the land (e.g., snow, soil water, canopy water), leaf and stem areas *for the next time step*, and zenith angle *for the next time step*. Calculating albedos for the next time step facilitates a simple interface between the atmosphere and land models. However, because the albedos are being calculated for the next time step, variables needed for surface radiation calculations in **surrad** (ground albedos; surface albedos; absorbed and transmitted fluxes) must be saved for the next time step. This subroutine is only called if the next time step is a radiation time step. This is needed because the atmospheric radiation (which requires surface albedos) may not be calculated every time step (e.g., only every three time steps). Because albedos are not necessarily updated every time step, leaf and stem areas are only updated if it is an albedo time step to ensure the same values used for the albedo calculations are also used for surface radiation, surface temperature, and energy flux calculations.

surbgc.F. This subroutine calculates (a) net primary production from photosynthesis and respiration and (b) other surface biogeochemical fluxes. Currently, only CO_2 fluxes are simulated.

surphy.F. This subroutine performs the surface biophysical calculations (energy and momentum fluxes, temperatures).

surrad.F. This subroutine uses relative reflected, transmitted, and absorbed solar fluxes (output from **suralb.F** and **twostr.F**) to calculate: (a) reflected solar radiation, (b) the solar radiation absorbed by vegetation and ground, for later use in the surface temperature and flux calculations, and (c) the photosynthetically active radiation absorbed by sunlit and shaded leaves, for use in the stomatal resistance calculations. Because the land surface model calculates its own absorbed solar radiation, one should ensure that when coupling to an atmospheric model the absorbed

solar radiation (averaged to the atmospheric grid) is the same as that calculated by the atmospheric model. This subroutine, which is called every time step, depends on output from **suralb.F**, which may be called less frequently. If albedos are only updated every three time steps, the result is that surface radiation is also only updated every three time steps *provided* that the incoming solar radiation from the atmosphere is also only updated every three time steps.

surtem.F. This subroutine calculates surface temperatures and fluxes. **stomata** is called twice to calculate leaf stomatal resistance and photosynthesis for sunlit and shaded fractions of the canopy.

tridia.F. This subroutine solves a tridiagonal system of equations using the algorithm discussed by Press et al. (1986), page 40.

twostr.F. The subroutine calculates the two-stream optical parameters and the fluxes absorbed, reflected, and transmitted by the vegetation per unit incoming flux for later use in **surrad**.

vegconi.F. This block data subprogram initializes the **vegcon** common block of vegetation-dependent parameters.

vegtypi.F. This block data subprogram initializes the **vegtyp** common block of multiple plant types and their fractional area for each surface type

verh2o.F. This subroutine performs the vertical (column) hydrology calculations.

wrtrdr.F. This subroutine writes a real data record (i.e., a vector of **kpt** points) to the current history file.